Investigating brain-derived α-synuclein fibrils and diagnostic biomarkers of synucleinopathies

Selene (Seoyun) Lee



A thesis submitted in partial fulfillment

of the requirements for the degree of

Doctor of Philosophy

Nuffield Department of Clinical Neurosciences

University of Oxford

Brasenose College

Trinity Term 2023

Declaration

I, Selene (Seoyun) Lee, confirm that the work presented in this thesis is my own. Where information has been derived from other sources or collaboration, the contributions are indicated as follows:

- **Figure 7.7**, Dr Rod Chalk performed LC-MS/MS and acquired raw data.
- **Table A.1**, Dr Michael Lawton performed statistical analysis.
- **Table A.2**, Dr Michael Lawton performed statistical analysis.
- **Table A.3**, Dr Michael Lawton performed statistical analysis.

Abstract

Synucleinopathies are associated with the aggregation of misfolded alpha-synuclein (αSyn) into fibrils. These αSyn fibrils are categorised into different 'strains' according to their biological properties. In vitro-seeded fibrils generated with seeding amplification assay (SAA fibrils) have facilitated αSyn strain research, but the question remains how well they replicate the brain-derived fibrils. The SAA also functions as a highly sensitive and specific diagnostic tool for Parkinson's disease (PD) and is usually carried out in cerebrospinal fluid (CSF), but other more accessible biofluids have also been studied, including saliva.

This thesis comprises four aims: 1) to investigate methods for characterising brain-derived αSyn fibrils, 2) to characterise biochemical and biophysical properties of brain-derived αSyn fibrils that are indicative of αSyn strains and compare these properties to the SAA fibrils, 3) to examine the diagnostic value of αSyn SAA in CSF of PD and multiple system atrophy (MSA) patients, 4) to examine saliva from PD patients for αSyn seeding activity and molecular signatures to identify biomarker candidates.

Findings revealed the biochemical and biophysical heterogeneity of αSyn fibrils from different synucleinopathies, but these properties were not replicated among the SAA fibrils. αSyn SAA with CSF samples were able to stratify between PD and MSA. The quantitative parameters correlated with MSA disease progression and PD clinical clusters. Preliminary investigation on PD saliva resulted in the detection of αSyn seeding activity and significant changes in the levels of oligomeric αSyn, alpha-1-antitrypsin (A1AT) and

chitinase-3-like protein-2 (CH3L2).

Overall, this thesis demonstrates biochemical and biophysical evidence of brain-derived αSyn strains, which the SAA fibrils fail to replicate. Results raise significant implications of using SAA fibrils to model synucleinopathies. The performance of CSF αSyn SAA illustrates its diagnostic value, and the molecular signatures observed in PD saliva offer a new outlook for diagnostic tools.

Acknowledgements

I am grateful to Prof Laura Parkkinen for her expert guidance and support throughout this journey. Your scientific endeavour has been contagious and sparked a constant inspiration. Thank you for sharing your expertise and the wonders of neuropathology. Also, in times of self-doubt, your encouragement was invaluable, especially amidst the challenges brought on by the pandemic.

Thanks also goes to my secondary supervisor, Dr Livia Civitelli. Every chapter and work done throughout my DPhil bears the mark of our invigorating discussion and your expert insight. All this work would not have existed without your endless support and supervision. My heartfelt thanks go to Dr Alan King Lun Liu, who offered clinical expertise and life advice that enriched this work. Your enthusiasm for research has been a motivator and lightened up our lab.

Some of the exceptional minds at Oxford have been my colleagues, and I was fortunate to work alongside them. Dr Rod Chalk, thank you for sharing your prowess in mass spectrometry and for your wise life advice. To Dr Errin Johnson, who made electron microscopy less intimidating and more fascinating, your patience and expertise are deeply appreciated. Thanks goes to Dr Aadil El-Turabi for our insightful discussions and creative ideas on not only alpha-synuclein but just about everything. I would also like to acknowledge the Oxford Brain Bank for providing the brain tissues used in this thesis.

Also, for the collaborators outside Oxford, I would like to thank them for the phenomenal contribution that made this work possible. Thanks go to Prof Hilal Lashuel from

EPFL for generously providing their homemade antibodies that were extremely useful for the work done in this thesis. Thanks to Prof Per Borghammer and Dr Tatyana Fedorova from Aarhus University, for providing the saliva samples. Thanks also goes to the Imperial Brain Bank for providing brain tissues used in this thesis.

I would like to thank all the patients and their families for the valuable donations and contributions for research.

A special thanks to Brasenose College for a supportive community that has enriched my student experience at Oxford. My sincere thanks to my college advisors, Prof William James and Prof Russell Foster, who made sure I was on track and reminded me there is still life outside research.

A constant source of comfort and strength, my family have been the biggest supporters, and I cannot thank them enough. This achievement is as much yours as it is mine. Oscar Lee, thank you for being my mental support and enduring endless ramblings about my DPhil. You have been inevitably chosen to be one of the five lucky people to read my thesis and know more about my research than you wanted to. Thanks go to my friends, who have been genuinely caring and ceaselessly asking when I finish. I think you can stop asking now.

Studies

Publications

- **Selene Seoyun Lee**, Livia Civitelli, Laura Parkkinen. *Brain-derived and in vitro-seeded αSyn fibrils exhibit distinct biophysical profiles*. eLife (in press). bioRxiv, 10.1101/2023.10.04.560803.

- Ilaria Poggiolini, Vandana Gupta, Michael Lawton, **Seoyun Lee**, Aadil El-Turabi, Agustin Querejeta-Coma, Claudia Trenkwalder, Friederike Sixel-Döring, Alexandra Foubert-Samier, Anne Pavy-Le Traon, Giuseppe Plazzi, Francesco Biscarini, Jacques Montplaisir, Jean-François Gagnon, Ronald B Postuma, Elena Antelmi, Wassilios G Meissner, Brit Mollenhauer, Yoav Ben-Shlomo, Michele T Hu, Laura Parkkinen. *Diagnostic value of cerebrospinal fluid alpha-synuclein seed quantification in synucleinopathies*. Brain, 10.1093/brain/awab431, December 2021.

- **Selene Seoyun Lee**, Rod Chalk, Livia Civitelli, Laura Parkkinen. *Investigation of salivary molecular signatures of Parkinson's disease*. (manuscript in preparation).

Contents

1 Introduction **1**

2 General background **3**

2.1 Synucleinopathies 3

2.1.1 Parkinson's disease (PD) 3

2.1.2 Dementia with Lewy bodies (DLB) 8

2.1.3 Multiple system atrophy (MSA) 9

2.2 α-Synuclein (αSyn) 10

2.2.1 Physiological αSyn 10

2.2.2 Pathological αSyn 14

2.3 αSyn strains 17

2.3.1 αSyn strain hypothesis 17

2.3.2 Evidence of αSyn strains in human brains of different synucleinopathies 20

2.3.3 Evidence of strains among in vitro-seeded αSyn fibrils 26

2.4 Biomarker for synucleinopathies 29

2.4.1 Seed amplification assay (SAA) 29

2.4.2 Salivary biomarkers 36

2.5 Thesis aims 40

3 Materials and Methods **42**

3.1 Human biosamples . . . 42

3.1.1 Brain samples . . . 42

3.1.2 CSF samples . . . 45

3.1.3 Saliva samples . . . 47

3.2 Extraction of αSyn fibrils from the human brain . . . 48

3.2.1 Sarkosyl-based extraction . . . 48

3.2.2 TritonX-100-based extraction . . . 48

3.2.3 RIPA-based extraction . . . 49

3.3 Biochemical characterisation of αSyn fibrils . . . 49

3.3.1 Slot blot . . . 49

3.3.2 Proteinase-K digestion . . . 50

3.4 Transmission electron microscope (TEM) imaging . . . 51

3.4.1 Negative stain TEM . . . 51

3.4.2 Immunogold TEM . . . 52

3.5 Measurement of protein concentration . . . 53

3.5.1 Bicinchoninic (BCA) protein assay . . . 53

3.5.2 Enzyme-linked immunosorbent assay (ELISA) . . . 54

3.6 Mass spectrometry . . . 54

3.6.1 ESI-TOF intact mass and data analysis . . . 54

3.6.2 LC-MS/MS and data analysis . . . 55

3.7 αSyn seed amplification assay (SAA) . . . 56

3.7.1 αSyn fibril SAA . . . 56

3.7.2 CSF SAA . . . 57

3.7.3 Saliva SAA . . . 58

3.8 Immunohistochemistry . . . 58

3.9 Graphic illustrations . . . 59

3.10 Statistical analysis 59

4 Investigating biochemical and biophysical methods to characterise αSyn fibrils from PD brain 60

4.1 Introduction 60

4.2 Results 62

4.2.1 Sarkosyl extraction of a PD brain yields optimal fibril integrity . . 62

4.2.2 Profiling the immunoreactivity of αSyn antibodies to sarkosyl-insoluble αSyn from PD brains 62

4.2.3 PK-resistance profiles of sarkosyl-insoluble αSyn from PD brains 66

4.2.4 αSyn fibrils from PD brains exhibit straight and twisted morphologies 68

4.2.5 Structural characterisation of αSyn fibrils using immunogold-TEM 69

4.3 Discussion 71

4.3.1 Experimental limitations 73

4.3.2 Summary 74

5 Brain-derived and in vitro-seeded αSyn fibrils exhibit distinct biochemical and biophysical profiles 75

5.1 Introduction 75

5.2 Results 76

5.2.1 Brain-derived αSyn fibrils from PD, PDD, DLB, and MSA display distinct seeding activity 76

5.2.2 Brain-derived and SAA αSyn fibrils show distinct biochemical profiles 78

5.2.3 Distinct morphologies of brain-derived and SAA αSyn fibrils revealed by TEM 81

5.3 Discussion 84

5.3.1 Investigation of biochemical and biophysical properties of brain-derived αSyn fibrils from different synucleinopathies. 84
5.3.2 SAA fibrils demonstrate distinct biochemical and biophysical properties to the brain-derived fibrils 87
5.3.3 Experimental limitations 88
5.3.4 Summary 89

6 Diagnostic value of cerebrospinal fluid αSyn seed quantification in synucleinopathies 91
6.1 Introduction 91
6.2 Results 92
6.2.1 αSyn seeding activity in CSF of PD and MSA patients 92
6.2.2 Correlation of the SAA parameters with PD disease severity and clusters 94
6.2.3 Correlation of the SAA parameters with MSA disease severity . . 95
6.3 Discussion 96
6.3.1 Experimental limitations 99
6.3.2 Summary 100

7 Salivary biomarker for PD 101
7.1 Introduction 101
7.2 Results 103
7.2.1 Immunoblot analysis of salivary αSyn 103
7.2.2 Measurement of salivary total and aggregated αSyn levels with ELISA 106
7.2.3 LC-MS intact mass analysis of PD saliva 108
7.2.4 Proteomic profiling of PD saliva 109
7.2.5 Detection of αSyn seeding activity in PD saliva 111

7.3 Discussion . . . 113
7.3.1 Salivary αSyn . . . 113
7.3.2 Salivary proteomic profiling . . . 113
7.3.3 αSyn seeding activity in PD saliva . . . 114
7.3.4 Experimental limitations . . . 115
7.3.5 Summary . . . 115

8 General discussion **116**
8.1 Key findings . . . 116
8.2 Implications of findings . . . 118
8.2.1 Characterisation of brain-derived αSyn fibrils . . . 118
8.2.2 Strain-like properties of the brain-derived αSyn fibrils from different synucleinopathies . . . 119
8.2.3 Brain-derived versus SAA αSyn fibrils . . . 120
8.2.4 Quantification of αSyn seeding in CSF of PD and MSA patients 121
8.2.5 Salivary biomarkers and its limitations . . . 122
8.3 Future directions . . . 123
8.4 Concluding remarks . . . 124

A Appendices **126**
A.1 Chapter 4 . . . 126
A.1.1 Immunogold-TEM analysis of αSyn fibrils from PD brains . . . 126
A.2 Chapter 5 . . . 128
A.2.1 Conformational stability of brain-derived and SAA αSyn fibrils . 128
A.2.2 Immunohistochemistry analysis of αSyn pathology in PD, PDD, DLB and MSA brains . . . 130
A.2.3 Phosphorylated αSyn fibrils in PD, PDD, DLB and MSA brains . 131
A.2.4 Measurement of fibrils from TEM images . . . 133

A.3 Chapter 6 134
A.3.1 Association between SAA parameters and clinical symptoms of PD patients 134
A.3.2 SAA parameter is associated with PD clinical clusters 135
A.3.3 SAA parameters correlate with MSA disease progression 136
A.4 Chapter 7 137
A.4.1 SynO4 detects salivary αSyn 137
A.4.2 HRP-conjugated αSyn antibodies detect salivary αSyn 137
A.4.3 Detection of αSyn seeding activity in PD saliva 139

Bibliography **142**

List of Figures

2.1 Symptoms associated with the progression of different synucleinopathies. 5
2.2 αSyn neuropathology. 7
2.3 Structure of αSyn monomer. 11
2.4 αSyn family members. 12
2.5 Role of αSyn in the synaptic vesicle cycle. 14
2.6 Balance of intracellular αSyn. 15
2.7 Conformational states of αSyn. 16
2.8 αSyn strain hypothesis. 19
2.9 Cryo-EM structures of brain-derived αSyn fibrils. 22
2.10 Distinct biochemical profiles of brain-derived αSyn fibrils from different synucleinopathies. 24
2.11 Structural comparison of brain-derived and SAA αSyn fibrils. 28
2.12 αSyn SAA mechanism. 31
2.13 αSyn SAA kinetic parameters. 32
2.14 Neural regulation of salivary glands. 37

4.1 Fibrils extracted from PD brain using different extraction methods. 63
4.2 Immunoreactivity profiles of αSyn antibodies towards sarkosyl-insoluble αSyn. 64
4.3 Semi-quantification of antibody immunoreactivity. 65
4.4 PK-resistant αSyn peptides. 67

4.5 Morphologies of the αSyn fibrils from PD brains. 68
4.6 Immunogold analysis of αSyn fibrils from PD brains. 70

5.1 SAA seeded with αSyn fibrils from different synucleinopathies. 77
5.2 SAA reaction kinetics. 78
5.3 Biochemical differences between brain-derived and SAA αSyn fibrils. . . 79
5.4 PK-resistance profiles of brain-derived αSyn fibrils. 80
5.5 Brain-derived and SAA αSyn fibrils show distinct morphologies. 82
5.6 Differences in phosphorylation between brain-derived and SAA αSyn fibrils. 84
5.7 Quantification of phosphorylated αSyn in brain-derived and SAA fibrils. . 85

6.1 αSyn SAA reactions of CSF from PD, MSA and HC and kinetic parameters. 93
6.2 Correlation between αSyn SAA parameters and clinical data of PD patients. 94
6.3 αSyn SAA parameters in PD clinical clusters. 95
6.4 Correlation between αSyn SAA parameters and clinical data of MSA patients. 96

7.1 Non-specific immunoreactivity of secondary antibodies towards salivary proteins. 104
7.2 SynO4 detection of salivary αSyn. 104
7.3 HRP-conjugated αSyn antibodies detect salivary αSyn. 105
7.4 Quantification of immunoreactivity from HRP-conjugated αSyn antibodies. 106
7.5 Concentrations of total protein and αSyn in PD and healthy saliva. 107
7.6 Intact mass analysis of pooled saliva from PD and HC. 108
7.7 Salivary protein differences between PD and HC. 110
7.8 Optimisation of salivary αSyn SAA. 111
7.9 SAA detection of αSyn seeding activity in PD saliva. 112

A.1 Immunogold-TEM images of unlabelled αSyn fibrils. 127

A.2 Conformational stability of brain-derived and SAA αSyn fibrils. 129
A.3 αSyn pathology in PD, PDD, DLB, and MSA brains. 130
A.4 Immunogold-TEM images of phosphorylated αSyn from PD, PDD, DLB and MSA brains. 132
A.5 Length and width measurements of the brain-derived and SAA fibrils. . . 133
A.6 Complete immunoblots of SynO4. 137
A.7 Complete immunoblots of HRP-conjugated antibodies. 138
A.8 Raw SAA measures of αSyn seeding activity in PD saliva. 140
A.9 Raw SAA measures of αSyn seeding activity in HC saliva. 141

List of Tables

2.1 Clinical features of the four clinical clusters of PD. 6
2.2 Summary of immunogold TEM studies of αSyn fibrils. 21
2.3 αSyn SAA kinetics parameters. 33
2.4 Salivary αSyn studies. 38

3.1 Clinicopathological summary of the cases used in Chapter 4. 43
3.2 Clinicopathological summary of the cases used in Chapter 5. 44
3.3 Demographics of PD, MSA and control subjects investigated in Chapter 6. 46
3.4 Demographics for the saliva study in Chapter 7. 47
3.5 Slot blot antibodies 50
3.6 Immunogold TEM antibodies 53
3.7 Buffer components of αSyn fibril and CSF SAA 57
3.8 Buffer components of saliva SAA 57

A.1 Correlation analysis between SAA parameters and clinical data of PD patients. 134
A.2 SAA parameters and PD clinical clusters. 135
A.3 Correlation analysis between SAA parameters and clinical data of MSA patients. 136

Chapter 1

Introduction

A city demolished by a hurricane leaves behind a trail of destruction. Similarly, neurodegeneration is catastrophic to the intricate system of the human brain. While the hurricane's aftermath is a chaos of broken trees and collapsed buildings, the degenerated brain is abandoned with disrupted neural pathways, aggregated proteins, and cellular dysfunction.

Soichiro Honda, the founder of Honda Motors, once noted, 'If you want to find out what is wrong with a car, go to the junkyard and see what parts are left over after everything else has broken.' The 'junkyard' is the neuropathological aftermath of the neurodegenerative 'hurricane'. Inspection of the 'junkyard leftovers', being the α-synuclein (αSyn) fibrils in the brain, unveils the underlying molecular mechanisms of synucleinopathies and their diverse clinicopathological features.

How can a single αSyn protein be linked to different synucleinopathies exhibiting diverse clinical and pathological characteristics? A prevailing hypothesis states that the different αSyn 'strains' might be the root contributor to such diverse disease phenotypes. The 'junkyard' αSyn fibrils in the post-mortem brain tissue serve as a valuable resource for investigating such αSyn strains. While efforts have been made to replicate these brain-derived fibrils in vitro using a seeding amplification assay (SAA), the biological relevance of such models remains an open question. Furthermore, the quest for a reliable, quanti-

tative and non-invasive biomarker for synucleinopathies has proven to be a formidable challenge.

The structure of this thesis is as follows. Chapter 2 reviews the distinct clinical and pathological features of the different synucleinopathies. The chapter also discusses αSyn protein, elucidating its physiological and pathological roles. It introduces αSyn strains and summarises current research on the brain-derived and SAA αSyn fibrils. The chapter concludes with αSyn biomarkers, providing an overview of SAA and a summary of salivary biomarkers for PD. Next, Chapter 3 outlines the experimental methodology and the demographic details of the patients whose biosamples were used in this thesis.

Chapters 4 through 7 each focus on an independent study that addresses each objective of the thesis. Chapter 4 explores various biochemical and biophysical methods for characterising αSyn fibrils from PD brains, emphasising the methodology and the biochemical variability observed within these fibrils. Chapter 5 investigates the strain-like properties of the brain-derived αSyn fibrils across different synucleinopathies and presents evidence that the SAA fibrils do not fully replicate the biological features of their brain-derived counterparts. Chapter 6 examines the diagnostic value of αSyn SAA and its crucial role as a molecular marker that may guide the identification of disease subtypes and progression. Chapter 7 takes a multifaceted approach to analysing the saliva of PD patients to identify signature molecular changes while also discussing the limitations and challenges of using saliva for biomarker discovery.

The concluding Chapter 8 synthesises the findings from the preceding chapters into an overarching discussion. This final chapter reflects on the conclusions drawn, the limitations encountered, and the future prospects of the research.

Chapter 2

General background

2.1 Synucleinopathies

Synucleinopathies are a group of heterogeneous neurodegenerative diseases characterised by the aggregation of the protein alpha-synuclein (αSyn) protein in the form of inclusions in the neurons and glial cells. According to neuropathological hallmarks, synucleinopathies are categorised into two main disease groups: Lewy body diseases (LBD) and multiple system atrophy (MSA). LBDs display αSyn inclusions in the form of Lewy bodies (LBs) and Lewy neurites (LNs) in the neurons[1]. More recently, astroglial pathology has also been characterised in LBDs[2]. Such αSyn pathology are observed among Parkinson's disease (PD), Parkinson's disease with dementia (PDD), and dementia with Lewy bodies (LBD), which importantly cannot be distinguished from on another. In contrast, MSA is characterised by its unique pathology, where αSyn inclusions form in oligodendrocytes in the form of glial cytoplasmic inclusions (GCIs). This section describes the clinical and pathological hallmarks of synucleinopathies. This leads to the central question of how one protein, αSyn, is associated with a diverse spectrum of diseases.

2.1.1 Parkinson's disease (PD)

PD is the second most common neurodegenerative disease after Alzheimer's disease (AD) and the most common movement disorder[3]. The disease affects 1 % of the population

over 60 years of age. It is an age-related disease as the prevalence is rare below 50 years of age and rises to 3 % in the population above 80 years of age.

2.1.1.1 Clinical hallmarks

Clinical symptoms of PD include resting tremor, rigidity, postural deformities and bradykinesia[4]. Diagnosis is made by observing the clinical symptoms, but it is difficult to distinguish PD from other Parkinsonian syndromes with clinical criteria alone (Fig. 2.1). Also, initial diagnostic misclassification is common with errors of 15-24% even by movement disorder specialists[5]. Therefore, the clinical diagnosis can only be confirmed with neuropathological assessment. Furthermore, making a clinical diagnosis at the early stages of the disease is challenging. A long prodromal phase, probably spanning 20 years, precedes the manifestation of motor disease. Hyposmia and constipation can precede motor symptom onset by decades, but these symptoms are not rare in older patients and, by themselves, are not useful in identifying prodromal PD. Rapid eye movement (REM) sleep behaviour disorder (RBD) is now recognised as the strongest risk factor for PD, with high conversion rate (approximately 80 %) to develop a synucleinopathy, highlighting its potential as a pre-clinical marker for PD at relatively early stages of the disease[6].

Some PD patients manifest cognitive impairment later on and are classified as PD with dementia (PDD)[7]. In the long-term PD progression, the prevalence of dementia is almost inevitable and rises up to 80 % with 20-year duration[8]. Nevertheless, there are no clear neuropathological differences between PD and PDD. Also, the overlapping pathological and clinical features between PDD and DLB expose ambiguity in the differentiation of the two diseases.

Due to the wide spectrum of clinical manifestations of PD, various clinical assessments are implemented to aid the diagnosis. Rating scales are used to measure motor impairment in PD patients. Movement Disorders Society Unified Parkinson's disease Rating Scale (MDS-UPDRS) parts I to IV is the most well-established scale that reflects

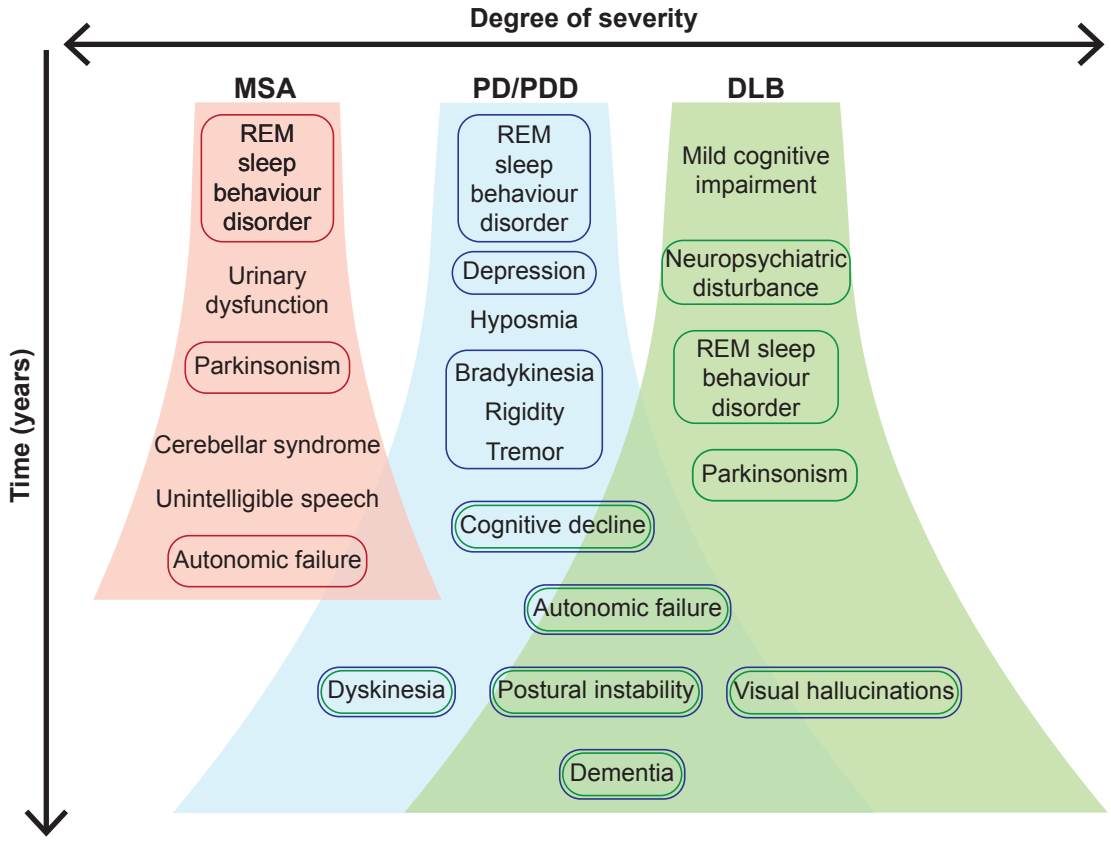

Figure 2.1 **Symptoms associated with the progression of different synucleinopathies.** PD/PDD is diagnosed at the onset of motor symptoms (bradykinesia, rigidity, tremor), but non-motor symptoms (REM sleep behaviour disorder (RBD), depression, hyposmia) can appear at an earlier prodromal phase of the disease. Non-motor symptoms are prevalent throughout the disease. As PD/PDD progresses, cognitive decline can appear, and the severity of the motor symptoms increases. DLB is diagnosed when dementia occurs before or concurrent with Parkinsonism. As the disease progresses, clinical symptoms overlap with PD/PDD. MSA progression is much more aggressive than PD/PDD and DLB. Symptoms such as RBD, parkinsonism, and autonomic failure overlap with PD/PDD and DLB. The overlapping symptoms across diseases are marked in circles.

the complex disabilities in PD, including non-motor symptoms[9]. The Hoehn and Yahr (H&Y) scale assesses disease progression from stage 0 to 5. For cognitive assessments, Mini-Mental State Examination (MMSE) and Montreal Cognitive Assessment (MoCA) are used to detect mild cognitive impairment (MCI) or dementia. Screening for cogni-

tive impairment is important as it can predict cognitive decline and stratify PDD patients. MMSE is commonly used as a primary screening tool, but MoCA has been reported to be a more sensitive and valid instrument for clinical assessment of PD patients[10].

However, PD is a complex syndrome rather than a single disease. Evaluating the baseline motor and non-motor symptoms, levodopa response and disease progression of PD patients from a well-characterised longitudinal cohort resulted in four different clinical clusters of PD[11] (Table 2.1). PD patients in cluster 1 had fast motor progression with mild and symmetrical motor disease. Their non-motor symptoms, including olfaction, cognitive impairment and postural hypotension, were prominent. Patients in cluster 2 manifested slow motor progression with mild motor and non-motor disease. Cluster 3 was associated with severe motor disease and poor non-motor symptoms, including psychological well-being and sleep. Cluster 4 patients had unilateral disease with severe tremors and slow motor progression. The different clusters of PD demonstrate the heterogeneity of clinical phenotypes and the possibility for targeted clinical trials and therapeutic interventions.

Table 2.1 Clinical features of the four clinical clusters of PD. Table adapted from Ref. [11].

Clusters	Motor progression	Motor disease	Levodopa response	Non-motor
Cluster 1	Fast	Symmetrical, mild	Poor	Prominent (hyposmia, hypotension, cognitive impairment)
Cluster 2	Slow	Unilateral	Good	Better than average
Cluster 3	Intermediate	More gait/posture problems	Intermediate	Poor well-being, poor sleep
Cluster 4	Intermediate	Unilateral, tremor dominant	Poor	Average

2.1.1.2 Neuropathological hallmarks

PD is neuropathologically characterised by the presence of Lewy pathology and loss of dopaminergic neurons in the substantia nigra pars compacta (SNpc)[12]. LBs are pigmented spherical inclusions found in neurons (Fig. 2.2a). LNs refer to neurites (axons and dendrites) that contain abnormal filaments similar to those found in LBs (Fig. 2.2b). Both LBs and LNs are mainly composed of oligomeric and filamentous αSyn[13]. Astroglial accumulation of αSyn is also prominent, but less addressed in PD[2] (Fig. 2.2c). This pathology is related to the loss of dopaminergic neurons in the SNpc, which primarily causes motor deficits in PD patients.

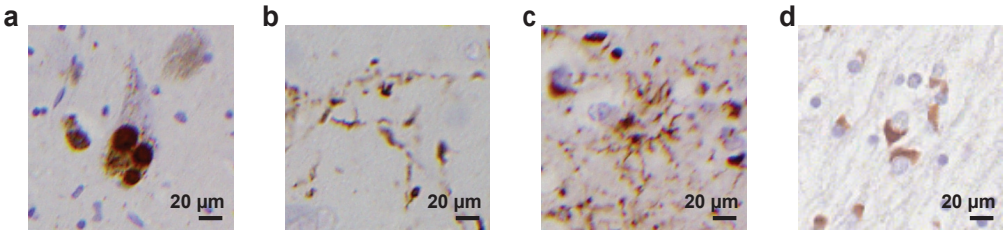

Figure 2.2 **αSyn neuropathology a-d**, αSyn inclusions in the form of Lewy body (LB) (**a**), Lewy neurite (LN) (**b**), astroglial pathology (**c**), and glial cytoplasmic inclusion (GCI) (**d**). (**a&b**) Lewy pathologies from the midbrain of a PDD case, stained with Syn1 (BD Biosciences). (**c**) Astroglial pathology from the amygdala of a PDD case, stained with LASH 80-96 (Lashuel lab). (**d**) GCI pathology from the striatum of an MSA case, stained with Syn1 (BD Biosciences). Scale bars = 20 µm.

In addition to SNpc, Lewy pathology is found throughout the brain. Braak and colleagues suggested that Lewy pathology spreads across the brain in a predictable manner as the disease progresses[14]. The authors characterised the stages of the disease progression regarding the presence of Lewy pathology throughout the nervous system. It starts in the peripheral autonomic neurons and olfactory regions (Braak stage 1), continues to spread in the lower brain stem (Braak stage 2), extends to the midbrain (Braak stage 3), forebrain and limbic system (Braak stage 4) and finally progresses to primary and association cortical areas (Braak stages 5-6). Although the prevailing view of PD pathology is that Lewy body pathology retrogradely spreads via synaptically connected networks,

there are limitations to this hypothesis.

Neuronal death occurs in the SNpc, pedunculopontine nucleus (PPN), locus coeruleus (LC), dorsal motor nucleus of the vagus (DMV), raphe nuclei (RN), nucleus basalis of Meynert (NBM) and ventral tegmental area (VTA)[15]. Neuronal death begins from the SNpc and later becomes apparent in the diencephalon, telencephalon and brainstem[16]. Interestingly, the pattern of Lewy pathology and that of neuronal loss differ significantly[17]. Also, the pattern of Lewy pathology in the brains of patients with PD is not always consistent with the Braak staging[18,19]. Therefore, the idea of selective vulnerability was suggested, which claims that specific neurons are at risk due to cell-autonomous characteristics and Lewy pathology can spread trans-synaptically[16]. This suggests that PD cannot be understood with the spread of Lewy pathology alone, and further understanding of the mechanistic link between Lewy pathology and neuronal death is needed.

2.1.2 Dementia with Lewy bodies (DLB)

DLB is another common neurodegenerative disorder that affects 7 % of the population above 65 years of age and 30 % of the population above 80 years of age[20]. It is the second most common cause of dementia after AD. Despite its impact on patients, it is not clear if DLB and PDD are distinct diseases with different underlying mechanisms or if they are clinical syndromes on a single mechanistic spectrum.

2.1.2.1 Clinical Hallmarks

The core clinical signs of DLB are fluctuating cognitive impairment, visual hallucinations and parkinsonism[21](Fig. 2.1). RBD was also added as one of the core clinical features in the most recent consensus criteria[22]. If dementia occurs concurrently or precedes parkinsonism within a year of the onset of parkinsonism, this is clinically diagnosed as DLB[23]. The sensitivity of clinical diagnosis is quite poor (12-32 %) but has high specificity (95 %)[24], which indicates that the significant number of DLB cases is missed, and the incidence of DLB is grossly underestimated. Furthermore, due to overlapping symp-

toms, DLB can be misdiagnosed with PDD. This results in inappropriate treatment, which imposes risk in DLB patients as some anti-parkinsonian treatments exacerbate neuropsychiatric symptoms[25]. Such risk stresses the importance of developing methods for the differential diagnosis of DLB and to better understand disease pathogenesis.

2.1.2.2 Neuropathological hallmarks

Similar to PD, DLB has a neuropathological feature of LBs, LNs and astroglial pathology (Figs. 2.2a-c). Also, the majority of DLB cases, but importantly not all, present a loss of dopaminergic neurons in the SNpc. Therefore, neuropathological differentiation between DLB, PDD and PD is impossible without any knowledge of the clinical information. However in DLB, Lewy pathology can be more predominant in the neocortex and limbic system compared to PD and often accompanied with concomitant AD-related challenges[26,27].

2.1.3 Multiple system atrophy (MSA)

2.1.3.1 Clinical hallmarks

Clinical features of MSA include parkinsonism, autonomic dysfunction, cerebellar dysfunction and additional motor and non-motor symptoms, including dystonia, RBD, and cognitive impairment (Fig. 2.1). Clinically, MSA is categorised into two primary motor phenotypes: the parkinsonian subtype (MSA-P) and the cerebellar subtype (MSA-C). Compared to PD and DLB, MSA disease progression is much faster and more aggressive, leading to death within ten years after symptom onset[28]. However, not all MSA patients follow a uniform clinical trajectory. Some patients can have prolonged disease duration longer than 15 years. Also, early autonomic failure has been associated with a worse prognosis in a USA cohort[29], but such correlation was absent in a Korean cohort[30]. Furthermore, in a European cohort, MSA-P showed faster disease progression than MSA-C[31], but in a USA cohort, MSA subtypes did not present such differences[29]. The mechanism behind the variability of clinical trajectories is unknown, but it demon-

strates the presence of diverse clinical subtypes of MSA.

The disease progression of MSA is commonly measured using a scale called, 'The Unified Multiple System Atrophy Rating Scale (UMSARS)'[32]. The gross assessment reflects patient history of disease-related impairments, motor and autonomic impairments, and global disability. The initial diagnosis of MSA can be challenging due to overlapping clinical features with PD. Especially due to the clinical overlap between MSA-P and PD, up to 10 % of MSA patients are misdiagnosed with PD[28]. In MSA-C, symptoms are difficult to distinguish from other cerebellar disorders, resulting in 30 % probability of patients with cerebellar ataxia having MSA. In order to stratify MSA from other synucleinopathies and diseases, neuropathological examination is essential.

2.1.3.2 Neuropathological hallmarks

MSA is associated with degenerating brain regions involved in autonomic function, including the cerebellum, pons and brainstem. The macroscopic changes are mostly seen either in the olivopontocerebellar system (MSA-C) or in the striatonigral system (MSA-P)[33]. MSA is characterised by cytoplasmic inclusions of filamentous αSyn aggregates in oligodendrocytes and neurons. Inclusions found in oligodendrocytes are defined as glial cytoplasmic inclusions (GCIs)[34] (Fig. 2.2d). GCIs are around 5–20 µm in diameter, surrounding the nucleus, with varied morphologies but very often this triangular or half-moon shape. Apart from CGIs, MSA is also characterised by some less prevalent neuronal aSyn aggregation. GCIs and neuronal inclusions are generally found in motor cortex, striatum, globus pallidus, pons and cerebellum[33].

2.2 α-Synuclein (αSyn)

2.2.1 Physiological αSyn

α-Synuclein (αSyn) is encoded by the *SNCA* gene located at position 21 on chromosome 4[35]. αSyn is a small protein composed of 140 amino acids (14.6 kDa) and its

primary sequence can be separated into three regions: N-terminus, the non-amyloid-β component (NAC) and the C-terminus[36,37] (Fig. 2.3a). The N-terminal domain (residues 1-60) is enriched with lysine and contains four repeats of the KTKEGV motif. This amphipathic region is essential for lipid binding[38]. The central domain (residues 61-95) is also known as the NAC domain, which is highly hydrophobic and essential for αSyn aggregation[39,40]. The C-terminus (residues 96-140) is rich in acidic amino acids and has an overall negative charge, allowing it to bind with different metal ions.

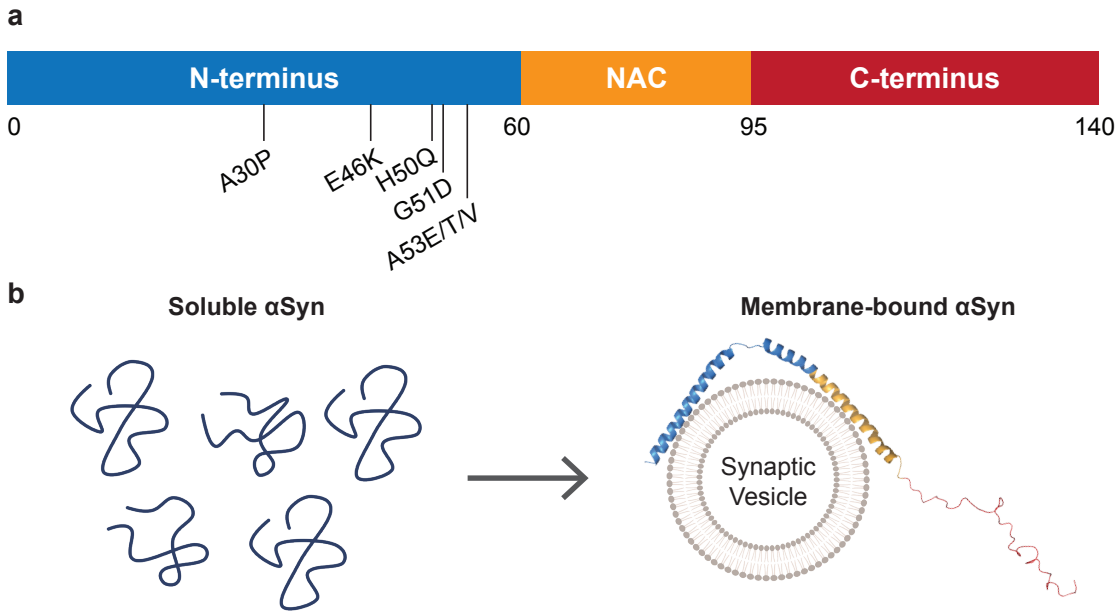

Figure 2.3 **Structure of αSyn monomer. a&b**, A schematic representation of the amino acid sequence of αSyn with its three main regions (**a**) and the disordered structures of αSyn in solution and the 3D tertiary structure when bound to a membrane (**b**). (**a**) The N-terminus contains the point mutations: A30P, E46K, H50Q, G51D, A53E, A53T, and A53V. (**b**) The 3D structure of the membrane-bound αSyn was generated using PyMOL[41] and PDB structure from Refs. [42,43].

In an aqueous solution, αSyn does not acquire a fixed three-dimensional structure (Fig. 2.3b). However, upon membrane and lipid binding, the amphipathic N-terminus and the NAC region form α-helices. These two regions are involved in binding to synaptic vesicles[44] (Fig. 2.3b). On the other hand, the C-terminus has high mobility and accessi-

bility. C-terminus truncation is commonly identified in normal and diseased brains[45].

Point mutations on αSyn associated with synucleinopathies are: A30P[46], E46K[47], H50Q[48], G51D[49], A53E[50], A53T[51], and A53V[52] (Fig. 2.3a). All mutations are on the N-terminal domain and do not have a significant impact on the structure of the monomeric αSyn except for A30P, which disrupts the wild-type (WT) regional α-helical structure[53]. Interestingly, these synucleinopathy-related point mutations do not significantly affect αSyn membrane association[54].

2.2.1.1 αSyn family

The synuclein family is made of three members: α, β, and γ-synucleins[55,56] (Fig. 2.4). The three synucleins are encoded by highly homologous genes where αSyn and β-synuclein (βSyn) themselves have higher sequence homology than γ-synuclein (γSyn). αSyn is the most abundant synuclein protein and βSyn provides a functional redundancy for dopamine level maintenance[57]. Likewise with αSyn, γSyn is involved in the cellular process for dopaminergic neuronal survival in the SNpc during development[58].

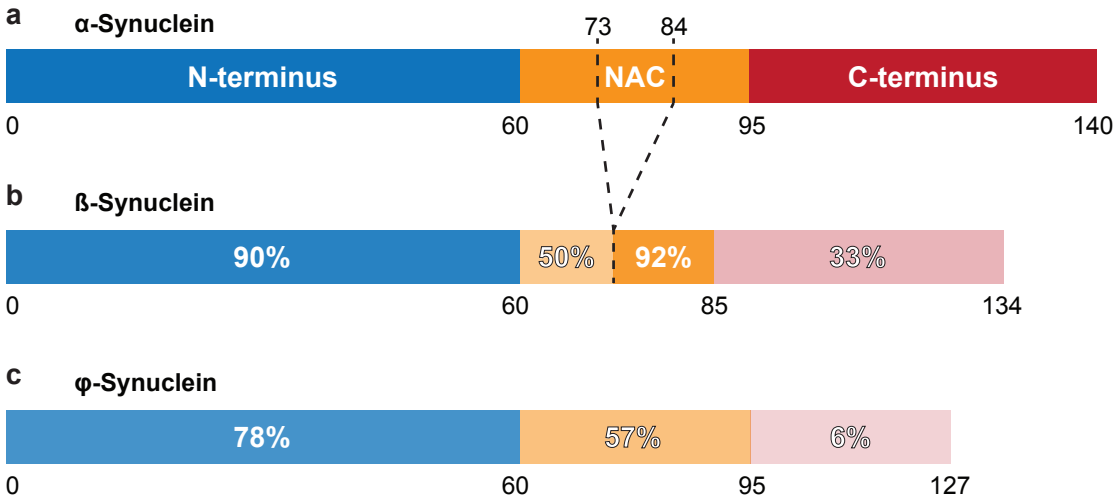

Figure 2.4 **αSyn family members. a-c**, Schematic representation of the amino acid sequences of αSyn (**a**), βSyn (**b**), and γ-Synuclein (**c**). (**b**) β-Synuclein missing the 73-84 NAC region sequence from αSyn. The sequence homology of each domain relative to αSyn is presented in percentages. Figure adapted from Ref. [59].

Unlike αSyn, βSyn lacks the major parts of the NAC region (Figs. 2.4a,b), which contributes to its inability to aggregate in physiological conditions. The NAC region of γSyn shares only 57 % sequence homology with αSyn (Fig. 2.4c). A study by Spillantini and colleagues identified αSyn, but not βSyn or γSyn, in LBs, which are the pathological hallmark of PD[60]. Furthermore, point mutations associated with synucleinopathies have not been observed in βSyn and γSyn[61] except for DLB, where two mutations on βSyn (V70M and P123H) have been found in sporadic and familial DLB patients, respectively[62].

Interestingly, βSyn and γSyn can inhibit αSyn fibrillation in vitro[63]. Another study showed that βSyn inhibits αSyn aggregation in transgenic mouse brain[64]. Furthermore, deletion of all three synucleins (αSyn, βSyn and γSyn) in a triple knockout (KO) mice resulted in neuronal dysfunction, changes in synaptic structure and reduced survival[65]. Both in vitro and in vivo studies suggest that the balance of the different synuclein levels may be critical for its physiological function in the brain.

2.2.1.2 Localisation and function

αSyn is produced and localised mainly in the central nervous system (CNS). It is located specifically in presynaptic terminals, reflecting its role involving synaptic vesicles[36,66].

The physiological function of αSyn has been studied with αSyn KO mice, which showed a significant reduction in both the reserve pool and docked synaptic vesicles and reduced striatal dopamine level[67,68]. Results indicate the role of αSyn in the maintenance, localisation and trafficking of synaptic vesicles. The N-terminus is especially important for this role because point mutations at the N-terminus disrupt αSyn association with synaptic vesicles[54].

Nevertheless, αSyn physiological function remains controversial, and it is difficult to define a specific function. However, studies point to its association with synaptic vesicles and regulation of neurotransmitter vesicle trafficking and life cycle[37,69]. As illustrated in Fig. 2.5, αSyn multimerises and forms a membrane-bound helical structure upon associ-

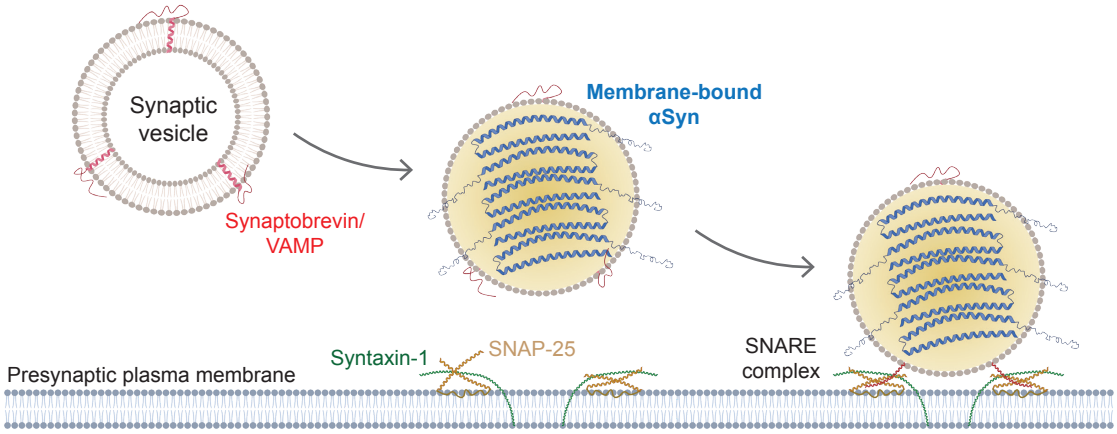

Figure 2.5 **Role of αSyn in the synaptic vesicle cycle.** Binding of αSyn multimers to the synaptic vesicles, together with synaptobrevin/VAMP chaperones, promotes the formation of the SNARE complex during the synaptic vesicle docking and fusion process.

ating with a synaptic vesicle. Then, αSyn acts as a chaperone, facilitating the formation of the SNARE-complex, a membrane fusion machinery crucial for neurotransmitter release at the synaptic terminal[70]. In dopaminergic neurons of αSyn knock-out mice, deletion of αSyn increased the refilling rate of the readily releasable pool (RRP) of dopaminergic vesicles and increased dopamine release[71]. On the other hand, mice with αSyn overexpression showed reduced dopamine release[72]. Although the mechanism of αSyn interaction and regulation of dopaminergic synaptic vesicles is unclear, the reported findings suggest a role of αSyn in dopaminergic neuronal function.

2.2.2 Pathological αSyn

2.2.2.1 Pathways to αSyn toxicity

The physiological function of αSyn is dependent on its cellular cycle of synthesis, aggregation, and degradation[73] (Fig. 2.6a). Imbalanced cycle caused by the dysfunction of the involved mechanisms can result in the misfolding, accumulation and aggregation of αSyn and its aggregation into oligomeric and fibrillar conformers that induce further cellular toxicity (Fig. 2.6b).

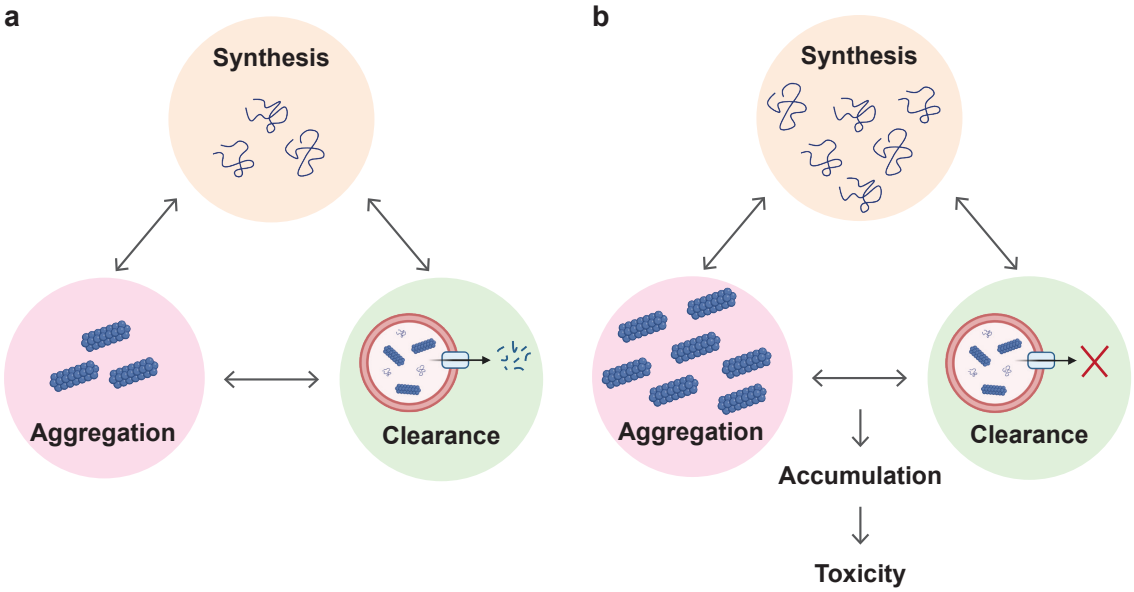

Figure 2.6 **Balance of intracellular αSyn. a&b**, Control of intracellular αSyn through a balance between the rate of synthesis, aggregation, and clearance mechanism (**a**) and dysregulation of each mechanism resulting in the accumulation of toxic αSyn species in synucleinopathies (**b**). Figure adapted from Ref. [73].

Imbalance is triggered by multiple mechanisms. For instance, multiplication of the *SNCA* gene in familial cases of PD increases αSyn expression, resulting in αSyn accumulation[74]. Also, a higher risk of PD from genetic point mutation of *SNCA* might be associated with increased αSyn protein expression[75]. In sporadic synucleinopathies, the αSyn mRNA levels remain unchanged, indicating that rather than protein expression, protein modifications or dysfunction of the clearance system may be associated with toxic αSyn. Indeed, impaired protein clearance mechanism plays a vital role in the pathogenesis of synucleinopathies. Clearance of αSyn occurs via various pathways, including proteolysis, chaperone-mediated, proteasome and autophagy[76]. Mutated and aggregated forms of αSyn were shown to disrupt chaperone-mediated autophagy, enhancing αSyn-mediated toxicity[77]. In addition, dysregulation of the key molecules of autophagy, such as ATG7 and mTOR, was reported in synucleinopathies[78]. Also, increased susceptibility of αSyn accumulation in lysosomal disorders such as Gaucher's disease highlights the connection

between dysfunctional protein clearance and αSyn toxicity[79].

2.2.2.2 αSyn aggregates

Impaired clearance of αSyn leads to accumulation and aggregation of αSyn. αSyn aggregation is a multi-step process as illustrated in Fig. 2.7. Aggregation begins with the misfolding of the monomeric protein, which then self-associates to form soluble oligomers. These oligomers can further aggregate to form protofibrils and, eventually, mature fibrils[80]. This process is believed to be a major contributing factor to the pathogenesis of synucleinopathies.

Oligomers are soluble, intermediate species formed early in the aggregation process. They are cylindrical in shape and can range in size from dimers to larger entities up to 560 kDa in molecular weight[81]. Therefore, oligomers exist as heterogeneous species that vary in size and resistance against protease degradation[82]. Oligomers are believed to be the most toxic species due to their ability to permeabilise cell membranes, leading to cell death[83,84].

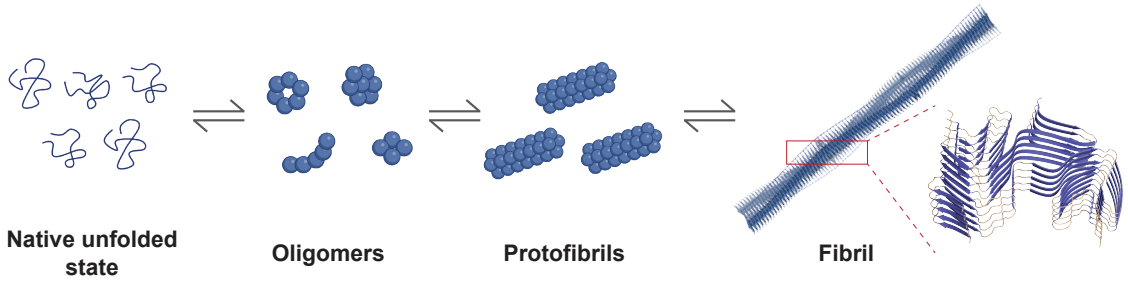

Figure 2.7 Conformational states of αSyn. Under physiological conditions, αSyn acquires a natively unfolded state. Certain environmental changes trigger αSyn organisation into soluble oligomers, which convert to β-sheet structures called protofibrils. Further elongation of the cross-linked β-sheet structures form highly structured and insoluble fibrils. The 3D structure of the αSyn β-sheets was generated using PyMOL[41] and PDB structure from Refs. [85,86].

In the early phase of fibril formation, relatively unstructured oligomers undergo structural reorganisation into fibrils rich in β-sheets (Fig.2.7). Fibrils are insoluble and elongated structures found in LB inclusions[60]. Fibrils are less toxic than oligomers but can

contribute to cell death by disrupting cellular processes, including the clearance mechanisms, causing further toxicity[73]. Also, fibrils can disaggregate into oligomers, suggesting a vicious cycle of αSyn aggregates involved in neurodegeneration that exacerbates αSyn toxicity[82].

2.3 αSyn strains

2.3.1 αSyn strain hypothesis

Extensive experimental evidence highlights the prion-like characteristics of αSyn aggregates. A well-characterised prion-like property of αSyn is the ability of αSyn misfolded species to induce aggregation of endogenous αSyn in vitro[63,87,88]. Another prion-like property is the ability of αSyn species to spread from one cell to another both in vitro and in vivo[89–91]. As a result, injection of synthetic αSyn fibrils into WT mice brains causes the spread of αSyn inclusions throughout the brain[92]. Nevertheless, it must be noted that although the prion-like spread of αSyn pathology was observed in mice, consequent neuronal loss or PD-like symptoms were absent[92,93]. Similar spreading of αSyn has also been suggested in host-to-graft spread of LB pathology in the human brain[94,95]. Yet, the Lewy pathology found in grafted neurons could have been caused by the microenvironment of the PD brain, such as inflammation, rather than the physical spread of αSyn seeds to the healthy neurons.

αSyn aggregates reflect many properties of prion, and emerging evidence suggests the existence of αSyn strains, similar to prion strains. Prion strains represent distinct conformations of aggregated αSyn, similar to prion strains in prion diseases. Prion strains are distinct infectious prion species that induce distinguishable disease phenotypes upon transmitting an identical host[96]. Thus, prion strains are defined by their transmission properties, such as incubation time and pathological profile. An additional indicator of prion strains includes conformational variants, proteinase-K digestion (biochemical) and glycosylation ratios. Whether the conformational and biochemical indicators reflect the

biological profiles of strains remains unclear. However, these indicators provide evidence of distinct strains and correlate with different disease phenotypes.

Hence, the study of αSyn strains is paramount as they can offer a molecular perspective into the diverse clinical and pathological manifestations observed across synucleinopathies (Fig. 2.8). Notably, different αSyn strains have been proposed to underlie the heterogeneity in disease phenotypes among patients with conditions such as PD, DLB and MSA[85]. Understanding the structural and functional properties of these strains could reveal deeper insights into disease mechanisms and therapeutic interventions.

Prions and prion-like proteins, including αSyn aggregate into conformational variants with distinguishable properties, which are used to characterise strains. Bousset and colleagues first characterised αSyn strains by generating in vitro αSyn aggregates using recombinant αSyn with distinct conformations called 'ribbons' and 'fibrils'[97]. The two polymorphs displayed distinguishable biochemical, structural and cytotoxic properties. Most importantly, 'ribbons' and 'fibrils' spread like prion strains in vitro as they propagated by recruiting soluble αSyn and establishing an assembly that inscribes their intrinsic biochemical and conformational properties. Thus, as the finding suggests, αSyn 'strains' are more than just structural polymorphs.

Since the first characterisation of αSyn strains, studies have reported additional indicators of αSyn strains. For example, different in vitro αSyn fibrils have shown differential interaction with the plasma membranes[98,99]. Further investigation on the fibrillar morphology[100], propagation patterns[101,102], and nanochemical properties[103] provided profound insight into the αSyn strains.

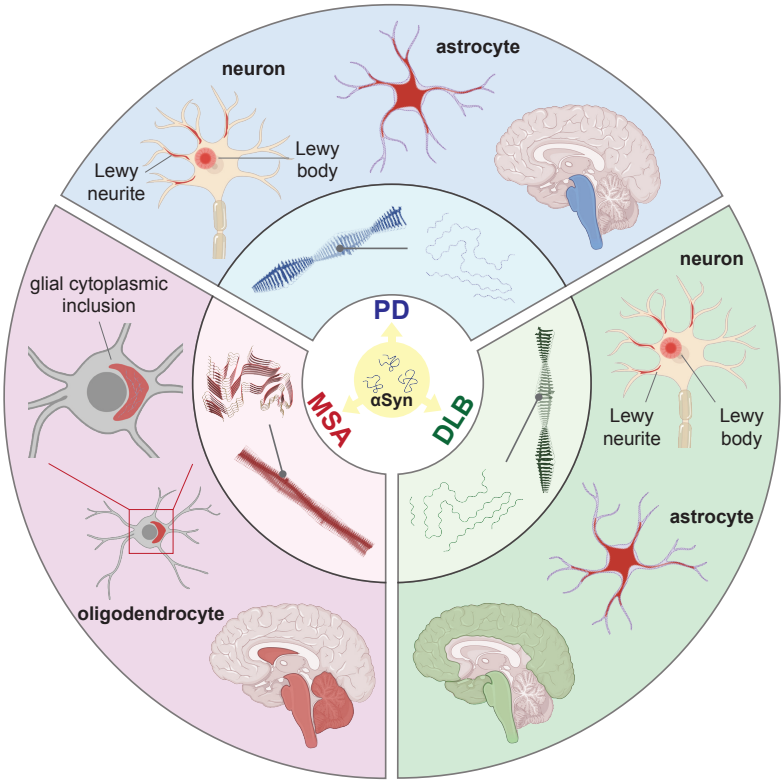

Figure 2.8 **αSyn strain hypothesis.** Distinct αSyn strains are associated with different neuropathological and clinical hallmarks of PD, DLB, and MSA. αSyn misfolds and aggregates into fibrils with distinct conformations. At the atomic level, PD and DLB strains share a 'Lewy fold' structure at the fibrillar core and comprise a single protofilament[104]. MSA strains are twisted with two protofilaments intertwined, forming a different core structure to the 'Lewy fold' [85]. At a cellular level, PD is characterised by significant neuronal loss at the brainstem, especially the SN, and the limbic region, highlighted in blue. LBs and LNs accumulate in neurons. αSyn also accumulates in astrocytes, forming astroglial pathology. In DLB, the brainstem, limbic and neocortex are all affected regions, highlighted in green. Here, LB and LN accumulate in neurons and astroglial pathology is also observed. In MSA, the cerebellum, basal ganglia and brainstem are the most affected, highlighted in red. Here, αSyn accumulates in the form of GCIs in the oligodendrocytes. SN: substantia nigra, LB: Lewy body, LN: Lewy neurite, GCI: glial cytoplasmic inclusion. The 3D structures of the αSyn fibrillar cores were generated using PyMOL[41], and the PDB structures from Refs. [85, 86, 104, 105]. Figure adapted from Ref. [106].

2.3.2 Evidence of αSyn strains in human brains of different synucleinopathies

Investigating human brain-derived αSyn fibrils is imperative to understanding αSyn strains and their role in synucleinopathies. While fibrils are an endpoint product of a disease, they nonetheless offer invaluable insights into the disease mechanism and the molecular underpinnings that differentiate various synucleinopathies. Furthermore, the meticulous characterisation of these strains may facilitate the development of diagnostic biomarkers and preventative interventions for fibril formation.

2.3.2.1 Morphological evidence

One of the pioneering efforts to isolate and characterise αSyn fibrils from human brains was undertaken by Spillantini and colleagues in 1998[13,107]. Utilising sequential extraction with the detergent sarkosyl, the team isolated αSyn fibrils from DLB and MSA brains and employed immunogold transmission electron microscopy (TEM) for morphological characterisation.

In the DLB brain's cingulate cortex, fibrils were prominently labelled with the PER4 antibody, targeting the αSyn C-terminus[107]. These long and single fibrils predominantly exhibited lengths ranging from 50-700 nm. Various morphologies were observed, including twisted fibrils of alternating widths (5 and 10 nm) and 90 nm twist periodicity. Interestingly, paired helical fibrils with pronounced twists were non-reactive to PER4. On the other hand, PER4 identified both twisted and straight fibrils from MSA brains[13]. The differential labelling patterns of PER4 suggest potential conformational differences between the DLB and MSA brain-derived αSyn fibrils.

Table 2.2 Summary of immunogold TEM studies of brain-derived αSyn fibrils.

Ref	Disease	Brain region	Fibril structure	Measurements
108	PD/PDD	Substantia nigra	Single and straight	Length: 200-600 nm Width: 5-10 nm
107	DLB	Cingulate	Single and twisted	Length: 50-700 nm Single fibril width: 5-10 nm Twisted fibril width: 5 and 10 nm Periodicity: 90 nm
13	MSA	Frontal cortex Cerebellum	Straight and twisted	Length: 50-1000 nm Straight fibril width: 10 nm Twisted fibril width: 5 and 18 nm Periodicity: 70-90 nm

Comparative analysis of αSyn fibrils from PD, DLB, and MSA brains revealed significant morphological differences, particularly in fibril length[13,107,108], as summarised in Table 2.2. The fibril widths varied, with PD and DLB fibrils ranging between 5 and 10 nm, while MSA fibrils consistently measured 10 nm. Also, both DLB and MSA fibrils exhibited a mix of straight and twisted structures, while the PD fibrils were predominantly straight and comprised of singular filaments. The early imaging studies of the brain-derived αSyn fibrils with antibody labelling provided an understanding of the morphological heterogeneity of fibrils and indication of distinct αSyn strains in different synucleinopathies.

2.3.2.2 Cryo-EM structural evidence

More recently, cryo-EM enabled in-depth analysis of the human-derived αSyn fibrils at the atomic level. Schweighauser and colleagues extracted sarkosyl insoluble αSyn fibrils from the putamen of MSA brains and obtained a high-resolution atomic model of MSA αSyn fibrils for the first time[85]. Two types of fibrils were identified, denoted as

types I and II, with each fibril type constituted of two distinct protofilaments (PF-IA/B and PF-IIA/B(1-2)) (Fig. 2.9). Each protofilament differs in the core residues, resulting in a different number of β-strands. Also, the packing and folding of the fibrillar core are different, resulting in conformational variability between the two types of fibrils. In addition, a few post-translational modifications (PTMs) were also identified. For instance, the ubiquitination of K80, a bulky modification, was spacious for PF-IIA but less compatible with PF-IA, PF-IB, and PF-IIB. The phosphorylation of T72 was more predominant in PF-IIA, and the position of the phosphorylation of T81 was different between PF-IIB1 and PF-IIB2. The study suggests that αSyn fibrils, even from a single disease (MSA), have structural differences at the atomic level, and the PTMs can add further variation.

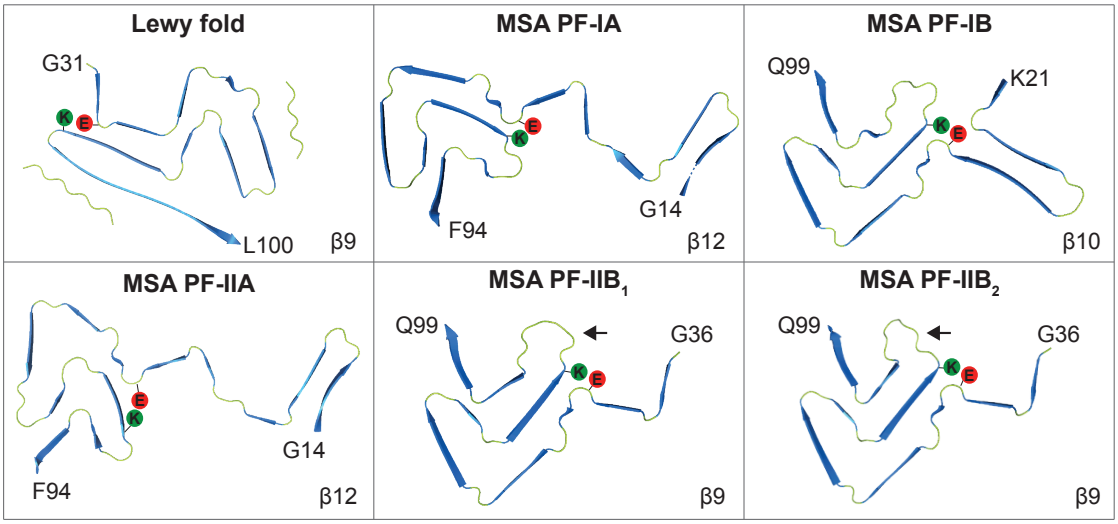

Figure 2.9 **Cryo-EM structures of brain-derived αSyn fibrils.** Secondary structures of the core of the αSyn fibrils extracted from PD/PDD, DLB, and MSA brains. PD/PDD and DLB brain-derived fibrils share a Lewy fold structure. The Lewy fold has 9 β-strands and a salt bridge between E35 (red) and K80 (green). MSA brain-derived fibrils comprise five protofilaments (PF-IA, IB, IIA, IIB1, IIB2). Each protofilament has 12, 10, 12, 9, and 9 β-strands, respectively and salt bridges between E46 (red) and K80 (green). MSA PF-IIB1 and PF-IIB2 have identical structures, except for the loop indicated by the black arrow. The β-strands are highlighted in blue. The secondary structures were generated using PyMOL[41] and PDB structures from Refs. [85, 86, 104, 105].

cryo-EM study has revealed a striking difference in the atomic structure of αSyn fibrils derived from PD, PDD and DLB compared to the MSA brains[104]. Interestingly, the αSyn fibrils from PD, PDD and DLB brains were composed of a single identical protofilament termed 'Lewy fold' (Fig. 2.9). Most of the fibrils were untwisted, and minor twisted fibrils had right-handed twists, whereas the MSA fibrils showed left-handed twists. Furthermore, different residues formed the salt bridge within the protofilament, where residues E35-K80 in Lewy fold and E46-K80 in MSA were involved. Differences in PTMs were also observed. Some MSA fibrils contained phosphorylation of Y39, which was absent in the Lewy fold fibrils. Atomic structures revealed characteristic structures and modifications of different αSyn fibrils, which added further evidence towards the existence of αSyn strains in synucleinopathies.

Nevertheless, the limitations of the cryo-EM studies must be noted. The complex sample preparation and image processing limit the observation of a wider fibril population in the brain. Such technical complications could limit the analysis of many samples, which is critical to understanding the structural heterogeneity of brain-derived αSyn fibrils in different patients. Yang and colleagues only included a single PD brain, two PDD and three DLB brains in their report[104]. Further structural characterisation of LBD brain-derived αSyn fibrils is essential to validate the findings. In addition, it is necessary to investigate different pathologically relevant brain regions (such as the substantia nigra, which was not investigated[104]). This might uncover potential structural differences among fibrils extracted from different brain regions. Also, exploring the correlation between the fibril structures and disease phenotypes would provide stronger evidence of αSyn strains.

2.3.2.3 Biochemical evidence

Resistance against protease (proteinase-K, PK) digestion and conformational stability are useful indicators of αSyn strains. PK cleaves non-specifically, digesting the flexible and accessible regions of αSyn fibril. Therefore, the PK-resistant fragments of the fibril, analysed with immunoblotting as illustrated in Fig. 2.10, can be utilised to understand

the fibrillar structure, especially the hydrophobic core. Furthermore, using a denaturant guanidine-hydrochloride (Gdn-HCl), it is possible to assess the conformational stability of the fibrils by examining their degree of resistance against denaturation.

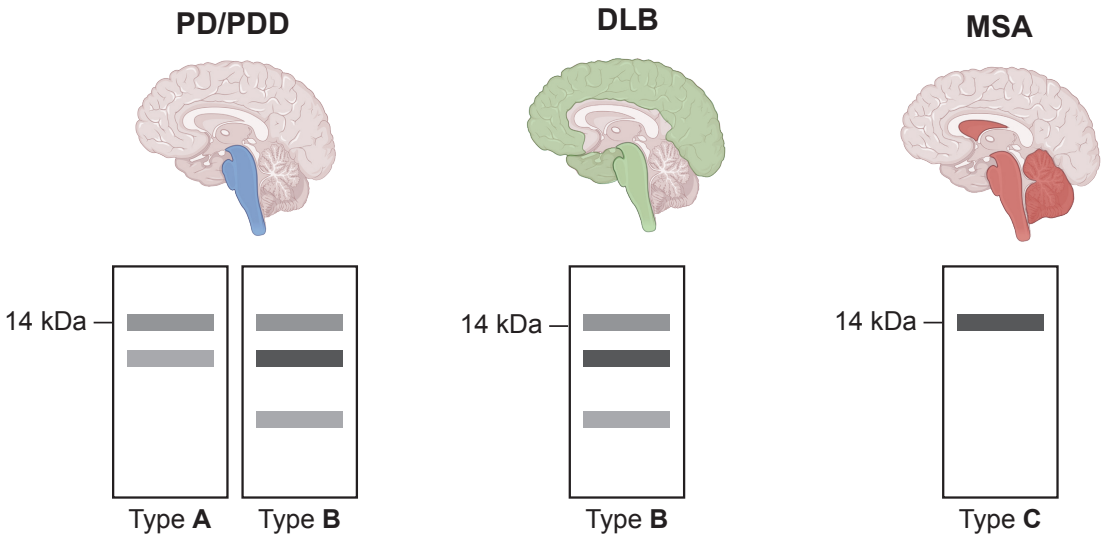

Figure 2.10 Distinct biochemical profiles of brain-derived αSyn fibrils from different synucleinopathies. Hypothetical immunoblot illustrations of the PK-resistant αSyn fibrils from PD, DLB, and MSA brains. Two studies[109,110] reported two distinct PK-resistance profiles of αSyn fibrils: types A and B. One study[110] also reported the common type B profile in αSyn fibrils from DLB brains and showed high PK-resistance of αSyn fibrils from MSA brains, represented by type C profile.

αSyn fibrils from different synucleinopathies have been characterised using PK and Gdn-HCl[109,110]. For example, Peng and colleagues demonstrated that MSA brain-derived αSyn fibrils are more PK-resistant than LBDs (Fig. 2.10)[110]. On the other hand, MSA αSyn was less conformationally stable and more prone to Gnd-HCl denaturation compared to DLB αSyn[92]. Also, distinct PK-resistant fragments were observed among different PDD cases (Fig. 2.10), indicating divergent αSyn fibril conformations between individuals of the same disease[109]. In human prion diseases, distinct biochemical profiles of prions correlate with different disease phenotypes[96]. Similarly, additional correlative study between the biochemical signatures of αSyn fibrils and disease phenotypes might offer compelling evidence of αSyn strains.

2.3.2.4 Evidence from αSyn seeding behaviour

Differential αSyn seeding kinetics across synucleinopathies has further reinforced the notion of distinct αSyn strains. 'Seeding' indicates the ability of pathological αSyn species to act as proteinaceous nuclei (seeds) capable of self-templated propagation. This intrinsic property has been translated into an in vitro amplification technology called the seed amplification assay (SAA), which has become instrumental in the investigation of αSyn strains (discussed in Section 2.4.1).

Studies demonstrated distinguishable αSyn seeding activities of CSF from PD and MSA patients, where the PD CSF showed higher seeding capacity than MSA[111,112]. A similar pattern of αSyn seeding activity was observed between the CSF from MSA and LBDs[113]. Such αSyn seeding signatures of biosamples from patients with different synucleinopathies support the notion that these diseases are associated with distinct αSyn strains.

An intriguing in vitro study using recombinant αSyn has unveiled the existence of a specific αSyn strain that escapes detection by Thioflavin-T (ThT), a commonly used fluorophore in the SAA, to monitor aggregation in real-time[114]. The distinct seeding kinetics in MSA biosamples could be related to these ThT-escaping αSyn conformers. These conformers, representing a distinct subset of αSyn strains, are detected using alternative fluorophores, such as SYBR-green or luminescent conjugated oligothiophenes (LCOs). Findings highlight the vast heterogeneity of αSyn strains and conformers, emphasising the continual evolution of methodologies for their characterisation.

Consequently, a multifaceted approach is essential to capture the complexity and diversity of αSyn fibrils. The aforementioned studies have employed αSyn-specific antibodies, imaging and biochemical techniques, and seeding assays to improve the understanding of αSyn fibrils. Nevertheless, systematic investigation of human brain-derived αSyn fibrils from different synucleinopathies is still limited. Such examination is necessary to characterise human disease-relevant αSyn strains of different synucleinopathies

and divergent disease phenotypes.

2.3.3 Evidence of strains among in vitro-seeded αSyn fibrils

In vitro-seeded αSyn fibrils represent a distinct category of αSyn conformers, diverging from both synthetic and human-derived fibrils. These αSyn fibrils are generated through templated aggregation using the SAA, where human-derived pathological αSyn species (seed) act as templates to promote the aggregation of recombinant monomeric αSyn. Theoretically, the resulting in vitro-seeded fibrils (SAA fibrils) are biological replicates of the human-derived αSyn seeds. Details of the SAA mechanism are outlined in Section 2.4.1. The SAA fibrils are pure and enriched with αSyn fibrils, overcoming the limitations associated with human-derived fibrils or even brain homogenates. However, it is crucial to note that these strains do not entirely replicate the human-derived strains in the atomic structural level[115]. Despite this limitation, they have provided new insights into αSyn strains and their role in synucleinopathies.

Structural characterisation has played a principal role in understanding the SAA αSyn fibrils. While PD-SAA fibrils presented diverse structures, MSA-SAA fibrils manifested a more consistent morphology[116]. Specifically, both PD and MSA-SAA fibrils adopted flat and twisted conformations, in contrast to the cylindrical, non-twisted architecture of DLB-SAA fibrils[117]. Advanced tomographic techniques further revealed that PD and MSA-SAA fibrils consist of two intertwined protofilaments with left-handed helical twists[111].

In addition, the SAA αSyn fibrils from different synucleinopathies exhibit distinct pathogenicity in vitro and in vivo. When seeded into primary neurons, PD and MSA-SAA fibrils induced neuritic or punctate phosphorylated αSyn (pαSyn) deposition, while DLB-SAA fibrils predominantly cause somal deposits[117]. In human induced pluripotent stem cell (hiPSCs) derived dopaminergic neurons, PD and MSA-SAA fibrils generate unique pαSyn pathologies, with MSA-SAA fibrils forming shorter neuritic aggregates compared to the longer aggregates by PD-SAA fibrils[118]. MSA-SAA fibrils also stim-

ulated a heightened inflammatory response in SH-SY5Y cells and were notably more potent in inducing phosphorylated αSyn (p-αSyn) pathology and motor deficits in rats, demonstrating higher toxicity than PD-SAA fibrils[117,119]. However, the MSA oligodendrocyte inclusions were absent consistent with previous reports[110,120,121]. In comparison, DLB-SAA fibrils were the least potent. These findings resonate with the characteristics of human-derived fibrils, where MSA-SAA fibrils are the most pathogenic. In contrast, PD and DLB-SAA fibrils were less pathogenic in vitro and in vivo. These insights underscore the utility of the SAA fibrils in discovering evidence of distinct αSyn strains across different synucleinopathies.

2.3.3.1 Human brain-derived versus in vitro-seeded αSyn fibrils

Before concluding on αSyn strains based on the investigation of the SAA fibrils, a fundamental question must be addressed: Are SAA fibrils representative models of the human-derived fibrils? High-resolution atomic structures highlight the striking differences between the human brain-derived and SAA αSyn fibrils. MSA brain-derived fibrils were used to seed the amplification of the corresponding SAA fibril to compare the structures[115]. Unlike the brain-derived, the SAA fibrils consist of a single protofilament with 9 β-strands. Also, K58 forms a salt bridge with an opposing protofilament in the brain-derived fibril. However, K58 is inverted towards the fibrillar core in the SAA fibril, as illustrated in Fig. 2.11a. Apart from these differences, the core structure between the MSA brain-derived and SAA fibrils overlay significantly.

Besides brain homogenates, cerebrospinal fluid (CSF) is a widely used seed for SAA as CSF contains seeding-competent αSyn species and can be taken from living patients. Figure 2.11b illustrates the core structure of the SAA fibril seeded with PD CSF[123]. The fibril's core overlays poorly with the brain-derived Lewy fold. The brain-derived versus the CSF-seeded fibrils may be incomparable due to different seed sources. However, the comparison highlights the limitation of the CSF-seeded SAA fibrils in reflecting the structure of the pathological fibrils in the brain. Also, such differences must be regarded

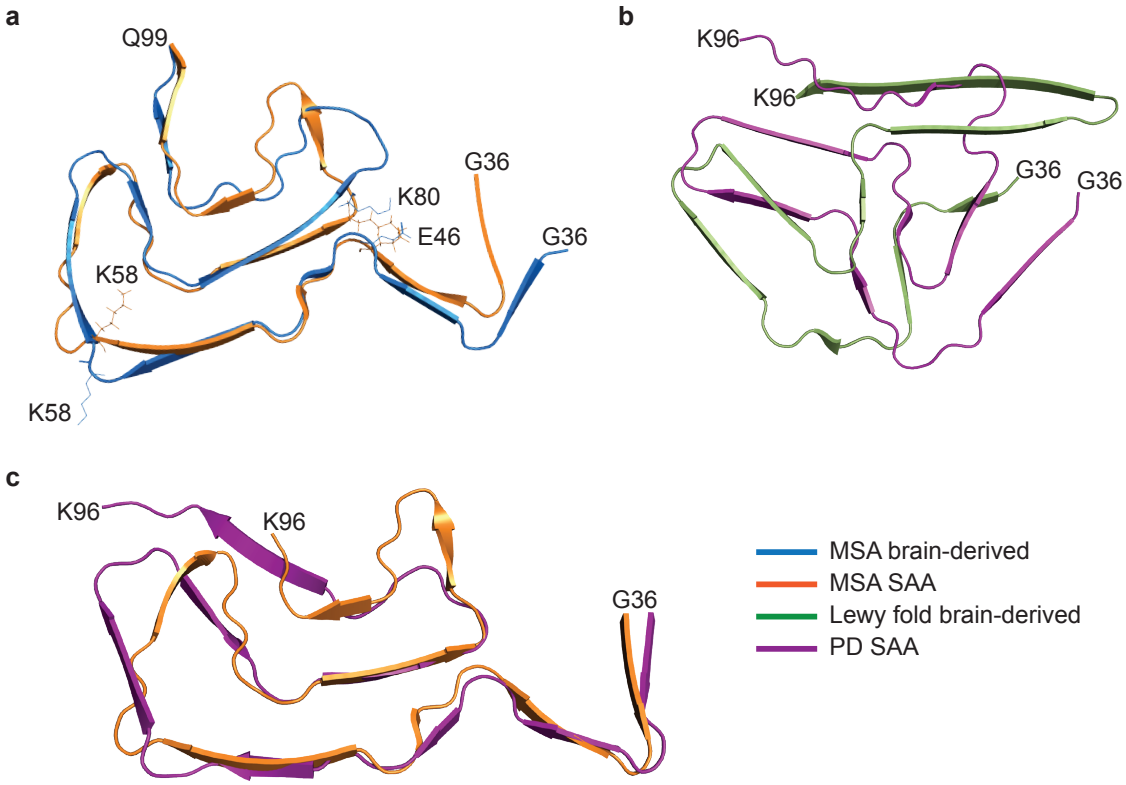

Figure 2.11 **Structural comparison of the brain-derived and SAA αSyn fibrils. a-c**, Overlay of the secondary structures of the cores of αSyn fibrils between MSA PF-IIB (blue) and MSA-SAA fibril (orange) (**a**), Lewy fold (green) and PD-SAA fibril (purple) (**b**), and MSA-SAA (blue) and PD-SAA fibril (purple) (**c**). (**a**) Residue K58 is inverted towards the fibrillar core in the SAA fibril. The secondary structures were generated using PyMOL[41] and PDB structures from Refs. [85, 86, 104, 105, 115, 122–124].

when investigating the αSyn fibrils and strains in living patients using the SAA fibrils seeded with patient biosamples.

Interestingly, one of the polymorphs of the PD CSF-seeded SAA fibril demonstrates a more significant similarity to the MSA brain-seeded SAA fibril, as seen in the overlay in Fig. 2.11c. Both fibrils comprise a single protofilament core with 8 β-strands. After second-generation seeded aggregation of the MSA-SAA fibrils, the structure of the SAA fibrils was conserved[115]. This suggests that the seed population and purity may affect

the templated propagation of the seed structure. Human-derived biosamples are complex fluids with unknown seed concentrations. In such an environment, buffer-dependent amplification might occur instead of templated aggregation by the seed. This mechanism might explain how the SAA fibrils seeded with different bio-fluids from distinct synucleinopathies share structural similarities.

To advance αSyn strain research, it is also crucial to compare other indicators of strain, such as biochemical and pathological properties. Understanding the gap between the αSyn fibrils from human and in vitro will allow the development of methods to generate αSyn fibrils in vitro that encompass the various properties of the human-derived fibrils. This will facilitate the development of improved models and advance the molecular understanding of synucleinopathies.

2.4 Biomarker for synucleinopathies

2.4.1 Seed amplification assay (SAA)

Seed Amplification Assay (SAA) is a powerful tool for studying neurodegenerative diseases characterised by protein aggregation. The core principle of SAA is detecting and amplifying minute amounts of misfolded protein seeds, enabling early-stage identification in human biosamples and amplifying SAA fibrils for downstream research.

The ability of SAA to detect seeding-competent αSyn aggregates in the biosamples from living patients enabled it to develop into a promising tool for biomarker discovery in synucleinopathies[125]. A biomarker, or biological marker, is a measurable indicator of some biological state or condition[126]. There is a vital unmet need for biologically relevant biomarkers for all neurodegenerative diseases, including synucleinopathies. Biomarkers facilitate early diagnosis and enable the monitoring of disease progression, stratification of patients into correct clinical trials and analysis of the efficacy of therapeutic interventions. Given the often insidious onset and progression of synucleinopathies, biomarkers offer multifaceted functions from symptomatic treatment to early intervention[127].

2.4.1.1 Principles of αSyn SAA

The αSyn SAA is based on seeded polymerisation, a process also seen in prion diseases[128]. As outlined in Fig. 2.12a, pathological αSyn, also known as "seeds", are added to a solution of buffer containing the following: monomeric recombinant αSyn, an amyloid dye ThT, and reaction buffer. The seeds can be derived from various human biofluids such as CSF[125], brain homogenate[129], olfactory mucosa[130], skin[131], blood[132] and saliva[133]. The mixture of seeds and monomeric recombinant αSyn in the reaction buffer is then incubated under specific conditions of temperature and shaking to allow for the seeded aggregation process to occur (Fig. 2.12b). This process is typically monitored in real time using a ThT fluorophore. ThT emits fluorescence upon association with the β-amyloid structures in the amplifying fibrils. The final readout of the assay is a non-linear sigmoidal fluorescence curve, which reflects the seeding activity of the αSyn aggregates present in the original seeds. Kinetic values can be extracted from the fluorescence curves to perform a quantitative analysis of the SAA reaction. It is crucial to note that the assay's performance is influenced by various factors, including the source and concentration of monomeric recombinant αSyn and seeds, the reaction conditions (e.g., temperature, pH, salt), and the presence of other molecules that can interact with αSyn (e.g., lipids, metals)[134].

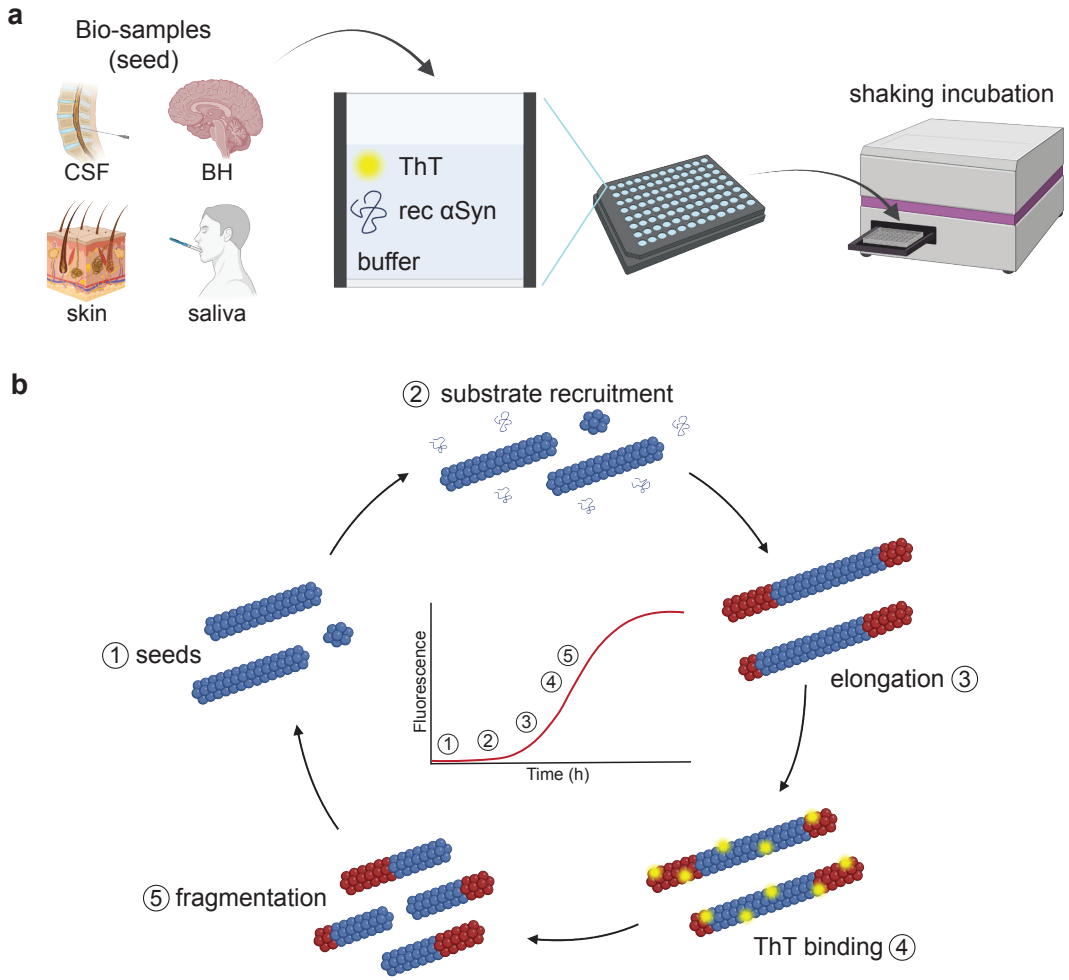

Figure 2.12 **αSyn SAA mechanism.** **a**, A biosample of interest (seed) is added to a reaction mixture containing ThT, monomeric recombinant αSyn (substrate, rec αSyn), and reaction buffer. The reaction mixture is loaded onto a 96-well plate, which is inserted into a plate reader. Samples are incubated with cycles of shaking, and fluorescence is measured throughout the reaction in real time. **b**, αSyn seeds in biosamples recruit substrates and induce elongation and amplification of new αSyn fibrils. ThT fluorophore (yellow) binds to the growing β-amyloid structures in the amplifying fibrils and emits fluorescence. Fibrils fragment during shaking and seeds further aggregation. These cycles are repeated, resulting in an exponential amplification of fibrils, reflected by the exponential rise of fluorescence emitted by ThT.

The resulting sigmoidal curve of positive αSyn SAA reaction embeds different kinetic parameters: Area under the curve (AUC), lag phase, time to reach 50 % of the maximum fluorescence (T_{50}), maximum fluorescence (F_{MAX}), and maximum velocity (V_{MAX})[135] (Fig. 2.13). The kinetic parameters provide an understanding of the various properties of the αSyn seeds, as described in Table 2.3. The quantitative values of these parameters are used to characterise αSyn strains and correlate with clinical measures, highlighting its potential as a differential diagnostic and progression biomarker.

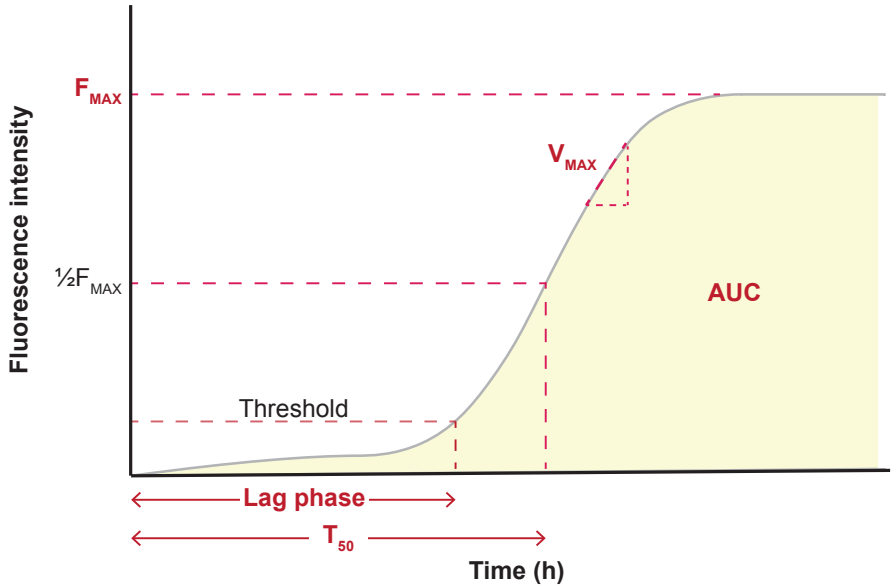

Figure 2.13 **αSyn SAA kinetic parameters.** Kinetics parameters from a αSyn SAA reaction curve. The grey curve represents an example sigmoidal curve of a positive SAA reaction. The highlighted region in yellow indicates the area under the curve (AUC). The lag phase is the time taken to reach the threshold, which ranges from 3-5 standard deviations from the minimum fluorescence. F_{MAX} is the maximum fluorescence. V_{MAX} is the maximum velocity, measured at the maximum slope on the fluorescence curve. T_{50} is the time taken to reach the 50 % of F_{MAX}.

Table 2.3 **αSyn SAA kinetics parameters.**

Parameter	Definition	Significance
AUC	Total area under the curve, representing the cumulative aggregation of αSyn over time.	Provides a holistic measure of the aggregation and used to compare the overall aggregation propensity.
Lag phase	Time taken to reach the threshold.	A shorter lag phase indicates a faster seeding kinetic.
T_{50}	Time required for the fluorescence to reach 50% of F_{MAX}.	A shorter T_{50} indicates a faster rate of aggregation, suggesting higher seeding activity.
F_{MAX}	The highest fluorescence intensity value reached during the assay.	The maximum amount of aggregated αSyn in the sample.
V_{MAX}	The maximum rate the fluorescence intensity increases, representing the steepest slope on the curve.	A higher V_{MAX} indicates a faster aggregation rate, suggesting higher seeding activity.

2.4.1.2 Diagnostic value of αSyn SAA

Extensive effort has been dedicated to optimising a diagnostic αSyn SAA as a diagnostic biomarker for synucleinopathies. The first study of αSyn SAA on synucleinopathies was performed by Fairfoul and colleagues, who successfully detected αSyn aggregation in the CSF of 99 pathologically confirmed patients and demonstrated 93 % overall sensitivity and 100 % specificity for PD and DLB[125]. All patients with pure AD pathology and a few cases that had atypical parkinsonism, such as PSP and CBD, were negative. Since then, numerous studies have reported results of robust αSyn SAA detecting synucleinopathies in CSF with sensitivity and specificity up to 98 % and 100 %, respectively[112,113,136,137].

Subsequently, studies further optimised αSyn SAA for differential diagnosis of

synucleinopathies. αSyn seeds in the CSF of MSA patients demonstrated significantly lower seeding activity than those of LBD patients[111–113]. Furthermore, when the wild-type (WT) αSyn SAA substrate was replaced with a C-terminally truncated αSyn monomer (1-130), PD showed more aggressive seeding than that of DLB[138]. An improved understanding of the SAA's seeding mechanism and quantitative readout might enable maximisation of the differential diagnostic potential of αSyn SAA.

In addition to differential diagnosis, early-stage disease detection is crucial for synucleinopathies. A high turn-over rate from RBD to PD suggests testing αSyn SAA in RBD patients could aid the early clinical diagnosis of PD. Isolated RBD (iRBD) refers to RBD without signs of neurological failure. The sensitivity of CSF αSyn SAA for iRBD varies from 75 % to 100 %[112,113,139–141]. Poggiolini and colleagues reported an overall 90 % sensitivity in four different iRBD cohorts combined, but a single cohort (DeNovo Parkinson Cohort (DeNoPa)) with 18 patients resulted in only 39 % sensitivity. Such difference was explained by earlier diagnosis and enrollment of iRBD patients than other cohorts. Positive αSyn seeding activity in iRBD patients has been observed using less invasive biosamples such as skin[131,142] and olfactory mucosa[143]. Although further optimisation is required for its translation into the clinic, studies illustrate the diagnostic potential of αSyn SAA for synucleinopathies even at the early prodromal stage, applying non-invasive interventions.

2.4.1.3 αSyn SAA and clinical measures

Monitoring disease progression is another essential biomarker function that is required. As a result, some studies have explored the correlation between αSyn SAA kinetic parameters and patient clinical measures. Clinical measures of synucleinopathies include the UPDRS scale, MMSE, H&Y scale and MoCA, which are described in detail in Section 2.1. Although these studies could distinguish the LBDs from MSA using the SAA kinetic parameters, they failed to identify any correlation with the clinical measures[112,113,144,145]. In contrast, only one study found a correlation between the H&Y

scale and T_{50} in 75 PD patients[146]. Moreover, motor deficit (MDS-UPDRS) had an inverse correlation with F_{MAX} and AUC in PD[145] and iRBD patients[112]. Among iRBD patients, moderate associations existed for higher V_{MAX} with worse MMSE scores[112]. Also, T_{50} was significantly lower in patients with probable RBD than non-RBD[145].

More recently, a study with the Parkinson's Progression Markers Initiative (PPMI) cohort reported findings on the association of αSyn SAA parameters with different clinical and genetic subtypes of PD[147]. *LRRK2*-PD group with negative SAA had lower MDS-UPDRS II scores and mild motor impairments (MDS-UPDRS III). Also, patients with *GBA*-PD had the highest proportion of positive SAA tests, followed by patients with sporadic and *LRRK2*-PD with the lowest. This finding builds evidence on how the αSyn SAA parameters could be associated with clinical heterogeneity and genetic subtypes of PD.

2.4.1.4 Limitations of αSyn SAA

Several fundamental challenges hinder the advancement of αSyn SAA. First, different laboratories developed diverse methods for αSyn SAA, limiting direct comparison of studies. To address this issue, three independent laboratories performed αSyn SAA according to their unique protocol using an identical cohort[148]. Interestingly, the SAA results were comparable between the laboratories, confirming the reproducibility of the assay despite the variations in the methods. Nevertheless, differences existed in sensitivity and specificity, ranging from 86-96 % and 93-100 %, respectively.

Next, the reproducibility of αSyn SAA is a greatly overlooked subject in this field. A study by Poggiolini and colleagues has been one of the very few that have assessed and reported reproducibility of their CSF αSyn SAA using different batches of recombinant αSyn[112]. Although two different batches did not seem to affect overall sensitivity and specificity, they did affect the SAA kinetics. Thus, the assay performance is highly dependent on the recombinant αSyn and currently, there is no consensus on methods on how to test its optimal function except testing it in the assay itself. How the recombinant protein affects the assay outcome must be better understood before the SAA can be used

in the diagnostic practice.

2.4.2 Salivary biomarkers

2.4.2.1 Saliva

Current efforts in searching for PD biomarkers have led to the development of various tools, such as neuroimaging and biofluid tests. Neuroimaging techniques have been implemented in clinics[149]. Nevertheless, the poor correlation between imaging and clinical progression and limited accessibility restricts their potential as a routinely used progression biomarker. Biofluid tests such as the CSF-based αSyn SAA detect pathological αSyn with significant sensitivity and specificity for PD. Although CSF contains markers associated with patients' clinical and pathological state, its major limitation lies in its invasive lumbar puncture procedure. Therefore, the search for a non-invasive biomarker has been increasingly important. Also, routine assessment of disease progression is critical for disease monitoring and clinical trials. Hence, studies have explored various easily acquired patient biofluids, including the olfactory mucosa[150], skin[151], and saliva[133], to identify biomarker candidates for synucleinopathies.

Saliva, a complex biological fluid produced primarily by the salivary glands, comprises a mixture of water, electrolytes, mucus, enzymes, and antimicrobial agents[152]. Its composition reflects both local oral and systemic physiological processes. Intriguingly, saliva is directly linked to the nervous system through the autonomic nervous system's regulation of salivary gland secretion (Fig. 2.14). Neurotransmitters, such as noradrenaline and acetylcholine, modulate salivary flow and composition, implying salivary changes can reflect neurological disorders[153].

PD patients often experience various oral pathologies, such as sialorrhea and xerostomia. Sialorrhea describes an increase in retaining saliva, and xerostomia is the opposite, describing a pathological oral cavity dryness due to reduced salivary secretion[155]. Such alterations in salivary function might be reflective of underlying neurodegenerative processes.

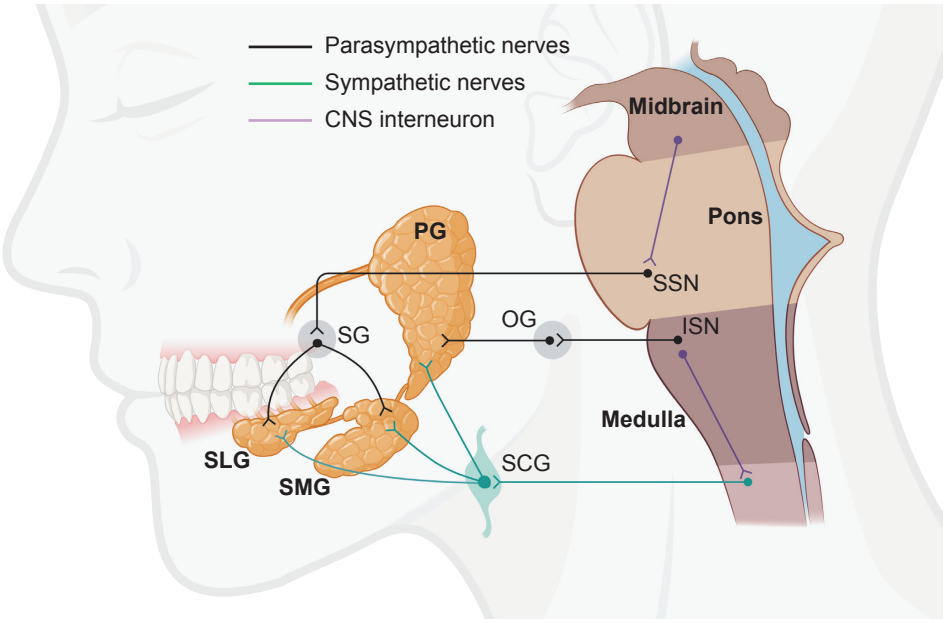

Figure 2.14 **Neural regulation of salivary glands.** Neural regulation of salivary glands via parasympathetic (black) and sympathetic (green) nerves. Salivary glands: parotid gland (PG), sublingual gland (SLG), submandibular gland (SMG). Brain stem: medulla, pons, midbrain. Brain stem nuclei: superior salivatory nuclei (SSN), inferior salivatory nuclei (ISN). Ganglia: submandibular ganglion (SG), otic ganglion (OG), superior cervical ganglion (SCG). Figure adapted from Ref. [154].

Furthermore, the non-invasive nature of saliva collection offers a significant advantage for frequent sampling, making it an attractive medium for longitudinal studies. Recent studies discovered changes in the level of αSyn and optimised salivary SAA, underscoring its potential as a diagnostic and prognostic tool[133,156]. In essence, the investigation of saliva as a PD biomarker is grounded in its physiological relevance and practical advantages in clinical and research settings.

2.4.2.2 Salivary αSyn

To date, αSyn is the most researched salivary protein for PD. An enzyme-linked immunosorbent assay (ELISA), as summarised in Table 2.4, was the most commonly used technique to detect αSyn in PD saliva. Several studies detected significantly lower levels of total αSyn in the saliva of PD patients compared to the healthy subjects[133,156–161].

In conflict, a few studies reported no change in the level of salivary total αSyn in PD compared to the healthy subjects[162–167].

Furthermore, the toxic conformers of αSyn, oligomers, were elevated in the saliva of PD patients compared to the healthy subjects (Table 2.4). Interestingly, the ratio of oligomers in total αSyn increased in PD patients with H&Y stage I to IV, indicating a correlation of oligomeric αSyn with disease progression[162]. On the contrary, one study reported the lack of statistical correlation between the amount of salivary total and oligomeric αSyn with H&Y scale and UPDRS scores in PD patients[159].

Table 2.4 **Salivary αSyn studies.** Summary of the studies investigating salivary αSyn levels in PD and healthy subjects using ELISA, Luminex, and electrochemiluminescence (ECL). PD ≈ HC, no significant difference between PD and HC; PD < HC, significantly lower levels in PD than HC; PD > HC, significantly higher levels in PD than HC; HC, healthy control.

Ref	Method	Total αSyn	Oligomeric αSyn	Oligomer/Total αSyn ratio
157	Luminex	PD < HC	NA	NA
158	ELISA	PD < HC	NA	NA
156	ELISA	PD < HC	PD > HC	PD > HC
162	Luminex	PD ≈ HC	PD > HC	PD > HC
163	ECL	PD ≈ HC	PD > HC	PD > HC
164	ELISA	PD ≈ HC	NA	NA
160	ELISA	PD < HC	PD > HC	PD > HC
159	ELISA	PD < HC	PD > HC	PD > HC
165	ELISA	PD ≈ HC	NA	NA
166	ELISA	PD ≈ HC	PD > HC	NA
133	ELISA	PD < HC	NA	NA
161	ELISA	PD < HC	NA	NA
167	ELISA	PD ≈ HC	PD > HC	NA

The correlation between salivary αSyn levels and disease progression or severity of PD remains controversial. Therefore, combining different proteins may be useful instead of a single αSyn biomarker. Indeed, it has been shown that combining salivary αSyn levels with additional salivary biomarkers improves the sensitivity and specificity in differentiating de novo PD from healthy controls[166]. For example, combining total αSyn with total-tau or microtubule-associated protein light chain 3 beta (MAP-LC3beta) improved diagnostic sensitivity for PD[166]. Misfolded tau protein aggregates into neurofibrillary tangles in AD brains. High CSF level of tau has been reported in PDD patients and accelerates αSyn aggregation[168,169]. MAP-LC3beta is an autophagy-related protein where high levels were detected in CSF of PD patients[170]. Combining total-tau and MAP-LC3beta with oligomeric αSyn also improved diagnostic accuracy. PD is a complex disease involving multiple molecular pathways. A combined investigation of various pathologically relevant molecules would contribute towards diagnostic accuracy even at early stages.

2.4.2.3 Salivary proteome

Studies of salivary proteins in PD patients have been performed using antibody-based assays such as ELISA. Although antibody-based assays are extremely sensitive, they pose a risk of non-specific binding to different complexes in the saliva matrix. Mass-spectrometry (MS) is a useful tool for a more integrated and quantitative analysis of salivary proteins.

Until now, only a single study has searched for potential salivary biomarkers for PD with MS. By analysing saliva from 24 PD and 15 healthy subjects, the authors identified 530 common proteins across all the samples[171]. Surprisingly, these common proteins were only, on average, 32 % of the total proteins in each sample. This finding highlights the heterogeneity of salivary proteins, which is important to consider for future saliva studies. Among the proteins identified, protein S100-A16, actin-related protein 2/3 complex subunit 1A (ARPC1A), and vacuolar protein sorting-associated protein 4B (VPS4B)

showed differential expression in PD versus healthy saliva. Findings allow speculation of potentially dysregulated pathways in PD, such as adipocyte differentiation, DNA repair mechanism, and endosomal pathway, respectively. The study unveiled novel directions for salivary biomarker research, and further investigation with larger PD cohorts and patients at different stages of PD progression will be imperative.

2.4.2.4 Salivary αSyn SAA

Following the discovery of elevated concentrations of oligomeric αSyn in saliva, more recent studies have evaluated the seeding capacity of PD saliva using αSyn SAA. The first salivary αSyn SAA study detected PD with 76.0 % sensitivity and 94.4 % specificity[172]. Also, MSA cases were detected with 61.1 % sensitivity. Interestingly, the lag phase of the salivary αSyn SAA was significantly shorter in PD than MSA, indicating the presence of more potent αSyn seeds in PD saliva than in MSA. Another study tested αSyn SAA with saliva samples from de novo PD patients[133]. The outcome sensitivity and specificity were 86 % and 78 %, respectively. Furthermore, SAA kinetic parameters F_{MAX} and AUC positively correlated with combined clinical measures of UPDRS III and the Non-Motor Symptoms Score (NMSS). Although promising methods have been reported, the reproducibility of the assays must be examined. In addition, further optimisation of the protocol with a larger and longitudinal cohort is essential to address the limitations of the assay and refine its clinical utility.

2.5 Thesis aims

As discussed, a growing body of evidence suggests the presence of αSyn strains of different synucleinopathies, and extensive αSyn strain characterisation has been performed with SAA fibrils. Furthermore, significant progression has been achieved in biomarker research through SAA diagnostics with patient CSF. Yet, a non-invasive biomarker supporting PD clinical diagnosis is still missing.

This thesis contains four aims that build upon these observations:

1. To explore methods to characterise the biochemical and biophysical properties of brain-derived αSyn fibrils. Chapter 4 will explore methodologies for systematic characterising αSyn fibrils from PD brains. Various biochemical and biophysical methods will be employed as current studies on brain-derived αSyn fibrils have focused primarily on structural aspects.

2. To expand the evidence for the existence of αSyn strains by investigating biochemical and biophysical properties of αSyn fibrils from different synucleinopathies and systematically comparing them to the SAA fibrils. Chapter 5 will assess the strain-like properties of brain-derived αSyn fibrils from brains of different synucleinopathies (PD, PDD, DLB, MSA) and compare them to the counterpart SAA fibrils. While structural differences have been reported, questions remain about biochemical and biophysical variability.

3. To assess the diagnostic value of αSyn SAA using CSF from a well-characterised longitudinal cohort of PD and MSA patients. Chapter 6 will examine the αSyn seeding activity in CSF of PD and MSA patients using αSyn SAA. The SAA quantitative parameters will be analysed against PD and MSA, clinical measures and PD clusters. This chapter will address the role of αSynSAA as a diagnostic tool and a molecular profile that provides information about disease progression and phenotypes.

4. To search for salivary molecules with distinguishable levels between PD and healthy patients. Chapter 7 will explore salivary biomarkers for PD. Biochemical methods, proteomics, and αSyn SAA will be used to identify molecular markers that are distinguishable between PD and healthy controls.

Chapter 3

Materials and Methods

3.1 Human biosamples

3.1.1 Brain samples

3.1.1.1 Patient demographics

Brain tissues from patients with PD and PDD were obtained from the Parkinson's UK Brain Bank (Imperial College London, UK) (Registered charity in England and Wales (258197) and in Scotland (SC037554)). Brain tissues from patients with DLB, MSA and healthy controls were collected from the Oxford Brain Bank (OBB, University of Oxford, UK) in accordance with approved protocols by the Ethics Committee of the University of Oxford (ref 23/SC/0241). All participants had given prior written informed consent for the brain donation. Both brain banks comply with the requirements of the Human Tissue Act 2004 and the Codes of Practice set by the Human Tissue Authority (HTA licence numbers 12275 for the Imperial and 12217 for OBB). Demographic and clinic-pathological data are summarised in Table 3.1 and Table 3.2.

Table 3.1 **Clinicopathological summary of the cases used in Chapter 4.** Only the entorhinal cortex was used for all these cases. Duration indicates the time (years) after the motor onset. CERAD, Consortium to Establish a Registry for Alzheimer's Disease; AD, Alzheimer's disease; MCI, mild cognitive impairment; CTR, healthy control; M, male; F, female.

Case	Sex	Duration (years)	Diagnosis	Braak αSyn	Braak tau	CERAD
PD 1	F	6	PD + AD	6	4	2
PD 2	F	18	PD + AD	6	4	2
PD 3	M	16	PDD	6	2	1
PD 4	M	11	PDD	6	3	3
PD 5	M	10	PDD	6	2	0
PD 6	M	11	PDD	6	2	3
PD 7	M	25	PDD	6	2	2
PD 8	M	11	PDD	6	2	3
PD 9	F	24	PD-MCI	5	2	2
PD 10	F	12	PD	6	3	1
CTR 1	F	N/A	Normal brain	N/A	N/A	N/A
CTR 2	F	N/A	Normal brain	N/A	N/A	N/A
CTR 3	M	N/A	Normal brain	N/A	N/A	N/A
CTR 4	F	N/A	Normal brain	N/A	N/A	N/A
CTR 5	M	N/A	Normal brain	N/A	N/A	N/A
CTR 6	M	N/A	Normal brain	N/A	N/A	N/A
CTR 7	M	N/A	Normal brain	N/A	N/A	N/A
CTR 8	F	N/A	Normal brain	N/A	N/A	N/A
CTR 9	F	N/A	Normal brain	N/A	N/A	N/A
CTR 10	M	N/A	Normal brain	N/A	N/A	N/A

Table 3.2 **Clinicopathological summary of the cases used in Chapter 5.** Duration indicates the time (years) after the motor onset. CERAD, Consortium to Establish a Registry for Alzheimer's Disease; AD, Alzheimer's disease; CVD, cardiovascular disease; CTR, healthy control; ECtx, entorhinal cortex; BG, basal ganglia; M, male; F, female.

Case	Brain region	Sex	Duration (years)	Clinical diagnosis	Neuropath diagnosis	Braak αSyn	Braak tau	CERAD
PD 1	ECtx	M	8	PD	PD	6	2	C0
PD 2	ECtx	M	6	PD	PD	6	2	C1
PD 3	ECtx	M	8	PD	PD	6	2	C1
PDD 1	ECtx	M	25	PDD	PDD	6	2	C2
PDD 2	ECtx	M	10	PDD	PDD	6	2	C0
PDD 3	ECtx	M	16	PDD	PDD	6	2	C1
DLB 1	ECtx	M	$<$1	Possible AD	DLB+AD	6	3	C2
DLB 2	ECtx	F	0	Possible AD	DLB+AD	6	3	C2
DLB 3	ECtx	M	3	AD+CVD	DLB+AD	6	3	C2
MSA 1	BG	M	5	PD	MSA	NA	0	C0
MSA 2	BG	M	NA	MSA	MSA	NA	0	C0
MSA 3	BG	F	2	MSA	MSA	NA	1	C0
CTR 1	ECtx	M	NA	NA	Normal brain	NA	NA	NA
CTR 2	ECtx	M	NA	NA	Normal brain	NA	NA	NA
CTR 3	ECtx	F	NA	NA	Normal brain	NA	NA	NA

3.1.2 CSF samples

3.1.2.1 Patient demographics

CSF samples of PD patients (n = 74) and healthy controls (n = 17) were from the Discovery cohort of the Oxford Parkinson's Disease Centre. An additional 32 CSF samples were taken from the OPTIMA cohort (Oxford Project to Investigate Memory and Ageing). CSF of 24 MSA patients was analysed, where 23 were from the longitudinal cohort from the French Reference Centre for MSA and one was from a Discovery PD patient re-diagnosed as MSA during clinical follow-up. Demographic and clinical data are outlined in Table 3.3.

The study was approved by the local ethics committees and all participants provided written informed consent according to the Declaration of Helsinki. The Discovery PD patients were diagnosed using UK Parkinson's Disease Brain Bank criteria[173], following specialist neurologist review. Clinical assessments included MDS-UPDRS parts I to IV, MMSE and MoCA. The Discovery PD patients were divided into four clusters according to the previously published data-driven approach[11], as shown in Table 2.1.

The diagnosis of 'probable' MSA was made using the consensus criteria[174]. Disease severity was assessed with the UMSARS. CSF was collected as part of the BIOAMS (NCT01485549) and BIOPARK (NCT02114242) cohort studies[175].

3.1.2.2 CSF collection and pre-treatment

Upon collection, CSF was centrifuged at 3,200 rpm for 10 min at 4 °C and aliquots were stored at -80 °C within 30 min of collection. CSF haemoglobin level was analysed using ELISA (Bethyl Laboratories) and samples with haemoglobin levels higher than 200 ng/ml were excluded from the study.

Table 3.3 Demographics of PD, MSA and control subjects investigated in Chapter 6. Data are mean ± SD. *P*-values were calculated with Kruskal-Wallis test or Mann-Whitney *U* test. LP, lumbar puncture.

	PD (*n* = 74)	**MSA (*n* = 24)**	**Controls (*n* = 55)**	***P*-value**
Sex (M/F)	48/26	14/10	28/27	0.13
Age at LP	65.3 ± 9.0	63.8 ± 8.2	76.4 ± 11.9	<0.001
Duration from diagnosis to LP (years)	2.1 ± 1.4	5.7 ± 3.2		
MDS-UPDRS I	8.9 ± 5.3			
MDS-UPDRS II	9.1 ± 6.2			
MDS-UPDRS III	26.8 ± 11.8			
MDS-UPDRS IV	0.6 ± 2.0			
H&Y stage	2.0 ± 0.4			
MMSE	27.6 ± 2.3		29.0 ± 1.1	0.009
MoCA	25.2 ± 3.1		27.6 ± 1.8	0.001
MSA subtype (MSA-P/MSA-C)		14/10		
UMSARS baseline		44.4 ± 17.5		
UMSARS follow-up		55.5 ± 21.3		
UMSARS change		10.2 ± 5.2		

3.1.3 Saliva samples

3.1.3.1 Patient demographics

Saliva was collected from PD patients (n = 33) and healthy controls (n = 41) from the movement disorder clinic at the Department of Neurology, Aarhus University Hospital. The study was approved by the local ethics committees and all participants provided written informed consent according to the Declaration of Helsinki. Saliva was collected as described in [176]. Demographic and clinical data are summarised in Table 3.4.

Table 3.4 Demographics for the saliva study in Chapter 7. Values are presented in average ± SD. *P*-values were calculated using Mann-Whitney *U* test.

Factors	**PD patients (n = 33)**	**Healthy controls (n = 41)**	***P*-value**
Age	62.8 ± 8.4	62.2 ± 9.8	0.81
Sex (M/F)	18/15	22/19	0.90
MMSE	28.6 ± 1.5	28.9 ± 1.1	0.5
Duration since diagnosis (years)	4.9 ± 3.5	N/A	N/A
UPDRS III	27.0 ± 12.8	N/A	N/A
H&Y stage	1.9 ± 0.5	N/A	N/A

3.1.3.2 Saliva collection and pre-treatment

The whole saliva was collected according to the standardised protocol[177,178]. Participants were asked to refrain from eating, smoking, and drinking for a minimum of four hours before the procedure and to rinse their mouths with still mineral water. Saliva collected in the first 5 min of the procedure was discarded, and saliva collected in the next 10-50 min was used for this study. Samples were immediately put on ice and centrifuged at 3,000 rpm for 30 min to remove large debris. The supernatant was sonicated and immediately frozen at -80 °C. Before analysis, saliva was thawed and treated with a protease inhibitor cocktail (Thermo Fisher). After a mild vortexing, samples were centrifuged at 2,600 *g* for 15 min

at 4 °C. The supernatant was collected and centrifuged again at a higher speed of 15,000 *g* for 15 min at 4 °C. The resulting supernatant was used for downstream analysis.

3.2 Extraction of αSyn fibrils from the human brain

3.2.1 Sarkosyl-based extraction

The extraction protocol was adapted from the method presented in [85]. Brain tissues (0.5 g) were homogenised in an extraction buffer (20 w/v) composed of 10 mM Tris-HCl, 0.8 M NaCl, 10 % sucrose and 1 mM EGTA (pH 7.5). Sarkosyl was added to the homogenates to a final concentration of 2 % and incubated for 30 min at 37 °C. Homogenates were centrifuged at 10,000 *g* for 10 min at 4 °C. The supernatants were centrifuged at 100,000 *g* for 60 min at 4 °C. The pellet was washed twice and resuspended in 500 µl/g of extraction buffer and centrifuged at 500 *g* for 1 min at 4 °C. The resulting supernatants were diluted 1/3 in buffer consisting of 50 mM Tris-HCl, 0.15 M NaCl, 10 % sucrose and 0.2 % sarkosyl (pH 7.5). The diluted supernatant was centrifuged at 100,000 *g* for 60 min at 4 °C. The resulting pellet was the sarkosyl insoluble fraction, washed twice and resuspended in 250 µl/g of 30 mM Tris-HCl (pH 7.5). The protein concentration of the sarkosyl insoluble fraction was determined using the bicinchoninic acid assay (BCA) (Thermo Scientific). The sarkosyl insoluble fraction was aliquoted in small volumes to prevent multiple freeze-thawing and stored at -80 °C after flash-freezing in liquid nitrogen.

3.2.2 TritonX-100-based extraction

The extraction protocol was adapted from the method presented in [179]. Brain tissues were homogenised in 4 % (w/v) extraction buffer containing tris-buffered saline (TBS - 20 mM Tris-HCl, 0.5 M NaCl, pH 7.5) and a complete protease-inhibitor (PI) tablet (Thermo Scientific). The homogenate was spun at 1,000 *g* for 5 min. The supernatant was spun at 175,000 *g* for 30 min at 4 °C. The supernatant was collected as a 'TBS soluble'

fraction. The pellet was rinsed twice with extraction buffer and added with 500 µl/g of TBS containing 1 % (w/v) TritonX-100. The resuspended pellet was centrifuged at 175,000 *g* for 30 min at 4 °C. The supernatant was collected as a 'TritonX-100 soluble' fraction. The final pellet was resuspended in 250 µl/g of 8 M urea and 5 % SDS in TBS.

3.2.3 RIPA-based extraction

The extraction protocol was adapted from the method presented in [180]. Brain tissues were homogenised in 10 % (w/v) of an extraction buffer containing 50 mM Tris-HCl, pH 7.4 containing 175 mM NaCl, 5 mM EDTA, and 0.1 mM PMSF. Homogenates were centrifuged at 1000 *g* for 5 min at 4 °C. Pellets were discarded, and the supernatants were ultracentrifuged at 120,000 *g* for 30 min at 4 °C. The resulting pellet was washed with extraction buffer and resuspended in 500 µl/g of extraction buffer containing 1 % of TritonX-100. The resuspended solution was ultracentrifuged at 120,000 *g* for 30 min at 4 °C. The resulting pellet was resuspended in 100 µl of RIPA buffer (Sigma) and ultracentrifuged at 120,000 *g* for 30 min at 4 °C. The final pellets were resuspended in 250 µl/g of 8 M urea.

3.3 Biochemical characterisation of αSyn fibrils

3.3.1 Slot blot

A nitrocellulose membrane (Amersham) was soaked in a transfer buffer containing 25 mM Tris, 192 mM glycine, pH 8.3 with 20 % methanol (vol/vol). The membrane was loaded onto a 48-slot slot blot apparatus (GE Healthcare), and a total of 2 µg of the sample was immobilised on a nitrocellulose membrane (Amersham) by filtration. After checking all the liquid passed through the membrane, the membrane was removed from the apparatus and blocked with 5 % skimmed milk and probed with primary antibodies summarised in Table 3.5 for overnight at 4 °C with mild shaking. All primary antibodies were prepared in 5 % BSA in 0.1 % TBST. Membranes were washed three times in 0.1 % TBST

for 10 min. After washing, the membrane was incubated with a secondary antibody as summarised in Table 3.5 for 45 min at room temperature (RT) with mild shaking. All secondary antibodies were prepared in 5 % skimmed milk in 0.1 % TBST. Membranes were washed again three times in 0.1 % TBST for 10 min. Membranes were developed using an ECL Western blot detection kit (Amersham) and imaged using a ChemiDoc imaging system (Bio-Rad). Semi-quantitative analysis of the slot blot data was performed using ImageJ.

Table 3.5 Slot blot antibodies. List of αSyn-specific antibodies used in slot blot and corresponding epitopes, manufacturers, dilutions, and host species. Ms: Mouse, Rb: Rabbit.

Antibody	Epitope	Manufacturer	Dilution	Host species
LASH 1-20	1-20	Lashuel Lab	1:10,000	Rb
LASH 34-45	34-45	Lashuel Lab	1:5,000	Ms
5G4	44-57	Millipore	1:3,000	Ms
LASH 80-96	80-96	Lashuel Lab	1:10,000	Ms
anti-aSyn clone 42	91-99	BD-Biosciences	1:2,000	Ms
LASH 110-115	110-115	Lashuel Lab	1:5,000	Ms
LB509	115-122	Abcam	1:2,000	Ms
MJFR-1	118-123	Abcam	1:10,000	Rb
Syn211	121-125	Abcam	1:2,000	Ms
EP1536Y	pS129	Abcam	1:3,000	Rb
Ab131508	134-138	Abcam	1:2,000	Rb
MJFR-14-6-4-2	Conformational	Abcam	1:5,000	Rb

3.3.2 Proteinase-K digestion

For the conformational stability assay, 10 µg of brain-derived αSyn fibrils and 1 µg of end-point seeded-amplified (SAA) fibrils were prepared. The samples were treated with

increasing concentrations of Gdn-HCl (0, 1, 2, 3, 4, 5 M) for 1 hour at 37 °C while shaking at 800 rpm. The Gdn-HCl treatment was stopped by reducing the concentration down to 0.5 M. Subsequently, the samples were treated with 1 µg/ml of proteinase-K (PK) for 30 min at 37 °C with shaking at 500 rpm. PK-treated samples were pulled down by ultracentrifugation at 100,000 *g* for 1 hr at 4 °C. The PK-treated pellet was resuspended in 30 mM Tris-HCl.

For PK profiling, 10 µg of brain-derived αSyn fibrils were treated with increasing concentrations of PK (0, 0.001, 0.01, 0.1, 1 mg/ml) for 15 min at 37 °C with shaking at 500 rpm.

Tricine sample buffer (Bio-Rad) was added to the Gdn-HCl and PK treated samples in a 1:2 ratio and boiled for 10 min in at 95 °C. Then, the samples were centrifuged briefly and loaded onto a 16.5 % Tris-Tricine gel (Bio-Rad) together with Precision Plus Protein Dual Xtra Prestained Protein Standard (Bio-Rad). SDS-PAGE was performed at 160 V for 1 hr at RT. Then, samples were transferred to a nitrocellulose membrane (Amersham) at 65 V for 1.5 hr at 4 °C. Membranes were blocked using 5 % skimmed milk in 0.1 % TBST for 1 hr at RT with mild shaking and probed with anti-αSyn clone 42 (BD Biosciences, 1:1,000 dilution in 5 % BSA) overnight at 4 °C with mild shaking. Subsequently, membranes were washed three times in 0.1 % TBST for 10 min and probed with anti-mouse secondary antibody (Abcam, 1:5,000 dilution in blocking buffer) for 45 min at RT with mild shaking. Membranes were washed again three times in 0.1 % TBST for 10 min. Membranes were developed using an ECL Western blot detection kit (Amersham) and imaged using a ChemiDoc imaging system (Bio-Rad).

3.4 Transmission electron microscope (TEM) imaging

3.4.1 Negative stain TEM

Ten µl of 2-fold diluted sample in 30 mM Tris-HCl was adsorbed onto carbon-coated 300 mesh copper grids (Agar scientific) for 2 min. The grids were washed with distilled water

for 30 sec and negative stained with 2 % uranyl acetate for 20 sec. The stained grids were imaged with an FEI Tecnai T12 transmission electron microscope (TEM) operating at 120 kV (Dunn School Bioimaging Facility, University of Oxford). For systematic imaging of the fibrils, magnification was set at 18,500 X, and one block of image at 18,500 X was considered as a single block on a mesh grid. On the mesh grid, one block of image was taken and observed for every five blocks while moving along the mesh from the top to the bottom. The TEM images were analysed using ImageJ.

3.4.2 Immunogold TEM

Ten µl of 2-fold diluted sample in 30 mM Tris-HCl was absorbed onto carbon-coated 300 mesh copper grids (Agar scientific) for 5 min. Grids were washed two times in PBS and blocked with blocking buffer (0.2 % fish gelatin in PBS) for 5 min. Then, grids were incubated with primary antibodies (antibodies and dilutions summarised in Table 3.6) diluted in blocking buffer for 60 min at RT. Grids were washed six times with blocking buffer and incubated with gold-conjugated secondary antibody (Abcam, diluted 1:20 in blocking buffer) for 30 min at RT. Grids were washed three times in blocking buffer and three times in PBS. Then, grids were fixed in 0.1 % glutaraldehyde in PBS for 15 min in RT. Finally, grids were washed four times in distilled water and negative stained with 2 % uranyl acetate for 30 sec. Grids were imaged with the same method outlined in Section 3.4.1.

Table 3.6 Immunogold TEM antibodies. List of αSyn-specific antibodies used in immunogold TEM and corresponding epitopes, manufacturers, dilutions, and host species. Ms: Mouse, Rb: Rabbit.

Antibody	Epitope	Manufacturer	Dilution	Host species
LASH 1-20	1-20	Lashuel Lab	1:10	Rb
LASH 34-45	34-45	Lashuel Lab	1:50	Ms
5G4	44-57	Millipore	1:20	Ms
LASH 80-96	80-96	Lashuel Lab	1:20	Ms
anti-αSyn clone 42	91-99	BD-Biosciences	1:20	Ms
LASH 110-115	110-115	Lashuel Lab	1:20	Ms
LB509	115-122	Abcam	1:20	Ms
MJFR-1	118-123	Abcam	1:20	Rb
Syn211	121-125	Abcam	1:20	Ms
EP1536Y	pS129	Abcam	1:20	Rb
Ab131508	134-138	Abcam	1:20	Rb
MJFR-14-6-4-2	Conformational	Abcam	1:50	Rb

3.5 Measurement of protein concentration

3.5.1 Bicinchoninic (BCA) protein assay

The total protein concentration of a sample was measured using the BCA assay (Pierce Rapid Gold BCA Protein Assay Kit, Thermo Fisher) following the manufacturer's protocol. Standards and samples were tested in duplicates, and the absorbance was measured at 480 nm using a FLUOstar Omega microplate reader (BMG Labtech). A standard curve was plotted using the averaged blank-corrected 480 nm absorbance readings.

3.5.2 Enzyme-linked immunosorbent assay (ELISA)

The level of total αSyn was measured using LEGEND MAX human αSyn ELISA kit (BioLegend), and the level of aggregated αSyn was measured using LEGEND MAX human αSyn aggregate ELISA kit (BioLegend) and Human αSyn PATHO ELISA kit (Roboscreen). The detection range of the target αSyn species of each ELISA kit was 10.2 – 650, 3.9 – 250, and 5 - 250 pg/ml, respectively. For each assay, 50 µl of undiluted or diluted sample was used tested duplicates. The following procedure followed the manufacturer's protocol.

3.6 Mass spectrometry

3.6.1 ESI-TOF intact mass and data analysis

Reversed-phase chromatography using an Agilent 1100 HPLC system (Agilent Technologies Inc., Palo Alto, CA, USA) was performed in line with mass spectrometry. The sample was diluted 1:10 with 0.1 % formic acid to make a 50 µl final volume and loaded onto a round-bottomed 96-well microplate (Agilent). Fifty µl of the sample was injected into a 4.6 mm x 150 mm (5 µm) Zorbax 300SB-C3 column with an oven set at 40 °C. Solvent A consisted of 0.1 % formic acid in LC-MS grade water, and solvent B consisted of 0.1 % formic acid in LC-MS grade methanol. Chromatography was performed as follows: Initial conditions were 95 % A and 5 % B and a flow rate of 0.5 mL/min. After 1 min at 5 % B, a gradient from 5 % B to 95 % B was applied over 20 min. Elution was performed isocratically at 95 % B for 2 min, and the system was equilibrated at initial conditions at 5 % B for 6 min. Intact protein mass was detected using an MSD-ToF electrospray ionization orthogonal time-of-flight mass spectrometer (Agilent Technologies Inc. – Palo Alto, CA, USA). The instrument was set up with an ESI source and operated in positive ion mode. The ion source operated with the gas temperature at 350 °C, drying gas flow rate at 12 L/min, nebulizer pressure at 45 psig, and capillary voltage at 4000 V. The MS ion optic operated with the fragmentor at 250 V, skimmer at 60 V, and octopole RF at

250 V.

The LC-MS data files were transferred to the data analysis software Masshunter Qualitative Analysis v 6.0 (Agilent, Santa Clara, CA, USA). A total ion chromatogram was used to select the elution time of interest. The mass-to-charge ratio (*m/z*) spectra were deconvoluted between the expected minimum mass of 5,000 Da and the maximum mass of 400,000 Da. The height of the mass peaks between PD and control samples were compared to analyse the differences in protein abundance. When a mass of interest was chosen, the UniProt search engine was used to find a matching protein. Then, the mass and the matched protein were searched in the LC-MSMS data of the corresponding sample to confirm the protein's identity. Post-translational modifications were identified by searching the mass shifts on the Unimod database.

3.6.2 LC-MS/MS and data analysis

Fifty µl of salivary sample was pre-digested with Lysyl endopeptidase (R) with a ratio of 1 µg of enzyme for 100 µg of protein for 2 hr shaking at 37 °C. The samples were digested with trypsin (Promega) for 16 hr at 37 °C shaking at 650 rpm. Trypsin was added with a ratio of 1 µg of enzyme for 40 µg of protein. Trypsin digestion was stopped by adding formic acid to a final concentration of 1 %. The digested sample was centrifuged at 17,000 *g* for 30 min at 4 °C to remove large aggregates. Digested peptides were desalted using handmade C18 stage tips.

Tryptic peptides were separated on a nanoliquid chromatography (EASY-nLC 1000 system, Thermo Fisher Scientific) connected in line with a Q Exactive mass spectrometer (Thermo Fisher Scientific) through an EASY-Spray nano-electrospray ion source (Thermo Fischer Scientific). Peptides were first trapped in C18 PepMac100 precolumn (300 µm inner diameter by 5 mm, 100 *Å* pore size; Thermo Fisher Scientific) using solvent A (0.1 % formic acid in water). Then, the peptides were separated on an analytical column (75 µm inner diameter by 500 mm, Reprosil C18, 1.9 µm particle size, 100 *Å* pore size) using a 60 min linear gradient (18 % to 30 % solvent B (0.1 % formic acid and 5 %

DMSO in acetonitrile) at a flow rate of 200 nl/min. The mass spectrometer operated in a data-dependent mode. Full-scan MS spectra were acquired in the Orbitrap (scan range of 350 to 1500 *m/z*, resolution 70,000, automatic gain control (AGC) target of 3×10^6, and maximum injection time of 50 ms). Following the MS scans, the 10 peaks with the highest intensities were selected for high-energy collisional dissociation (HCD) fragmentation at 30 % of normalised collision energy. HCD spectra were also acquired in the Orbitrap.

Tandem mass spectra were analysed with SEQUEST from Proteome Discoverer 1.4 (Thermo Fischer Scientific) using a protein database for Homo sapiens. Contaminant protein sequences, including Lys-R and trypsin were included in the database. For the database search, cysteine residues were considered fully carbamidomethylated (+57 Da statically added), methionine was considered oxidised (+16 Da dynamically added), and two missed cleavages were allowed. Peptide mass tolerance was set at 50 ppm and 0.02 Da on the precursor and fragment ions, respectively. The protein identification was filtered at a false discovery rate below 1 %.

3.7 αSyn seed amplification assay (SAA)

3.7.1 αSyn fibril SAA

Brain-derived fibrils were diluted 1:1,000 in 30 mM Tris-HCl (pH 7.4). Each sample was tested in six replicates, and 2 µl of diluted samples were added to 98 µl of reaction buffer. The reaction buffer consisted of listed components, each prepared with specific treatment before making up the master mix, which is outlined in Table 3.7. A total 100 µl of reaction mixture was transferred onto a Nunc MicroWell 96-well Optical-Bottom Plates (Thermo Scientific) and sealed. The plate was inserted into a FLUOstar Omega plate reader (BMG). The plate was incubated at 42 °C and went through a double-orbital shaking for 1 min and rest for 1 min at 400 rpm. The fluorescence was measured with bottom-reading at 2,000 gain setting every 30 min for 100 hr using 440/490 (excitation/emission) filters. Data analysis was performed using the MARS software (BMG).

3.7.2 CSF SAA

The reaction mixture was composed of 85 µl of the reaction buffer (Table 3.7) and 15 µl of neat CSF. The reaction was performed in triplicates, using the same conditions and shaking methods as the αSyn fibril SAA (Section 3.7.1). Reactions with RFU (at 120 h) higher than 5 SD from the average initial fluorescence were considered positive SAA reaction.

Table 3.7 Buffer components of αSyn fibril and CSF SAA.

Buffer component	Final concentration	Treatment method
recombinant αSyn	0.1 mg/ml	Filtration with 100 kDa MWCO filter (PALL) by 3,300 *g* centrifugation for 15 min at 4 °C
PIPES pH 7	100 mM	Filtration through a 0.22 µm filter (Millipore)
NaCl	150 mM	Filtration through a 0.22 µm filter (Millipore)
ThT	10 µM	Filtration through a 0.22 µm filter (Millipore)

Table 3.8 Buffer components of saliva SAA.

Buffer component	Final concentration	Treatment method
recombinant αSyn	0.06 mg/ml	Filtration with 100 kDa MWCO filter (PALL) by 3,300 *g* centrifugation for 15 min at 4 °C
PBS pH 7.4	10 mM	Filtration through a 0.22 µm filter (Millipore)
ThT	10 µM	Filtration through a 0.22 µm filter (Millipore)

3.7.3 Saliva SAA

Saliva samples were diluted 1:10,000 in PBS (pH 7.4). Each sample was tested in triplicates, and 2 µl of diluted samples were added to 98 µl of reaction buffer. The reaction buffer consisted of listed components, each prepared with specific treatment before making up the master mix, outlined in Table 3.8. A total 100 µl of reaction mixture and one 1 mm silica bead was transferred onto each well of a Nunc MicroWell 96-well Optical-Bottom Plate (Thermo Scientific) and sealed. The plate was inserted into a FLUOstar Omega plate reader (BMG). The plate was incubated at 37 °C and went through a double-orbital shaking for 1 min and rest for 29 min at 400 rpm. The fluorescence was measured with bottom-reading at 2,000 gain setting every 30 min for 100 hr using 440/490 (excitation/emission) filters. Data analysis was performed using the MARS software (BMG).

3.8 Immunohistochemistry

Six µm thick sections of formalin-fixed paraffin-embedded (FFPE) human brain tissue sections were de-paraffinized in xylene for 5 min three times. Tissues were rehydrated through decreasing concentration of industrial denatured alcohol (IDA) (100 %, 100 %, 90 %, 70 % for 5 min each) and subsequently in distilled water for 5 min. For antigen retrieval, sections were treated with 70 % formic acid for 15 min. Endogenous peroxidase was blocked with 3 % H_2O_2 for 20 min with mild shaking. Tissues were further blocked with 10 % fetal bovine serum (FBS) in PBS for 30 min. Sections were incubated with anti-αSyn clone 42 (Syn1) (BD Biosciences) diluted 1:1,000 in 10 % FBS overnight at 4 °C. After washing with PBS for 5 min three times, sections were incubated with mouse-HRP secondary antibody (Agilent Technologies) for 30 min at RT. Sections were developed with Dako DAB (Agilent Technologies) and counterstained with haematoxylin. Finally, sections were mounted with coverslips using DPX (Thermo Scientific).

3.9 Graphic illustrations

Graphic illustrations were generated using BioRender (BioRender.com) and Adobe Illustrator software.

3.10 Statistical analysis

SPSS version 29.0 and GraphPad were used for all the statistical analyses. Statistical tests used for different analyses are specified in each figure legend.

Chapter 4

Investigating biochemical and biophysical methods to characterise αSyn fibrils from PD brain

4.1 Introduction

The αSyn strain hypothesis has gained prominence as a molecular basis of the clinical and pathological heterogeneity observed in synucleinopathies[181]. This hypothesis is supported by observations of distinct structures in brain-derived αSyn fibrils from different synucleinopathies. Cryo electron-microscope (cryo-EM) studies have revealed a common 'Lewy fold' structure in αSyn fibrils from PD, PDD, and DLB brains, characterised by a right-handed twist[85,104]. In contrast, αSyn fibrils from MSA brains exhibited a distinct 'MSA fold' composed of two protofilaments with a left-handed twist. Distinct αSyn conformers in LBDs and MSA suggest that these diseases could be associated with distinct αSyn strains. This is analogous to tauopathies, where distinct tau conformers are associated with different disease phenotypes[182].

Distinct cellular infectivity of αSyn aggregates from different synucleinopathies also supports the existence of αSyn strains. αSyn aggregates from MSA brains induced more

severe in vitro αSyn pathology in compared to PDD and DLB[110,183,184]. Furthermore, transmission profiles of αSyn aggregates have been investigated using mouse models of synucleinopathy. The findings from these studies vary depending on the model used, the method of inoculation, and the incubation periods. However, a common observation is that αSyn aggregates from MSA brains induce more severe αSyn deposition and pathology in mouse brains compared to PDD and DLB[92,120,128,184–188].

While the structural, cellular toxicity and transmission properties of αSyn aggregates are thoroughly characterised, the biochemical and biophysical profiles of αSyn fibrils from human brains have not been examined extensively. Biochemical and biophysical characterisation are conventional methods of defining prion strains[189]. Biochemical characterisation is typically performed by assessing resistance against proteinase-K (PK) digestion. For instance, sarkosyl-insoluble αSyn fibrils from PD brains are PK-resistant, and individual cases can exhibit unique patterns of PK-resistance[109,110]. Therefore, the PK-resistance provides a biochemical fingerprint of αSyn fibrils, which could be used to profile strains. Biophysical characterisation includes structural imaging techniques such as immunogold labelling and transmission electron microscopy (TEM). Previous studies reported TEM images of PD brain-derived αSyn fibrils with straight morphologies[108]. Moreover, distinct immunolabelling patterns of antibodies such as PER1 (epitope 11-34) and H3C (epitope 131-140) to brain-derived αSyn fibrils provided evidence of their structural heterogeneity[108].

This chapter will utilise various biochemical and biophysical techniques to systematically examine the αSyn fibrils from PD brains. The aims of this chapter are the following:

1. Present methods for biochemical and biophysical characterisation of αSyn fibrils from PD brains.

2. Examine the immunoreactivity of αSyn antibodies, PK-resistance and TEM morphologies of αSyn fibrils from PD brains.

3. Identify biochemical and biophysical signatures indicative of αSyn strains.

4.2 Results

4.2.1 Sarkosyl extraction of a PD brain yields optimal fibril integrity

The integrity of isolated αSyn fibrils from the human brain is crucial for downstream characterisation. Here, three detergent-based extraction protocols were evaluated: sarkosyl, Triton X-100, and RIPA. The entorhinal cortex from a PD patient's brain was used to test these protocols, and the extracted fibrils were visualised using TEM.

The sarkosyl extraction yielded a dense and clean population of fibrils, with visible morphological features such as straight and twisted fibrils (Figs. 4.1a&b). The average length of the straight fibrils (n = 50) was 507 ± 258 nm (standard deviation, SD), while the twisted fibrils (n = 50) had an average twist periodicity of 101 ± 16 nm.

The RIPA-insoluble fraction contained fibrils and membranous structures, as shown in Fig. 4.1c. However, the fibril density was lower compared to the sarkosyl-insoluble fraction. Additionally, the fibrils were shorter, with an average length of 131 ± 67 nm. The background noise and artefacts limited the resolution of the fibril morphology.

The Triton X-100 - insoluble fraction also contained insolubilised membranous structures and low-resolution fibrils (Fig. 4.1d). Consequently, fibril identification was challenging, and observation of morphological features was limited. In the given area, only 20 fibrils were observed with an average length of 244 ± 141 nm.

Sarkosyl isolated a relatively purer fraction of intact fibrils from the PD brain with observable morphology. Therefore, the sarkosyl-based extraction protocol was selected for extracting αSyn fibrils from the PD brains.

4.2.2 Profiling the immunoreactivity of αSyn antibodies to sarkosyl-insoluble αSyn from PD brains

The immunoreactivity of 12 αSyn antibodies to the sarkosyl-insoluble αSyn was systematically assessed using immunoblotting. The entorhinal cortex from 10 PD patients and 10 healthy control (HC) brains were selected to isolate the sarkosyl-insoluble frac-

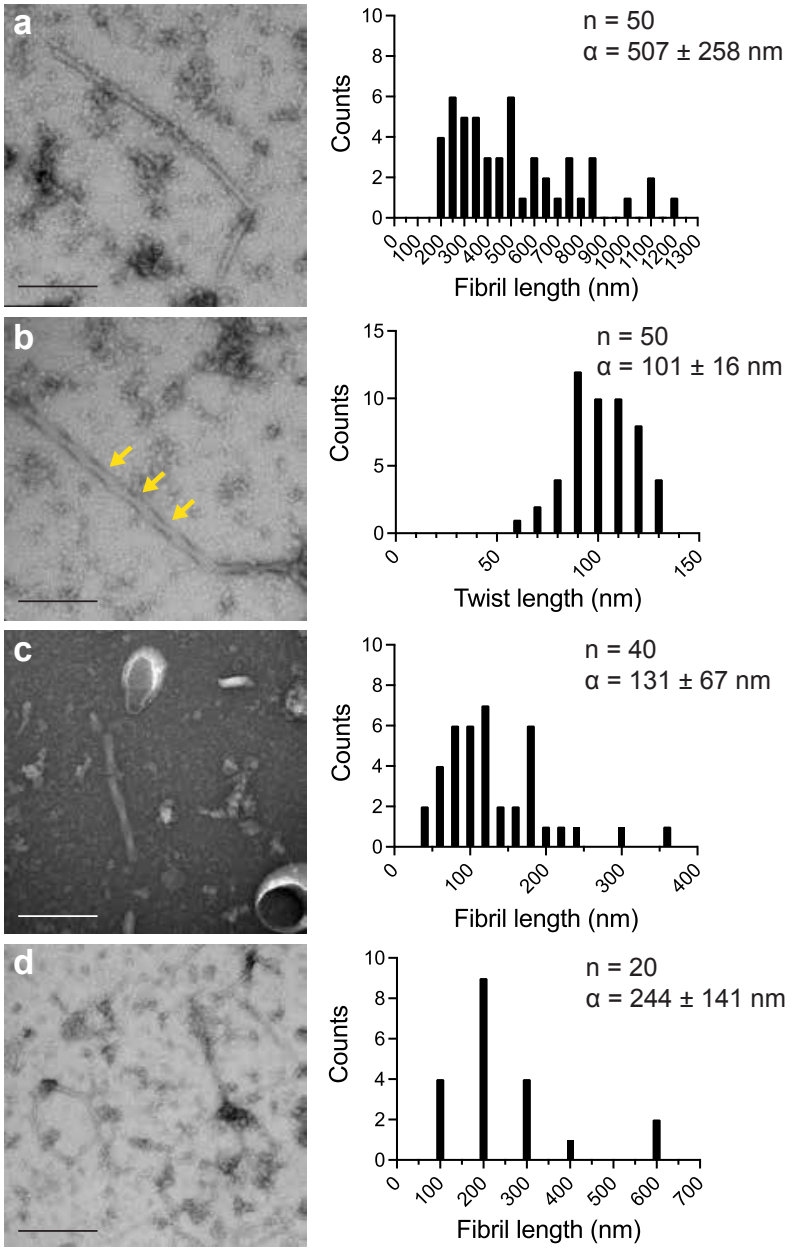

Figure 4.1 **Fibrils extracted from PD brain using different extraction methods. a-d**, TEM images and measurements of the lengths of the fibrils (white arrows) extracted from a PD brain using sarkosyl (**a&b**), RIPA (**c**), and Triton X-100 (**d**). (**a**) Straight and (**b**) twisted fibrils in the sarkosyl-insoluble fraction. Twisted fibrils are marked in yellow arrows and the distribution of the twist length (periodicity) is plotted. (**c&d**) Membranous structures in RIPA and Triton X-100 insoluble fractions are marked in red arrows. n = number of total fibrils counted, α = average length $\pm$ SD (nm), scale bar = 200 nm.

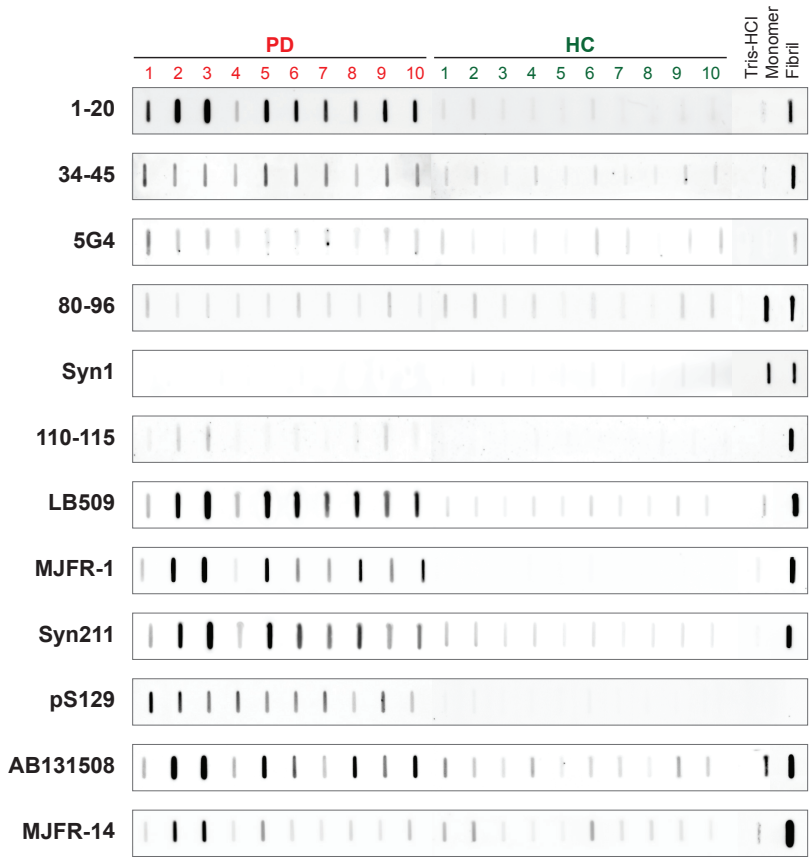

Figure 4.2 Immunoreactivity profiles of αSyn antibodies towards sarkosyl-insoluble αSyn. Slot blots showing immunoreactivity of 12 αSyn antibodies towards sarkosyl-insoluble αSyn from 10 PD and 10 HC brains. A negative control buffer (Tris-HCl), recombinant αSyn monomer (Monomer), and synthetic αSyn fibrils (Fibril) were used as controls. HC, healthy control.

tions. BCA was used to measure the total protein concentrations and 2 µg was loaded for immunoblotting. Tris-HCl (pH 7.4), monomeric recombinant αSyn and synthetic αSyn fibrils were included in the immunoblot as blank and positive controls. The 12 antibodies used in this study recognise epitopes spread across αSyn, specified in Table 3.5. Among these, two antibodies (MJFR-14, 5G4) are aggregate-specific.

The panel of slot blot results are summarised in Fig. 4.2. Antibodies 1-20, LB509, MJFR-1, Syn211, pS129 and AB131508 demonstrated stronger immunoreactivity to sarkosyl-insoluble αSyn from PD brains compared to HC (Fig. 4.3). Notably, antibodies

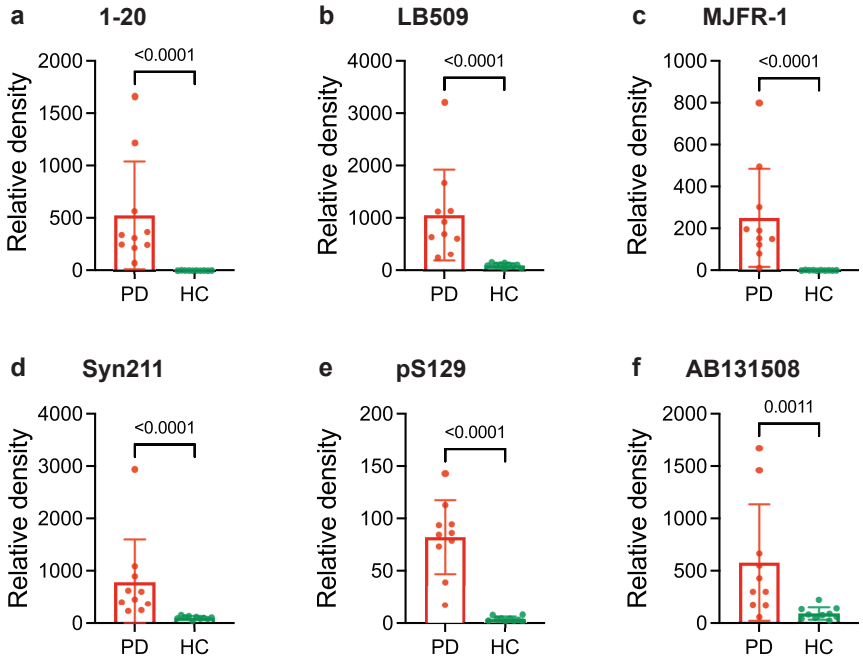

Figure 4.3 **Semi-quantification of antibody immunoreactivity towards sarkosyl-insoluble αSyn. a-f**, Immunoblot densities were measured for αSyn antibodies 1-20 (**a**), LB509 (**b**), MJFR-1 (**c**), Syn211 (**d**), pS129 (**e**), and AB131508 (**f**). These antibodies showed significantly stronger immunoreactivity to the sarkosyl-insoluble αSyn from PD than HC brains. Histograms represent average density with error bars indicating SD. *P*-values were calculated using Mann-Whitney *U* test and indicated on each histogram.

1-20, LB509 and Syn211 exhibited low or no immunoreactivity to the monomeric recombinant αSyn but reacted strongly with synthetic αSyn fibrils, which highlights their specificity towards αSyn fibrils. pS129 did not bind to the monomeric recombinant αSyn due to the absence of phosphorylation. These observations underscore the specificity of 1-20, LB509, MJFR-1, Syn211, pS129 and AB131508 antibodies in detecting pathological αSyn fibrils in PD brains.

In contrast, antibodies 80-96, Syn1 and 110-115 displayed weak immunoreactivity towards sarkosyl-insoluble αSyn from PD (Fig. 4.2). However, these three antibodies strongly detected synthetic fibrils, suggesting structural differences between the human brain-derived and synthetic αSyn fibrils.

The 5G4 antibody showed weak immunoreactivity towards all the samples. Although 5G4 is aggregate-specific, the weak immunoreactivity might be caused by low antibody sensitivity. Also, another aggregate-specific antibody, MJFR-14, did not show distinguishable immunoreactivity between PD and HC. It also weakly detected monomeric recombinant αSyn, suggesting that MJFR-14 does not preferentially detect a single αSyn conformer.

Overall, antibodies 1-20, LB509, MJFR-1, Syn211, pS129 and AB131508 showed preferentially stronger immunoreactivity towards sarkosyl-insoluble αSyn from PD than HC. Interestingly, the aggregate-specific antibodies (MJFR-14, 5G4), 80-96, Syn1 and 110-115 showed no difference between PD and HC.

4.2.3 PK-resistance profiles of sarkosyl-insoluble αSyn from PD brains

αSyn fibrils form a PK-resistant core, and mapping this core can reveal insights into the fibrillar conformation and heterogeneity. Here, 10 µg of the sarkosyl-insoluble fractions were treated with increasing concentrations of PK and the resulting PK-resistant peptides were revealed by Western blot using Syn1 antibody.

The panel of PK-resistance profiles are summarised in Fig. 4.4. When undigested, a smear of bands from 15 to 250 kDa was observed. Also, three additional lower molecular weight (MW) bands between 5-10 kDa were detected in most samples. Upon digestion with the lowest concentration of PK (0.001 mg/ml), the monomeric αSyn band at 15 kDa disappeared in most of the samples, and lower MW bands between 10 and 15 kDa appeared. As the concentration of PK increased from 0.01 to 1 mg/ml, the higher MW smears disappeared and left with a single PK-resistant band of approximately 10 kDa.

Variability among PK-resistance profiles was observed when samples were digested with lower concentrations of PK at 0.001 and 0.01 mg/ml (Fig. 4.4). Specifically, when digested with 0.001 mg/ml of PK, samples 1,2 and 10 revealed a single PK-resistant band around 11 kDa. Others revealed more than a single band that ranges from 8 to 15 kDa.

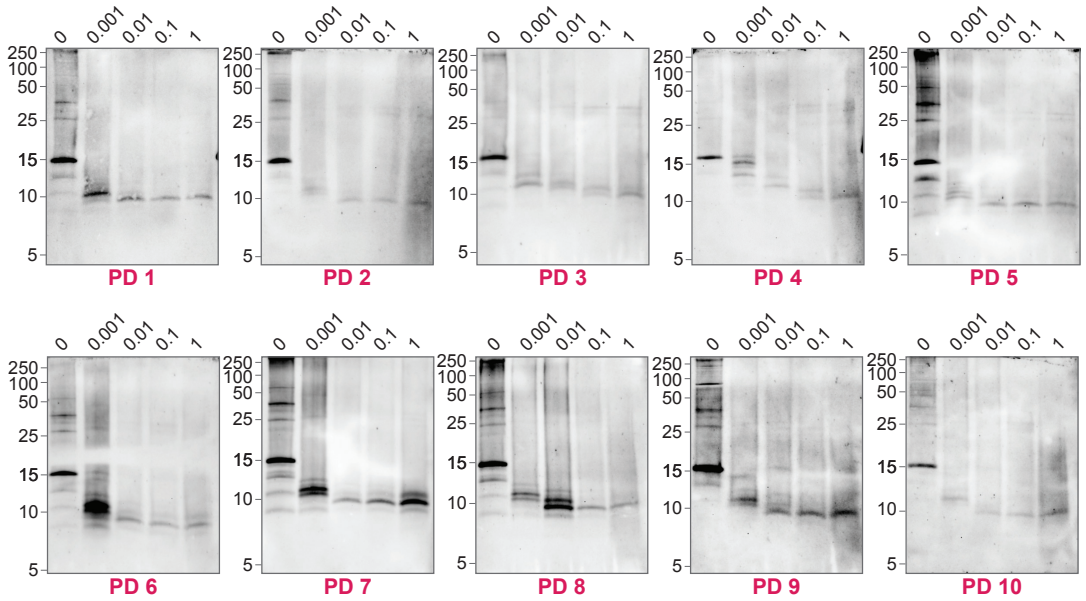

Figure 4.4 PK-resistant αSyn peptides. Immunoblots showing PK-resistant αSyn peptides from 10 PD brains. αSyn fibrils were subjected to increasing concentrations of PK (0, 0.001, 0.01, 0.1, and 1 mg/ml). PK-resistant species were characterised by Western blotting with Syn1. Molecular weights are indicated on the left of each immunoblot.

In addition, at 0.01 mg/ml of PK, samples 1, 2, 5, 6, 7, 9 and 10 revealed a single PK-resistant band near 10 kDa. Samples 3 and 4 showed a PK-resistant band of 12 kDa. Sample 8 showed a strong smear of bands and multiple PK-resistant bands ranging from 9 to 12 kDa.

Findings demonstrate that the strongest PK treatment reveals a common PK-resistant core among all the fibrils, and using a weaker PK concentration exposes the variability in PK resistance in different cases. The heterogeneous PK resistance fingerprints of αSyn fibrils uncover the structural variability of the αSyn fibrils, which may be correlated with distinct clinical phenotypes of PD.

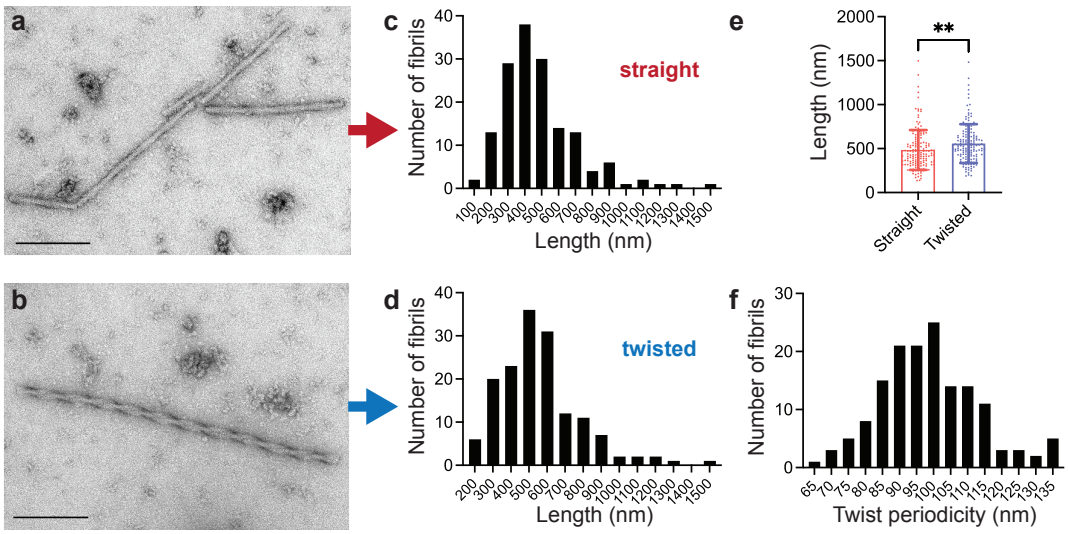

Figure 4.5 **Morphologies of the αSyn fibrils from PD brains.** **a&b**, TEM images of the straight (**a**) and twisted (**b**) fibrils from PD brains. **c&d**, Length distribution of the straight (**c**) and twisted (**d**) fibrils. **e**, Twisted fibrils are significantly longer than straight fibrils. Histograms represent the average, and the error bars indicate SD. Mann-Whitney *U* test was used. $P^{**} < 0.01$. **f**, Distribution of the twist periodicity of the twisted fibrils. Scale bar = 200 nm.

4.2.4 αSyn fibrils from PD brains exhibit straight and twisted morphologies

Subsequently, the sarkosyl-insoluble αSyn fibrils were subjected to negative staining and visualised using TEM. At high magnification, two dominant morphologies were observed: straight and twisted (Figs. 4.5a&b). A total of 155 fibrils (approximately 15 for each PD case) of each morphology were imaged and analysed using ImageJ software.

The straight fibrils exhibited an average length of 484 $\pm$ 226 nm (SD) (Fig. 4.5c), while the twisted fibrils had a longer average length of 557 $\pm$ 221 nm (Fig. 4.5d). Notably, the twisted fibrils were significantly longer than the straight fibrils (Fig. 4.5e). Moreover, the twist periodicity of the twisted fibrils averaged 98 $\pm$ 14 nm (Fig. 4.5f). These observations from TEM demonstrate the morphological variability of αSyn fibrils, further highlighting the complex population of αSyn fibrils.

4.2.5 Structural characterisation of αSyn fibrils using immunogold-TEM

To confirm that the fibrils observed using TEM are αSyn, immunogold TEM was performed using the 12 sets of antibodies previously assessed by immunoblot. The specific dilutions used are outlined in Table 3.6.

Antibodies targeting the N-terminus of αSyn (1-20 and 34-45) displayed strong immunolabelling towards straight fibrils (Fig. 4.6). However, 34-45 also labelled the background, potentially indicating the presence of smaller monomers or oligomers. Additionally, only 34-45 labelled the twisted fibrils out of all the antibodies tested. Antibodies 80-96 and Syn1, which target the NAC region of αSyn, did not exhibit any immunolabelling towards straight and twisted fibrils (Fig. A.1). Among the six antibodies with epitopes against the C-terminus of αSyn (110-115, LB509, MJFR-1, Syn211 and Ab131508), only MJFR-1 and Ab131508 showed immunolabelling towards straight fibrils, but not the twisted (Fig. 4.6). None of the C-terminus antibodies labelled the twisted fibrils. The aggregate-specific antibody 5G4 did not label any fibrils (Fig. A.1). MJFR-14 labelled the straight fibrils but not the twisted ones (Fig. 4.6). Similarly, the pS129 antibody displayed strong immunolabelling towards the straight fibrils and not the twisted (Fig. 4.6).

The observations from immunogold TEM provide multiple indications of the structure of the αSyn fibrils. The lack of labelling from the NAC-region-specific antibodies suggests that this region is embedded in the core of both straight and twisted fibrils. The N-terminal and C-terminal ends seem more exposed in the straight fibrils, whereas they are more embedded in the twisted fibrils. Also, the straight fibrils are phosphorylated, and the twisted are not, but this epitope could be embedded, restricting antibody labelling.

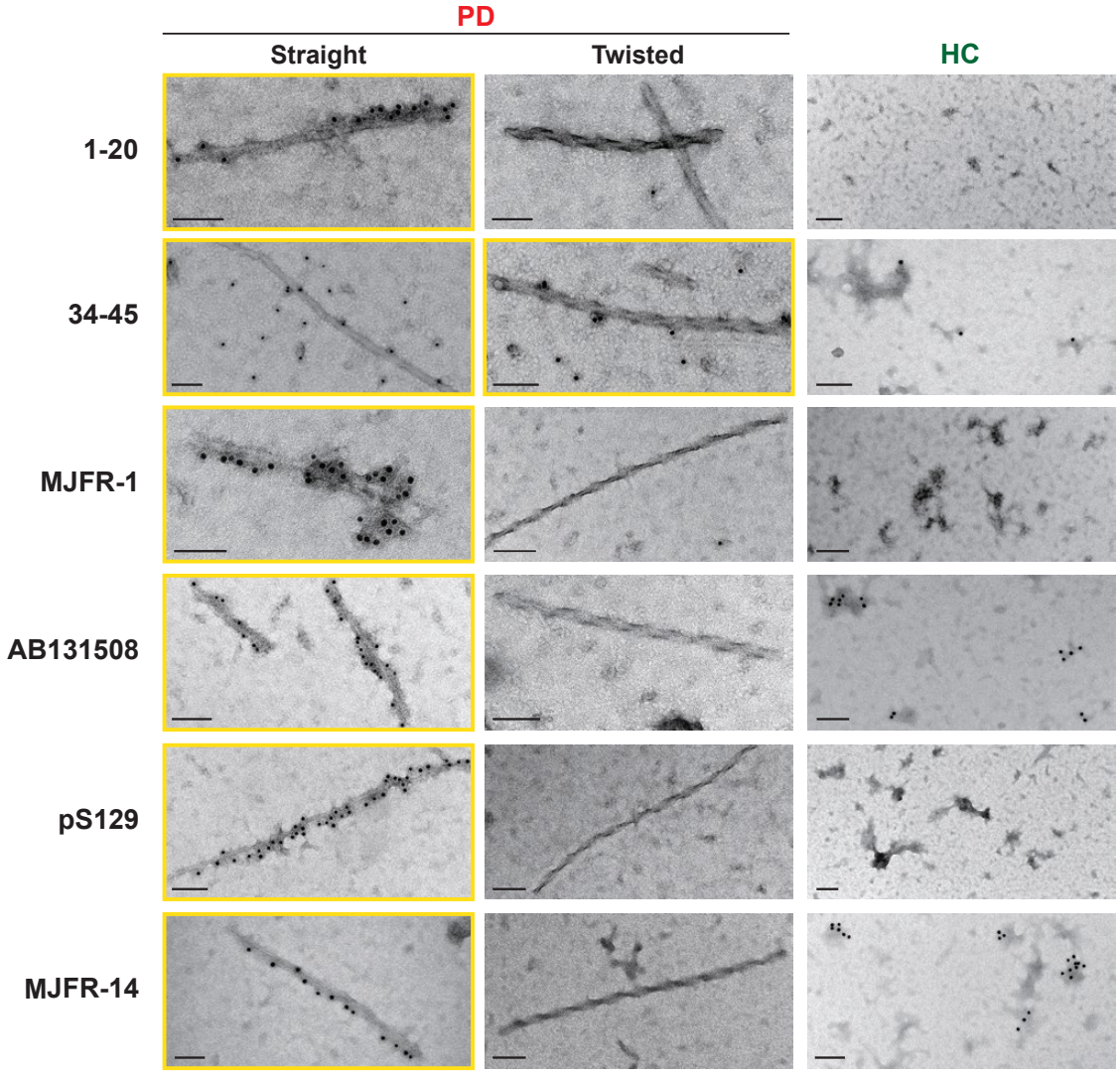

Figure 4.6 Immunogold labelling of different antibodies towards αSyn fibrils from PD brains. Immunogold-TEM images showing the different immunolabelling patterns of αSyn antibodies (1-20, 34-45, MJFR-1, AB131508, pS129, MJFR-14) to αSyn fibrils (straight and twisted). Immunogold labelled fibrils are highlighted in yellow boxes. Sarkosyl-insoluble fraction from HC brain was used as a negative control. Scale bar = 100 nm.

4.3 Discussion

Recent studies have evaluated the atomic structures of human brain-derived αSyn fibrils, contributing to our understanding of their heterogeneity and αSyn strains[85,104,115]. This study further expands on this knowledge by investigating the biochemical and biophysical characteristics of the αSyn fibrils in PD brains.

The sarkosyl extraction method, consistent with previous studies[85,104,110,115], yielded a relatively clean fraction of intact αSyn fibrils. The sarkosyl-insoluble fraction contained more fibrils with intact structures than the RIPA and Triton X-100-insoluble fractions, indicating the enhanced preservation and isolation of fibrils achieved by the sarkosyl method. The differences in the detergent-insoluble fraction might result from multiple variables, such as the ultracentrifugation protocols and wash steps. Also, the ionic nature and the mild denaturing strength of sarkosyl might make it an effective agent for αSyn fibril extraction from the human brain.

Profiling the immunoreactivity of αSyn antibodies against sarkosyl-insoluble αSyn revealed the specificity of the N and C-terminal antibodies towards that of PD. In contrast, the NAC region and aggregate-specific antibodies failed to show differential immunoreactivity between PD and HC.

These findings align with cryo-EM studies, which reported that residues 1-30 and 101-140 extend from the 'Lewy fold' core of PD αSyn fibril and are accessible for antibody detection[104]. Antibodies 1-20, LB509, MJFR-1, Syn211, pS129 and AB131508, which target these residues, demonstrated strong immunoreactivity to αSyn fibrils from PD. Interestingly, although residues 34-45 form a β-strand, five residues (K34, V37, Y39, K43, and K45) form a cavity where the 34-45 antibody might be able to engage with the exposed residues[104]. The 110-115 antibody showed strong immunoreactivity to the synthetic αSyn fibril but weak towards the PD αSyn fibrils. Its contrasting immunoreactivity might indicate structural differences in the 110-115 region between the synthetic and brain-derived αSyn fibrils.

Furthermore, antibodies 5G4, 80-96 and Syn1, exhibited weak immunoreactivity towards sarkosyl-insoluble αSyn from PD, likely due to epitope inaccessibility. The aggregate-specific antibody MJFR-14, despite its conformation-specific epitope, did not show a significantly stronger immunoreactivity to PD than HC. As MJFR-14 detects monomeric αSyn, the immunoreactivity towards the HC samples likely resulted from monomer recognition. Indeed, conformational-specific antibodies do not show preferential specificity towards a single αSyn species[190]. The findings also illustrate the complex composition of human brain-derived sarkosyl-insoluble fraction, which might not be a pure αSyn fibrillar fraction, unlike the in vitro-generated synthetic fibrils[191].

The PK resistance of PD αSyn fibrils revealed distinct molecular fingerprints of different PD cases. A 10 kDa PK-resistant peptide, potentially representing a common core in PD αSyn fibrils, was exposed in all cases with the strongest PK treatment. This core might correspond to the 'Lewy fold' residues 31-100, according to the cryo-EM structure[104]. In addition, at lower PK concentrations, a ladder of bands below 15 kDa was observed, which aligns with previous findings[110]. Also, variations in PK resistance were more evident at the lowest PK concentration, where different cases showed distinct numbers of PK-resistant peptides with varying sizes. Similarly, Guo and colleagues reported, using five PDD brains, variations in the PK-digestion profiles of the sarkosyl-insoluble αSyn fibrils[109]. For future investigation, it is vital to build PK profiles of more cases to confirm whether the biochemical fingerprint represents distinct αSyn strains.

Lastly, TEM revealed two predominant αSyn fibril morphologies: straight and twisted. Previously, straight and twisted structures have been characterised using TEM in DLB brains, but not in PD[107]. Immunogold-TEM revealed additional structural information, such as the exposed regions on the fibrils (amino acid sequences 1-20, 34-45, 118-123 and 134-138). It also suggested that the unlabelled epitopes may be core-embedded. Antibodies LB509 and Syn211 showed different immunoreactivity in slot blot and immunogold-TEM. They demonstrated strong immunoreactivity towards the

sarkosyl-insoluble αSyn from PD in slot blot but failed to label the fibrils in immunogold-TEM. These differences may be attributed to these antibodies labelling the non-fibrillar αSyn conformers on slot blot. The sarkosyl-insoluble fraction could contain non-fibrillar αSyn aggregates, which cannot be distinguished on slot blot, but on TEM, it is possible to visualise and select fibrils.

4.3.1 Experimental limitations

Using sarkosyl-based isolation of αSyn fibrils requires careful consideration while interpreting results from this chapter. Different αSyn strains demonstrate distinct sarkosyl solubility[192]. Using sarkosyl might have resulted in a selective isolation of specific αSyn fibril populations. Therefore, it must be noted that the sarkosyl-insoluble fibrils characterised in this chapter may not be representative of the larger population of fibrils that includes the sarkosyl-soluble.

In addition, the PK-resistant peptides of αSyn fibrils were examined using a single antibody Syn1. As a result, PK profiling was limited to peptides containing the 91-99 region. The peptides without the 91-99 region were left undetected. Thus, additional analysis is required using various antibodies targeting different regions on αSyn such as LB509 and LASH1-20 (C- and N-terminus). Fingerprints from different antibodies would provide more complete and representative profiles of the PK-resistant peptides.

Lastly, TEM imaging inherently offers limited structural resolution and two-dimensional visualisation. Consequently, this chapter could only categorise fibrillar structures into two broad categories: straight and twisted. While these classifications provide valuable insights, they may not capture the full spectrum of atomic-level structures of fibrils. Advanced techniques such as cryo-EM would be indispensable for a more high-resolution structural characterisation.

4.3.2 Summary

This chapter underscores the utility of biochemical and biophysical methodologies in characterising PD brain-derived αSyn fibrils. αSyn antibodies serve as potent tools for identifying pathological αSyn and evaluating fibril structures. PK-resistance profiles revealed unique biochemical fingerprints of αSyn fibrils, which require further characterisation with different αSyn antibodies. Concurrently, TEM demonstrated the morphological heterogeneity of αSyn fibrils from PD brains. These observations enhance the understanding of brain-derived αSyn fibrils. Creating a library of the molecular fingerprints of brain-derived αSyn fibrils could facilitate molecular characterisation of distinct synucleinopathies and build evidence of distinct αSyn strains.

Chapter 5

Brain-derived and in vitro-seeded αSyn fibrils exhibit distinct biochemical and biophysical profiles

5.1 Introduction

αSyn strains have been extensively characterised in αSyn fibrils generated in vitro under various experimental conditions [92,97,100,101,193]. However, to what extent the in vitro fibrils reflect the human αSyn fibrils remains questionable. To address this problem, a number of studies demonstrated the evidence of αSyn strains in the human brain by investigating the structures[85], infectivity in vitro[186,187,194], and animals[92,121,195]. Nevertheless, further work is required to systemically investigate different fingerprints of human brain-derived αSyn strains and their correlation to different synucleinopathies.

Due to its versatility, the seed amplification assay (SAA) has become a useful tool to amplify in vitro-seeded αSyn fibrils (SAA fibrils) using human biosamples to seed the reaction. The seeding mechanism of SAA is hypothesised to generate SAA fibrils that encode the intrinsic properties of the original pathological αSyn that seeds the amplification. Therefore, it has been assumed that the SAA fibrils replicate the endogenous and

pathological αSyn in the human system. As a result, studies have been utilising the SAA fibrils to characterise αSyn strains[116,117,159,196]. Nevertheless, recent studies highlighted the significant differences between the human brain-derived and SAA fibrils in structure and the pathology induced in vivo[115,117]. The differences are discussed in detail in Chapter 2.3. However, there is a limited understanding of whether the SAA fibrils preserve not only the structure but also the biochemical and biophysical properties of the seed fibrils.

This chapter explores the biochemical and biophysical characteristics of brain-derived αSyn strains among different synucleinopathies. Also, the SAA fibrils were examined to assess whether they maintain the strain-like properties of the brain-derived αSyn fibrils. The aims of this chapter were the following:

1. Investigate the biochemical and biophysical properties of the brain-derived αSyn fibrils in PD, PDD, DLB and MSA to identify evidence indicating the presence of αSyn strains.

2. Compare the biochemical and biophysical properties of the brain-derived and the SAA αSyn fibrils and examine whether the SAA fibrils replicate these properties of the brain-derived fibrils.

5.2 Results

5.2.1 Brain-derived αSyn fibrils from PD, PDD, DLB, and MSA display distinct seeding activity

αSyn fibrils were extracted from the frozen brains of patients diagnosed with PD (n = 3), PDD (n = 3), DLB (n = 3), MSA (n = 3), and healthy controls (n = 3) as specified in Table 3.2. The entorhinal cortex, the primary region affected by αSyn pathology in each disorder, was selected for PD, PDD and DLB, while the striatum was used for MSA. These brain-derived fibrils served as seeds in an SAA reaction to produce in vitro amplified fibrils (SAA fibrils).

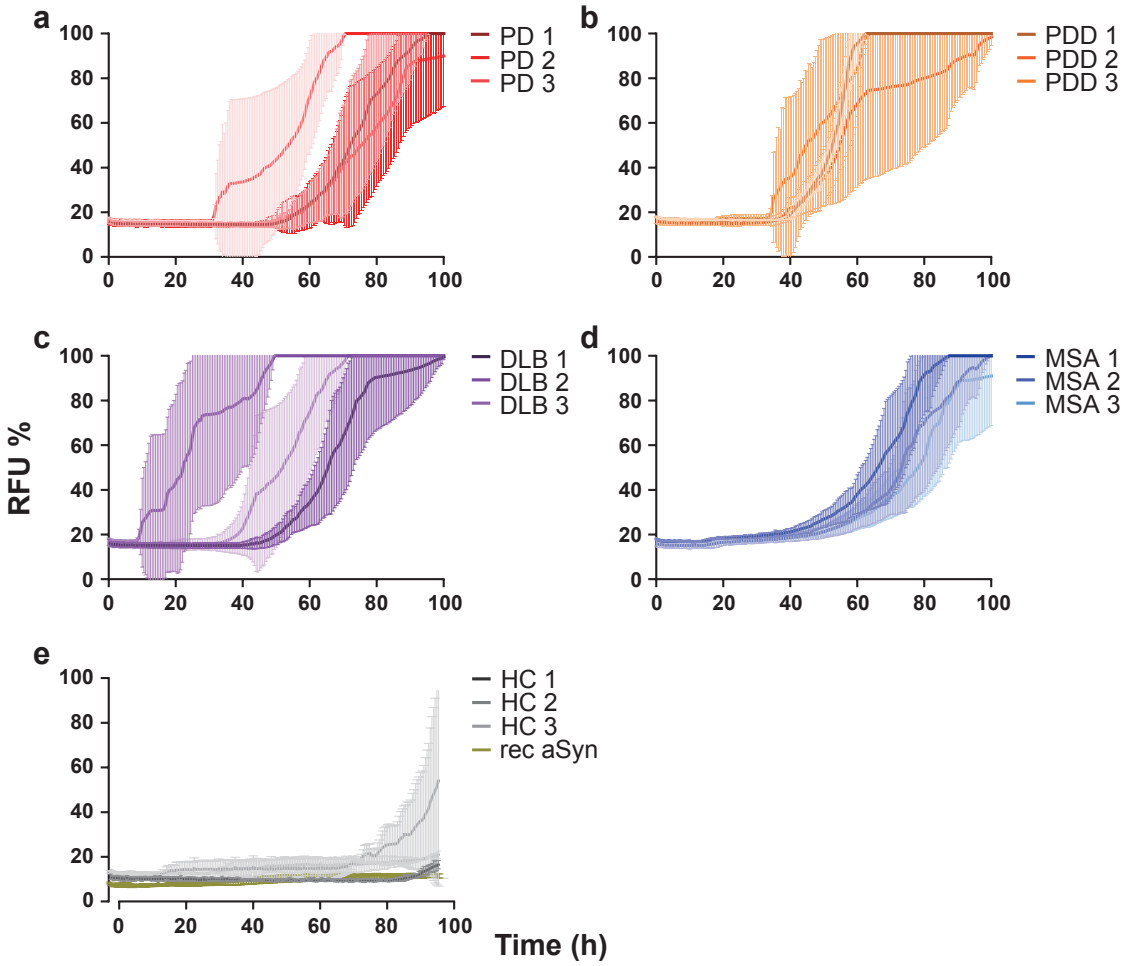

Figure 5.1 **SAA seeded with αSyn fibrils from different synucleinopathies. a-e**, SAA reactions seeded with sarkoyl-insoluble αSyn fibrils from PD (n = 3) (**a**), PDD (n = 3) (**b**), DLB (n = 3) (**c**), MSA (n = 3) (**d**), and HC (n = 3) (**e**) brains. (**e**) Recombinant αSyn represents a negative control reaction without seeds. Each case was repeated in six replicates and averaged into a single curve with error bars indicating standard deviation.

Brain-derived fibrils from PD, PDD, DLB and MSA reached peak ThT fluorescence within 100 hr (Figs. 5.1a-d). Healthy controls exhibited no seeding potential, except case 2 (HC 2), which showed an increasing signal towards the end of the reaction (approximately 91 hours) as shown in Fig. 5.1e. Kinetic parameters revealed a significant difference in seeding activities between PD/MSA and PDD/DLB. The time to reach 50% of maximum fluorescence (T_{50}) and the lag phase, the time to reach 5 standard deviations

(SD) from the average minimum fluorescence[112], were significantly lower in PDD/DLB than in PD/MSA (Figs. 5.2a&b). Consequently, the area under the curve (AUC) was statistically higher in PDD/DLB than in PD/MSA (Fig. 5.2c). However, other parameters such as the maximum rate of increase in fluorescence (V_{max}), did not significantly differ among the diseases. In summary, SAA kinetic parameters suggest that brain-derived fibrils from PDD and DLB possess a more aggressive seeding capacity than those from PD and MSA.

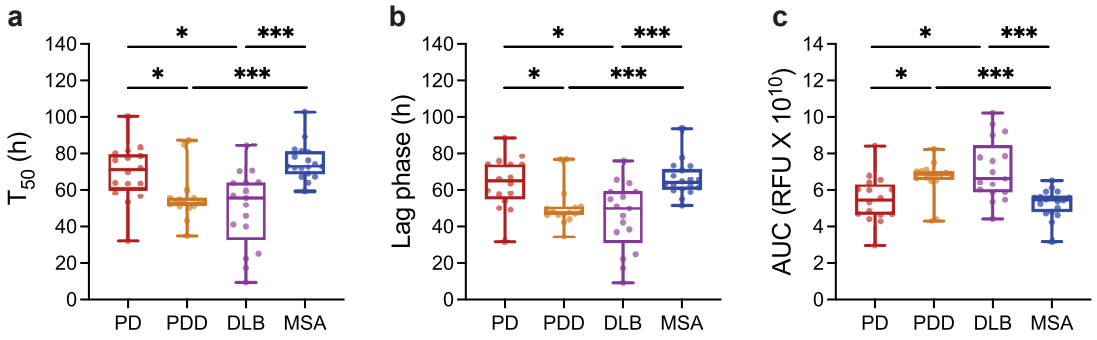

Figure 5.2 **SAA reaction kinetics.** **a-c**, Calculation of the SAA reaction kinetics T_{50} (**a**), lag phase (**b**) and area under the curve (AUC) (**c**) from the reaction curves of PD, PDD, DLB and MSA. Mann-Whitney U test was used for statistical comparison. $*P \leq 0.05$, $***P \leq 0.005$.

5.2.2 Brain-derived and SAA αSyn fibrils show distinct biochemical profiles

Upon completion of the SAA reaction, SAA fibrils were concentrated via ultracentrifugation. Given that prion strains can be distinguished by unique biochemical profiles[92,111,197], these characteristics were examined in the brain-derived and SAA fibrils. The fibrils were denatured with increasing concentrations of guanidine hydrochloride (GdnHCl, 0-5 M), followed by digestion with proteinase-K (PK, 1 µg/ml).

First, examining the brain-derived fibrils, the mildest GdnHCl treatment (1 M) en-

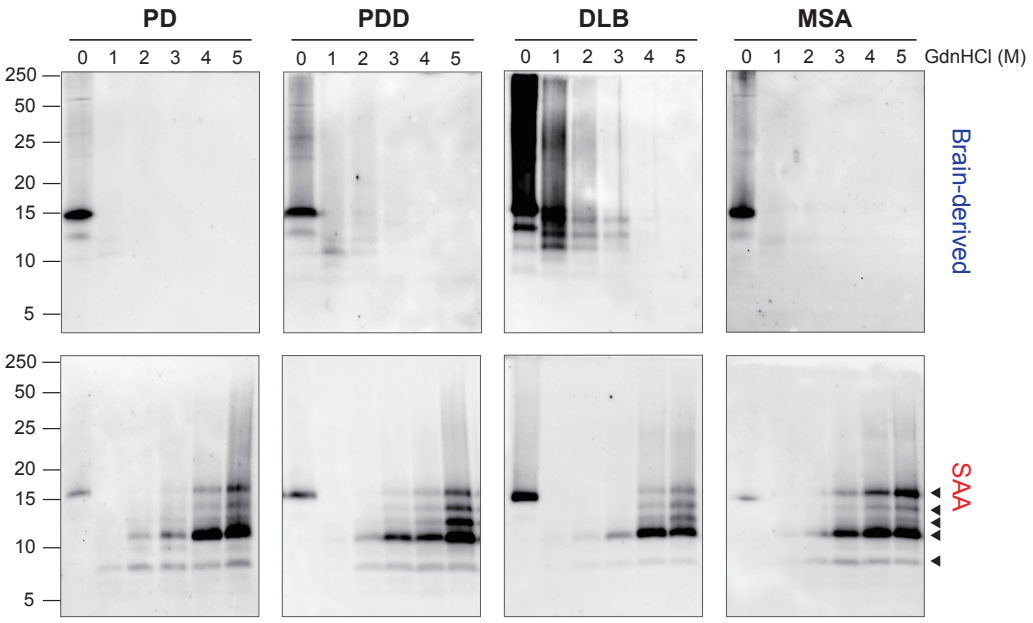

Figure 5.3 Biochemical differences between brain-derived and SAA αSyn fibrils. Brain-derived and SAA fibrils were digested with increasing concentrations of GdnHCl (1-5 M), 1 µg/ml of PK, and resolved with Western blot using Syn1 (BD Biosciences) antibody. The 0 M GdnHCl represents a non-treated, raw sarkosyl-insoluble sample (no PK digestion). Results from one representative case are shown. Black triangles mark the five unique PK-resistant peptides in the SAA fibrils. Molecular weights (kDa) are indicated on the left of the immunoblot.

tirely denatured the PD and MSA fibrils, as shown in the immunoblots in Fig. 5.3. Higher GdnHCl concentrations of 2 M and 3 M denatured PDD and DLB brain-derived fibrils (Fig. 5.3). These observations were consistent across all three cases analysed (Figs. A.2a-d). These results underscore that PD and MSA brain-derived fibrils exhibit lower biochemical stability than PDD and DLB.

Comparative study of the brain-derived fibrils across synucleinopathies was limited by the fast denaturation of the fibrils following GdnHCl treatment. To enhance the visualisation of the biochemical profiles, the experiment was repeated using only PK. The fibrils were subjected to five PK concentrations: 0, 0.001, 0.01, 0.1 and 1 mg/ml. At 0 mg/ml PK, PD revealed a monomeric band (15 kDa), which degraded instantly at the

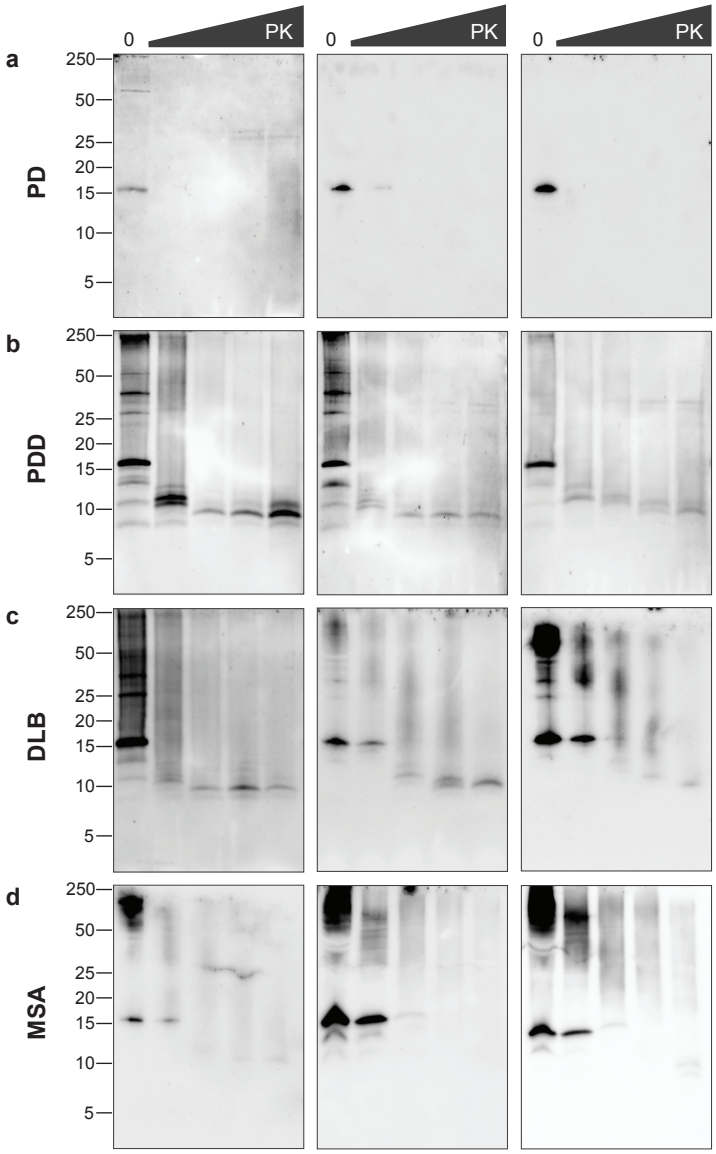

Figure 5.4 PK-resistance profiles of brain-derived αSyn fibrils. Brain-derived αSyn fibrils from PD, PDD, DLB, and MSA were digested with increasing concentrations of PK (0, 0.001, 0.01 0.1 and 1 mg/ml) and resolved with Western blot using Syn1 (BD Biosciences) antibody. Black triangles on the top of the immunoblot indicate increasing PK concentrations. Molecular weights (kDa) are indicated on the left of the immunoblot.

lowest PK concentration (0.001 mg/ml) (Fig. 5.4a). PDD, DLB, and MSA fibrils at 0 mg/ml PK revealed high MW bands above 15 kDa, as seen in Figs. 5.4b-d, indicative of

αSyn aggregates. Additionally, lower MW bands (∼13, 10, 7 kDa) were also detected. As the PK concentration increased, the PDD and DLB fibrils gradually degraded, with high MW bands starting to disappear and low MW bands below 15 kDa beginning to appear (Figs. 5.4b&c). The MSA fibrils also gradually degraded as the PK concentration increased (Fig. 5.4d), but low MW bands below 15 kDa were less prominent compared to those of PDD and DLB.

Despite using an identical amount of total protein (10 µg) in the experiments, the quantity of αSyn fibril could vary in each sarkosyl-insoluble fraction. Immunohistochemistry revealed a lower burden of αSyn pathology in PD brains than in PDD, DLB and MSA brains (Fig. A.3). Additionally, immunogold-TEM images using pS129 antibody in Fig. A.4 revealed that PD and MSA cases contain less number of phosphorylated fibrils than PDD and DLB at a given magnification. Therefore, the lower amount of αSyn fibrils in the PD and MSA brains could have contributed to the higher vulnerability against protein denaturation and digestion.

The biochemical profiles of SAA fibrils displayed significant differences compared to the brain-derived fibrils. Immunoblots in Fig. 5.3 illustrate that all the SAA fibrils from PD, PDD, DLB and MSA demonstrate identical biochemical profiles. PK-resistant bands of 7 and 10 kDa began to appear following treatment with 2 M GdnHCl. However, as the concentrations of GdnHCl increased, specific PK-resistant peptides appeared, consisting of five bands (∼7, 11, 12, 13, 14 kDa). These observations suggest stronger denaturing conditions are required to destabilise the SAA fibrils and expose PK digestion sites. In conclusion, SAA fibrils were more conformationally stable and characterised by distinct biochemical properties than the brain-derived fibrils.

5.2.3 Distinct morphologies of brain-derived and SAA αSyn fibrils revealed by TEM

Next, the morphologies of the brain-derived and SAA fibrils were investigated using TEM. Brain-derived fibrils from PD, PDD and DLB displayed two morphologies: straight

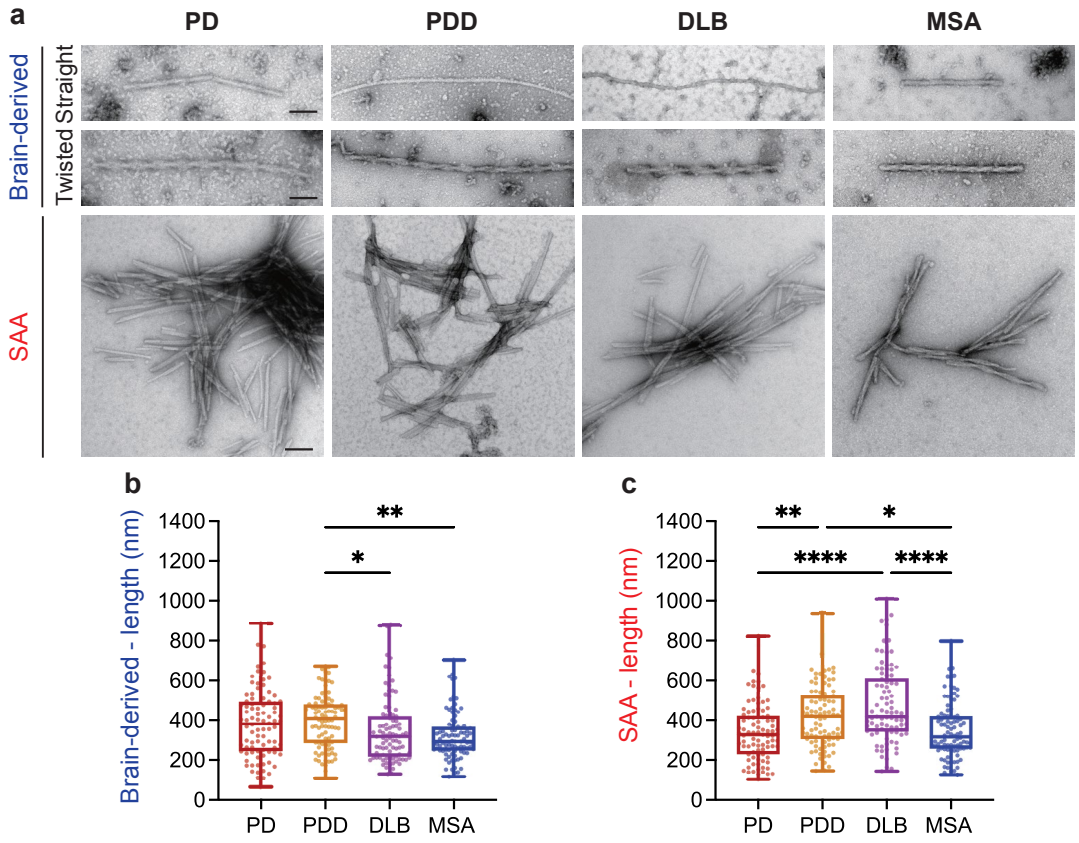

Figure 5.5 **Brain-derived and SAA αSyn fibrils show distinct morphologies.** **a**, TEM images illustrating the structures of the brain-derived and SAA fibrils. Brain-derived fibrils displayed two distinct structures: straight and twisted. Scale bar = 50 nm. **b&c**, Lengths of the brain-derived (**b**) and SAA (**c**) fibrils. A total of 30 fibrils were measured for each disease case. Mann-Whitney U test was used for statistical comparison. *$P \leq 0.05$, **$P \leq 0.01$, ****$P \leq 0.001$.

and twisted, while fibrils from MSA were predominantly straight with rarely twisted forms (Fig. 5.5a). Consequently, only straight fibrils were selected to measure their lengths, presented in Fig. 5.5b. Fibril lengths varied between 68 to 885 nm, with PDD fibrils significantly longer than those from DLB and MSA.

In contrast, SAA fibrils exhibited a single dominant structure. PD, PDD and DLB SAA fibrils were straight, while MSA SAA fibrils were twisted (Fig. 5.5a). Also, the SAA fibrils were clustered, while the brain-derived fibrils existed in singular filaments. The lengths ranged from 104 to 1008 nm, with PDD/DLB SAA fibrils significantly longer

than those from PD/MSA (Fig. 5.5c). Interestingly, the differences in lengths follow the pattern of SAA kinetic differences shown in Fig. 5.2. This suggests that the SAA reaction kinetics might determine the length of the SAA fibrils. Also, no significant differences in lengths were found between the brain-derived and SAA fibrils, except for DLB, where the SAA fibrils were significantly longer (Fig. A.5a). The widths of the brain-derived and SAA fibrils are significantly different for PDD and DLB (Fig. A.5b). Overall, the results demonstrate that the SAA fibrils do not replicate the structures of the brain-derived fibrils, and SAA reaction kinetics affects the SAA fibrillar dimensions.

5.2.3.1 Brain-derived and SAA αSyn fibrils exhibit dissimilar phosphorylation patterns

The fibrils imaged by TEM were confirmed as αSyn fibrils through immunogold labelling with αSyn fibril conformation-specific (MJFR-14) and pS129-specific (pS129) antibodies. As illustrated in Fig. 5.6a, MJFR-14 and pS129 antibodies showed strong immunoreactivity to the straight brain-derived fibrils across all synucleinopathies. However, the twisted brain-derived fibrils were not labelled by either MJFR-14 or pS129 (Fig. 5.6b). Slot blot results in Fig. 5.7a confirmed the immunogold-TEM results.

The immunogold TEM images of the SAA fibrils shown in Fig. 5.6a illustrate strong MJFR-14 labelling, also confirming that the fibrils are αSyn. However, pS129 labelling was absent in PD and MSA SAA fibrils, but weak labelling was observed in PDD and DLB SAA fibrils. Slot blots in Fig. 5.7b, performed with the same antibodies, confirmed these immunogold-labelling results. The pS129 showed immunoreactivity to the SAA fibrils from PDD and DLB but not with those of PD and MSA.

The immunoreactivity of pS129 towards the SAA fibrils differed significantly from the brain-derived fibrils. However, interestingly, for both brain-derived and SAA fibrils, the amount of phosphorylated fibrils was higher in PDD/DLB than in PD/MSA (Figs. 5.7a&b). Findings suggest that when a significant amount of phosphorylated seeds are present, the phosphorylation may be incorporated into the newly amplifying fibrils.

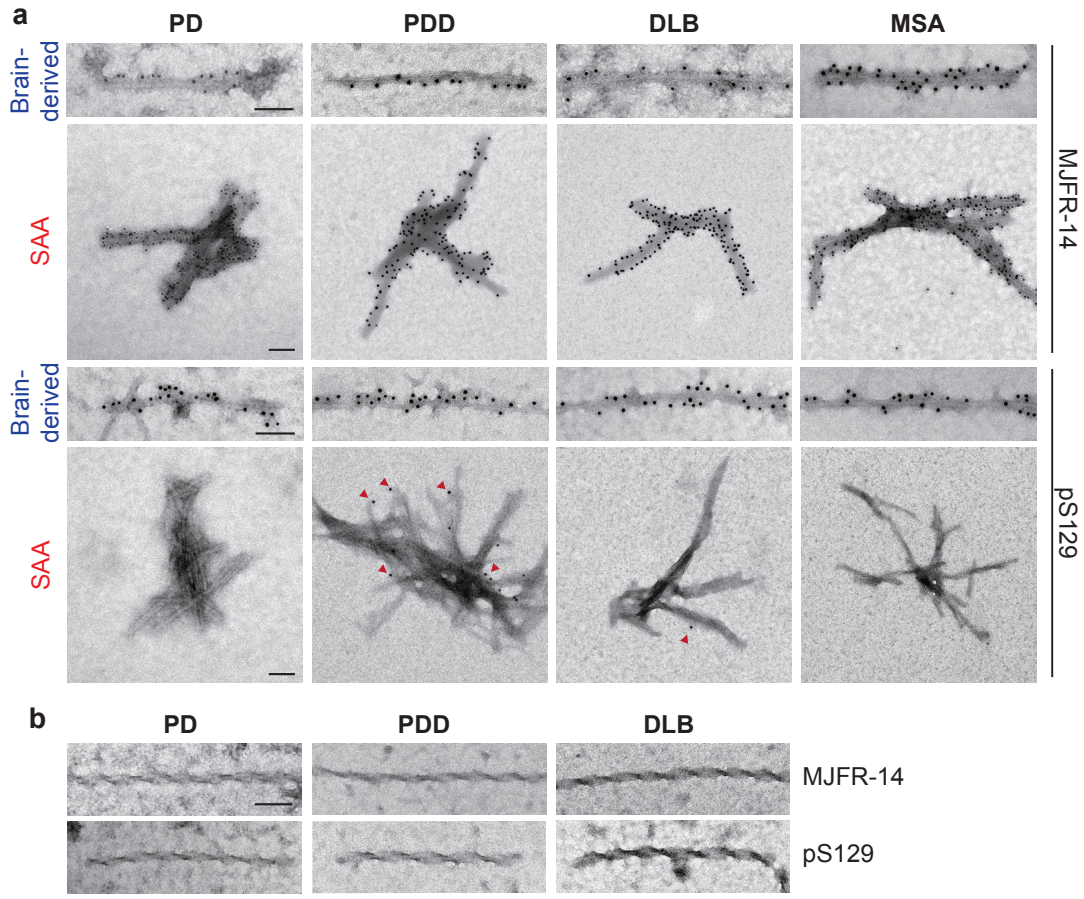

Figure 5.6 **Differences in phosphorylation between brain-derived and SAA αSyn fibrils. a**, TEM images illustrating the brain-derived and SAA fibrils labelled with MJFR-14 and pS129 antibodies. The red arrows indicate pS129 immunogold labelling on the SAA fibrils. **b**, The twisted brain-derived fibrils were not labelled with MJFR-14 and pS129 antibodies. Scar bar = 50 nm.

5.3 Discussion

5.3.1 Investigation of biochemical and biophysical properties of brain-derived αSyn fibrils from different synucleinopathies.

This study investigated the biochemical and biophysical properties of brain-derived αSyn fibrils from different synucleinopathies. The fibrils from demented brains (PDD and DLB) exhibited faster seeding kinetics, whereas the PD and MSA fibrils showed milder

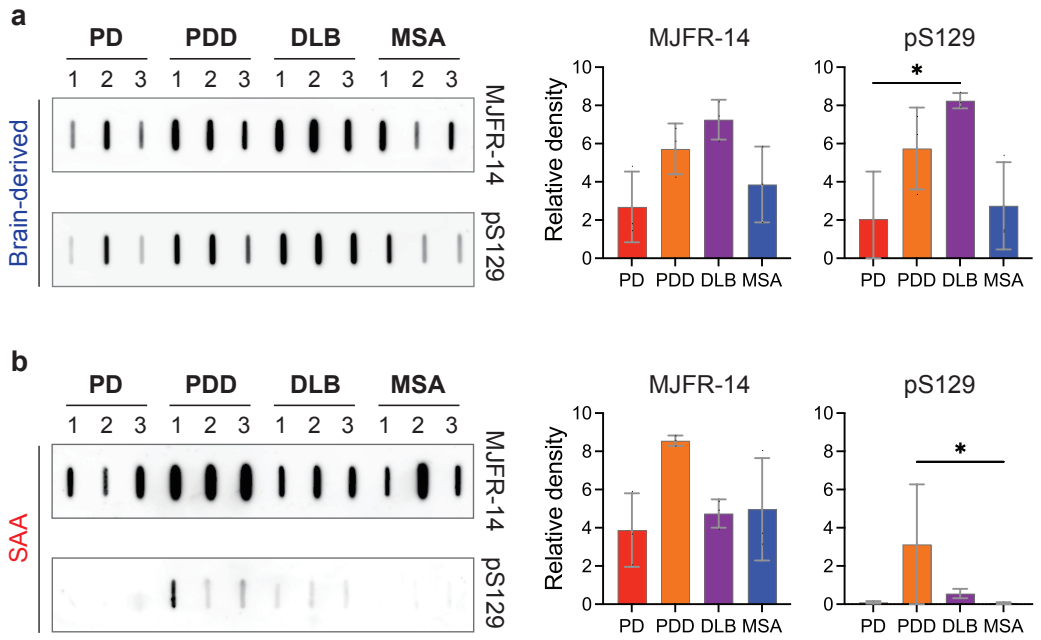

Figure 5.7 **Quantification of phosphorylated αSyn in brain-derived and SAA fibrils. a,b**, Semi-quantification of the immunoreactivity of MJFR-14 and pS129 towards brain-derived (**a**) and SAA (**b**) fibrils. The averages of the three cases are presented with error bars indicating standard deviation. Mann-Whitney U test was used for statistical comparison. $^*P \leq 0.05$.

seeding capacity. The aggregation kinetics were not distinguishable between PD and MSA in the SAA reaction, unlike previous CSF αSyn SAA studies[111,112]. It must be noted that the choice of biosample significantly affects the seeding kinetics[198]. Here, the isolation of sarkosyl-insoluble αSyn species allowed selective assessment of the seeding kinetics of pathological αSyn fibrils.

A potential correlation between the amount of phosphorylated αSyn (p-αSyn) and rapid seeding kinetics was observed in this study. Previous studies have shown conflicting roles of p-αSyn in αSyn aggregation, with some suggesting an enhancing effect[199,200] and others a potential neuroprotective role[201,202]. Findings in this chapter suggest that a higher amount of p-αSyn could be associated with the aggressive seeding kinetics observed in PDD and DLB brain-derived fibrils.

Furthermore, the amount of p-αSyn has been shown to correlate with the disease du-

ration of synucleinopathies. Higher amounts of accumulated p-αSyn fibrils were reported in demented brains of PDD and DLB than in PD without dementia and MSA[110,203]. The patients with PDD and DLB in this study had longer disease duration than those with PD and MSA, indicating a possible correlation between p-αSyn and disease duration. Indeed, an inverse relationship between the level of non-p-αSyn and disease duration has been characterised previously[202]. This suggests that p-αSyn might accumulate in a time-dependent manner and contribute to the development of αSyn strain-like properties.

Interestingly, PD and MSA fibrils were more susceptible to GndHCl denaturation, which might indicate their conformational instability. This aligns with previous findings that DLB brain-derived αSyn fibrils were more stable than those of MSA[92]. Also, the less stable MSA fibrils propagated faster in TgM83 mice than the more stable DLB fibrils. Such inverse correlation between conformational stability and disease propagation has been characterised in prion disease[204]. Therefore, our findings on the differential conformational stability could reflect the strain-specific characteristics of αSyn fibrils. Subsequently, it could be related to the fast disease progression of MSA compared to PDD and DLB.

PK profiles of αSyn fibrils also revealed their molecular diversity. PD fibrils degraded entirely at the lowest PK concentration, possibly due to low fibril deposition in PD brains. PDD and DLB fibrils showed different sizes of PK-resistant peptides between different individuals. MSA fibrils gradually disappeared upon PK treatment without being digested into small fragments, indicating a distinct αSyn strain. In order to confirm whether such variability in the molecular profiles corresponds to αSyn conformational variants, PK-resistance must be examined further in a larger number of cases.

TEM analysis revealed distinct structures of brain-derived αSyn fibrils across synucleinopathies. 'Straight' fibrils were predominant in MSA brains, while PD, PDD and DLB brains had both 'straight' and 'twisted' fibrils. This structural dichotomy might suggest a 'strain-like' profile of the fibrils, separating LBDs from MSA. The 'straight'

fibrils, densely decorated with MJFR-14 and pS129 antibodies, were confirmed as phosphorylated αSyn fibrils. In contrast, the 'twisted' fibrils, potentially composed of a different protein like tau[169], were not recognised by these antibodies. Similarly, 'twisted' fibrils from DLB cingulate cortex were not recognised by αSyn antibody in a previous immunogold-TEM study[107]. Another explanation is that the epitopes of the tested antibodies might not be accessible in the 'twisted' fibril structure. Nevertheless, a higher resolution imaging such as cryo-EM would be necessary to characterise the 'twisted' fibrils.

Distinct fibrillar structures of brain-derived αSyn fibrils have been identified in previous studies using TEM (Table 2.2) and cryo-EM (Fig. 2.9). TEM structures demonstrated in this study may differ from the published findings due to the selection of different brain regions and the limitation of the resolving power of TEM. Future cryo-EM studies of αSyn fibrils from various synucleinopathies, brain regions, and clinical subtypes will enhance the understanding of the diversity of αSyn conformers in synucleinopathies.

5.3.2 SAA fibrils demonstrate distinct biochemical and biophysical properties to the brain-derived fibrils

The biochemical and biophysical properties of the brain-derived αSyn fibrils and their corresponding SAA fibrils were compared, revealing significant differences. The SAA fibrils displayed greater resistance to GdnHCl and PK digestion, indicating enhanced stability compared to the brain-derived fibrils. Furthermore, while the brain-derived fibrils from PD, PDD, DLB and MSA exhibited distinct PK resistance patterns, the SAA fibrils from all four synucleinopathies showed identical patterns. This suggests that SAA amplifies fibrils with uniform biochemical features, losing the intrinsic properties of the original seed fibrils.

The observed differences in biochemical stability could be attributed to fibril distribution. TEM revealed that SAA fibrils were clustered, while brain-derived fibrils were distributed as single filaments, which could be more easily denatured and digested. Also,

the artificial in vitro environment of the SAA process, including the use of a PIPES-based buffer[112], could favour the formation of specific three-dimensional structures that are more conformationally stable[110,205]. Thus, future tests could assess whether conditions mimicking the original cellular environment generate SAA fibrils that replicate the true nature of brain-derived fibrils.

TEM images of brain-derived fibrils exhibited a mix of straight and twisted morphologies, whereas SAA fibrils were uniform, either straight or twisted. Interestingly, straight fibrils were dominant in MSA brains, but the corresponding SAA fibrils were twisted. Indeed, cryo-EM analysis revealed significant structural differences between the MSA brain-derived and SAA αSyn fibrils[85,115]. The structural difference could be due to a dominant seeding fibril in the brain-derived fibrils mixture, seeding a single standardised SAA fibril. Other factors, such as metal ions, the absence of PTMs on SAA fibrils, and the PIPES-based SAA buffer, could contribute to this[63,206].

Lastly, the differences in phosphorylation levels between brain-derived and SAA fibrils were investigated. Brain-derived fibrils exhibited higher phosphorylation levels than SAA fibrils, suggesting a lack of PTM conservation in SAA fibrils. Notably, the pattern of PDD and DLB brain-derived fibrils containing more p-αSyn fibrils than PD and MSA was also observed in SAA fibrils. It is likely that a high amount of pαSyn from the seed carries over the pαSyn to the newly amplifying SAA fibrils.

5.3.3 Experimental limitations

The methodology of SAA for PD, PDD, DLB and MSA brain-derived αSyn fibrils must be revisited to evaluate results in this chapter. The assay involved 1:1,000 dilution of the sarkosyl-insoluble fraction, independent of the amount of the fibrils. The amount of seeds was not normalised and, therefore, inconsistent among PD, PDD, DLB, and MSA. Observations in this chapter demonstrate that PDD and DLB brains contain higher amounts of p-αSyn fibrils than PD and MSA brains. As a result, the diluted seeds from PDD and DLB possibly contained more seeds than PD and MSA and led to faster seeding

activity.

Normalising the amount of seeds in SAA would be integral to assess the intrinsic seeding capacity of the αSyn fibrils. Thus, for example, an αSyn ELISA could be performed to measure total αSyn in the sarkosyl-insoluble fractions and adjust the amount of seeds used in the reaction.

In addition, SAA was conducted under specific buffer conditions, which could have influenced the specific biochemical and biophysical properties of the SAA fibrils observed in this chapter. It is well-established that αSyn amplification is highly sensitive to its microenvironment, including factors such as ionic concentration[134]. Consequently, the buffer conditions selected for this study may have generated a particular fibrillar subtype, potentially accounting for the uniform PK profiles observed across all SAA fibrils. Additionally, de novo αSyn fibrils could be amplified using the SAA buffer and generate a control PK profile. This can be used to confirm that the PK profiles of the SAA fibrils are unique to the seeded fibrils compared to the non-seeded fibrils.

Furthermore, the concentration of fibrils in the sarkosyl-insoluble fraction requires consideration when examining the PK profiles. Sarkosyl-insoluble fraction of PD, compared to PDD, DLB and MSA, contained less αSyn fibrils according to the PK profiles. Thus, the rapid degradation of the PD fibrils on the immunoblot (Fig. 5.4a) is likely due to the undetectable amount of PK-resistant peptides rather than low protease resistance. These limitations underscore the need for careful interpretation of the data and potentially warrant the exploration of more sensitive and quantitative methodologies for a more robust analysis.

5.3.4 Summary

The distinct biochemical and biophysical profiles of brain-derived αSyn fibrils from different synucleinopathies have been investigated in this chapter. Also, the SAA fibrils demonstrated different biochemical, structural, and phosphorylation properties from the brain-derived fibrils. This finding underscores the need to improve understanding of SAA

fibrils. It also emphasises the importance of investigating human-derived αSyn fibrils to explore αSyn strains and conduct disease-relevant studies.

Chapter 6

Diagnostic value of cerebrospinal fluid αSyn seed quantification in synucleinopathies

6.1 Introduction

αSyn seed amplification assay (SAA) is a powerful assay optimised to detect αSyn aggregation in the cerebrospinal fluid (CSF) of patients with pathologically confirmed synucleinopathies[125]. Detection of αSyn aggregation in such accessible biosample highlights the role of αSyn SAA as a biomarker tool for diagnosing synucleinopathies. Differential diagnosis of the different synucleinopathies is difficult due to the overlapping clinical symptoms, resulting in misdiagnosis up to 40 %[207]. Also, early clinical diagnosis has been a major challenge. Accurate and early diagnosis of different synucleinopathies would facilitate the delivery of appropriate therapeutic intervention and recruitment for clinical trials.

Previous studies have reported highly sensitive and specific αSyn SAA that detected αSyn aggregation in CSF of patients with synucleinopathies[111,113,125,136,137,144,148]. However, it was unclear whether αSyn SAA could produce reproducible and robust quan-

titative measurements that can stratify between different synucleinopathies and correlate with disease severity, progression and clinical phenotypes. This study examines CSF from well-characterised longitudinal cohorts of PD and MSA patients to perform SAA and investigate whether the resulting quantitative measurements can be used to distinguish PD and MSA. Furthermore, the quantitative output of the CSF αSyn SAA was assessed with clinical data to identify its correlation with disease progression and different PD phenotype clusters[11].

This chapter examined CSF from well-characterised longitudinal cohorts of PD and MSA patients to perform αSyn SAA. The working hypothesis was that the αSyn SAA quantitative measures can distinguish between PD and MSA and show a significant correlation with the clinical symptoms. The aims of this chapter are the following:

1. Detect αSyn seeding activity in CSF of PD and MSA patients using αSyn SAA.
2. Extract quantitative parameters from the αSyn SAA reactions and compare the parameters between PD and MSA.
3. Examine the correlation between the αSyn SAA parameters and PD/MSA disease progression.
4. Examine the correlation between the αSyn SAA parameters and PD clinical subtype clusters.

6.2 Results

6.2.1 αSyn seeding activity in CSF of PD and MSA patients

αSyn seeding activity was examined in the CSF of PD (n = 74), MSA (n = 24) and control (n = 55) subjects. αSyn seeding activity was detected in 66 out of 74 PD patients and 2 out of 55 control subjects, resulting in the assay sensitivity of 89 % and specificity of 96 % (Fig. 6.1a). Two control subjects showed αSyn seeding activity. One control

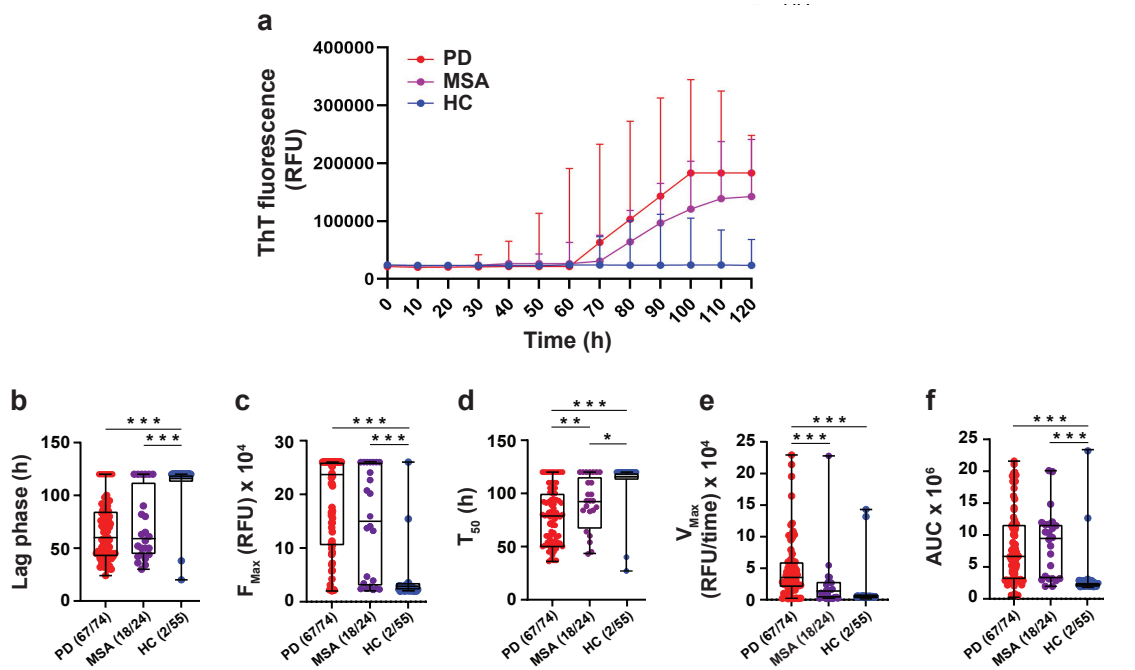

Figure 6.1 **αSyn SAA reactions of CSF from PD, MSA and HC and kinetics parameters.** **a-f**, Averaged αSyn SAA reaction curves of CSF from PD (n = 74), MSA (n = *24*) and HC (n = 55) (**a**) and kinetic parameters: lag phase (**b**), F_{MAX} (**c**), T_{50} (**d**), V_{MAX} (**e**) and AUC (**f**). (**a**) Each reaction curve represents an average of ThT fluorescence from each group. Vertical bars represent one SD. (**b-f**) The Kruskal-Wallis test was used for statistical analysis. $*P \leq 0.05$, $**P \leq 0.01$, $***P \leq 0.005$.

demonstrated normal MDS-UPDRS and olfaction testing. The other control had normal MDS-UPDRS, autonomic, cognition, olfaction and quantitative motor testing but demonstrated bilateral action tremor. To date of this analysis, none of the two controls met the criteria for PD or other neurodegenerative diseases. αSyn seeding activity was absent in eight PD patients. These patients performed better in olfaction testing, but there was no difference in the motor scores compared to those who tested positive for αSyn SAA.

In MSA patients, 18 out of 24 showed αSyn seeding activity, resulting in 75 % sensitivity. Interestingly, all nine MSA-C patients but only 8 out of 14 MSA-P patients showed αSyn seeding. However, no significant differences in the SAA kinetic parameters were observed between MSA-C and MSA-P patients.

Next, the αSyn SAA kinetic parameters were compared between PD and MSA

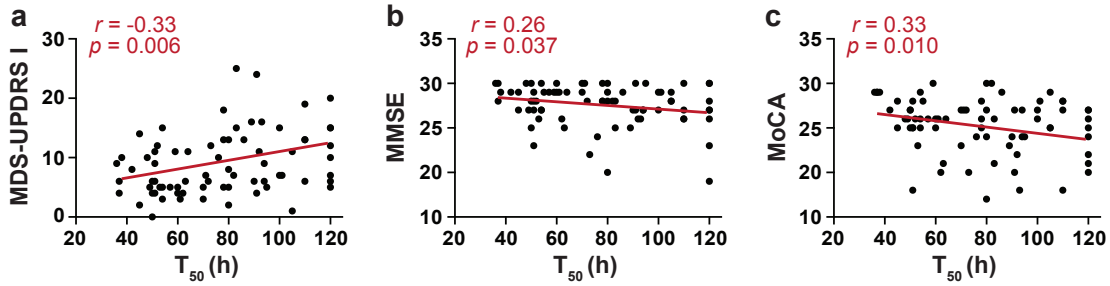

Figure 6.2 **Correlation between αSyn SAA parameters and clinical data of PD patients. a-c**, Among 74 PD patients, significant correlation was observed between T_{50} against MDS-UPDRS I (**a**), MMSE (**b**) and MoCA (**c**). Spearman rank correlation analysis was used. Spearman correlation coefficient (r) and P-value (p) are specified on each plot. The linear plot in red represents the best-fit regression.

(Figs. 6.1b-f). The average T_{50} of PD was 77 h and MSA was significantly longer with 93 h (Fig. 6.1d). The average V_{MAX} was significantly higher in PD with 4.9 x 10^4 and MSA with 2.4 x 10^4 (Fig. 6.1e). The lag phase, F_{MAX} and AUC showed no significant difference between PD and MSA (Figs. 6.1b,c,f). Overall, the longer lag phase and lower V_{MAX} of MSA compared to PD suggest slower αSyn seeding activity in MSA CSF.

6.2.2 Correlation of the SAA parameters with PD disease severity and clusters

The αSyn SAA kinetic parameters and PD clinical measures did not show a meaningful correlation, where a higher seeding activity indicates a more severe disease phenotype. The full analysis is summarised in Table A.1. A correlation was identified between T_{50} and MDS-UPDRS I score, but the correlation was in an unexpected direction (Fig. 6.2a). Longer T_{50} indicates stronger αSyn seeding activity, thus expected to be higher with severe disease phenotype. In addition, MMSE and MoCA scores demonstrated a significant correlation with T_{50}, but also in an unexpected direction (Figs. 6.2b,c).

The Discovery cohort PD patients were grouped into four clinical clusters and their αSyn SAA kinetic parameters were compared. A summary of the parametric values of each cluster and statistical analysis is outlined in Table A.2. V_{MAX} was significantly

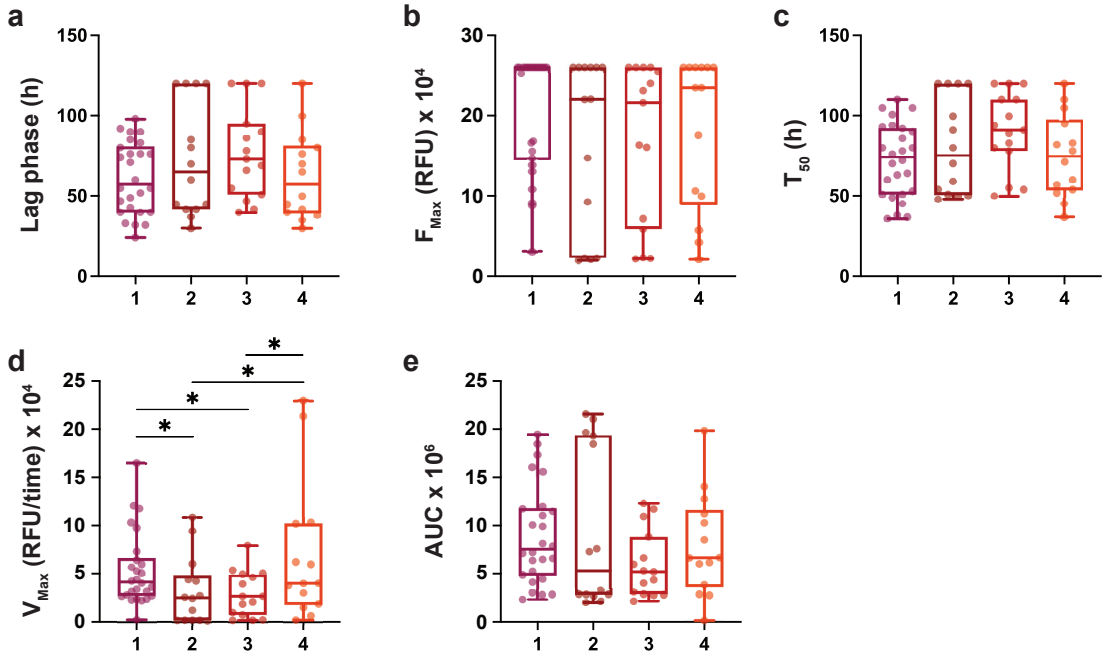

Figure 6.3 **αSyn SAA parameters in PD clinical clusters. a-e**, Discovery cohort PD clinical clusters 1-4 and their αSyn SAA lag phase (**a**), F_{MAX} (**b**), T_{50} (**c**), V_{MAX} (**d**) and AUC (**e**). The Kruskal-Wallis test was used for statistical analysis. $^*P \leq 0.05$.

different across the clusters where clusters 1 and 4 showed higher V_{MAX} than clusters 2 and 3 (Fig. 6.3d). The other four SAA parameters showed no significant difference between the clusters (Figs. 6.3a-c,e).

6.2.3 Correlation of the SAA parameters with MSA disease severity

Correlation analysis was also performed with the αSyn SAA kinetic parameters and the clinical data of MSA patients. The complete analysis is summarised in Table A.3. All five SAA parameters were significantly correlated with change in the UMSARS score from baseline to follow-up (Figs. 6.4a-e). The correlations were in the expected direction, where a shorter lag phase and T_{50} are expected with worse disease severity. Also, higher F_{MAX}, V_{MAX} and AUC are expected with severe disease phenotype.

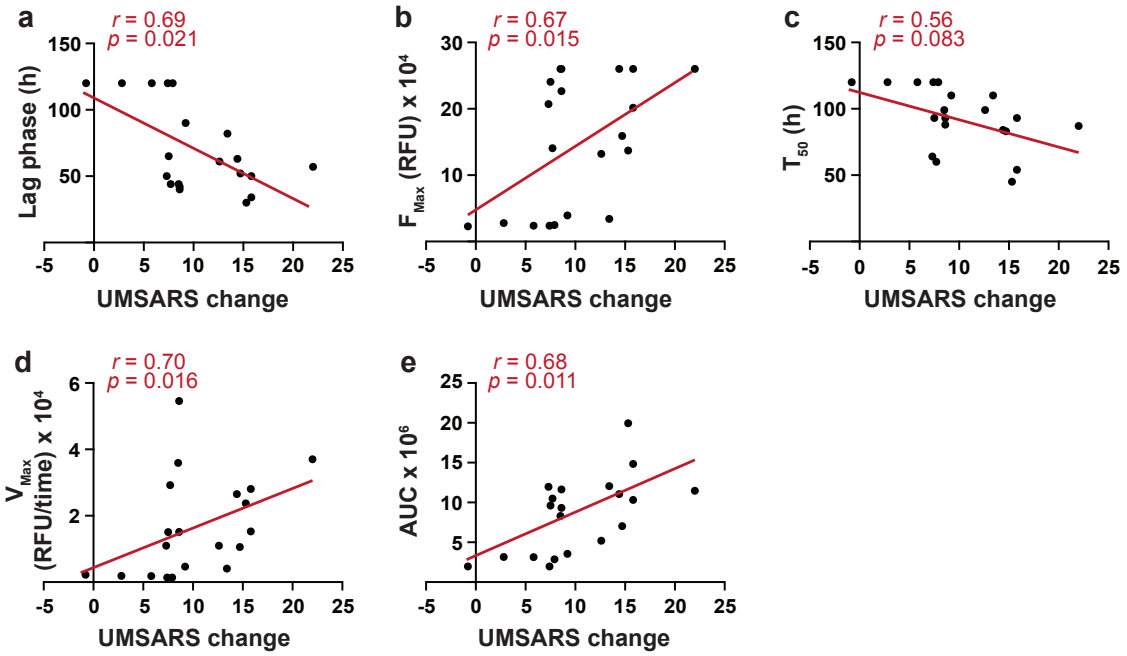

Figure 6.4 **Correlation between αSyn SAA parameters and clinical data of MSA patients.** **a-e**, Among 20 MSA patients, significant correlation was observed between the change in UMSARS (from baseline to follow up) against lag phase (**a**), F_{MAX} (**b**), T_{50} (**c**), V_{MAX} (**d**), and AUC (**e**). Spearman rank correlation analysis was used. Spearman correlation coefficient (r) and P-value (p) are specified on each plot. The linear plot in red represents the best-fit regression.

6.3 Discussion

In this chapter, αSyn SAA was used to assess the diagnostic value and clinical correlations of the SAA parameters for PD and MSA. αSyn SAA identified PD with 89 % sensitivity and 96 % specificity. The sensitivity for MSA was 75 %. T_{50} and V_{MAX} were distinguishable between PD and MSA, suggesting a more aggressive seeding capacity of PD CSF. Further associations of T_{50} with PD clinical measures (MDS-UPDRS I, MMSE, MoCA) were observed, although they were not as hypothesised (i.e. higher seeding activity associated with more severe disease phenotype). Also, V_{MAX} was distinguishable between different clinical clusters of PD. The change in UMSARS in the MSA patients was associated with all five SAA parameters.

Previous αSyn SAA study before this work achieved sensitivity and specificity of 95 % and 100 %, respectively[125]. Another study detected αSyn seeding activity in PD CSF with sensitivity and specificity of 93.6 % and 100 %, respectively[111]. The sensitivity and specificity of the PD αSyn SAA reported in this chapter are slightly lower, likely due to the differences in the cohort sizes. Nevertheless, the consistent performance of αSyn SAA with PD CSF highlights its diagnostic function.

No clear correlations were identified between the SAA parameters and PD clinical data. Similar findings were reported by others[144,208], where αSyn SAA parameters from 105 PD patients demonstrated no correlation between clinical measures. In contrast, one study reported that T_{50} correlates with the H&Y stage of 75 PD patients. However, H&Y is a relatively rough score dividing patients from only 1 to 5, whereas this study and others examined motor function on UPDRS III (score range of 0-132). The negative findings in this chapter could be due to Discovery patients being moderately affected (mean MDS-UPDRS III score of 27) at the time of CSF collection. However, to further analyse whether the seeding capacity of pathogenic αSyn changes during disease progression, one should examine larger cohorts with longitudinal CSF samples representing a wider spectrum of disease severity.

The SAA parameters were further analysed in four different PD clinical subtypes[11]. Cluster 2 is associated with a milder form of disease, and patients in this cluster demonstrated the lowest proportion of αSyn seeding activity across all clusters. On the other hand, all patients in cluster 1, with fast motor progression and worse non-motor symptoms, showed positive αSyn seeding activity. In addition, V_{MAX} significantly differed across the clusters. Such differences in αSyn seeding activity might represent distinct αSyn 'strains' associated with PD clinical clusters. Previous chapters discussed the evidence of αSyn strains between synucleinopathies and within a single disease entity. Investigating how the molecular 'strain' profiles relate to different clinical clusters might provide further insight into the molecular basis of the great variability of disease pheno-

types in PD.

Recently, a study performed with the Parkinson's Progression Markers Initiative (PPMI) cohort reported variable αSyn seeding activities between different PD genetic subgroups[147]. The highest portion of positive SAA was found among *GBA* PD patients, followed by sporadic and *LRRK2* PD patients with the lowest SAA activity. Interestingly, hyposmia showed a strong association with positive SAA. Other clinical data was also significantly associated with SAA outcome but was only observed in the *LRRK2* PD group. For example, the *LRRK2* PD patients with negative SAA had lower MDS-UPDRS II scores and less severe motor impairments (MDS-UPDRS III). This finding builds evidence on the association between αSyn SAA and PD genetic and clinical heterogeneity. Also, combined with the findings from this chapter, it highlights the role of αSyn SAA as a molecular signature that may improve stratification of different clinical and genetic subtypes.

αSyn seeding activity was detected in 75 % of the MSA cases, which is lower compared to the 94 % sensitivity achieved previously with CSF of 65 MSA patients[111]. These results are strikingly different from studies demonstrating much lower and below-threshold αSyn seeding activity in MSA CSF samples[113,209]. However, a slower seeding activity of MSA CSF compared to PD is a consistent finding in these studies. Clinically, MSA is a faster-progressing disease than PD. Also, PD-derived αSyn induces weak or no disease in cell and animal models, while MSA induces rapid disease propagation and cellular infectivity[181]. Therefore, slower seeding activity in MSA than in PD was unexpected. Nevertheless, it is important to note that differential ThT-kinetics might not reflect their differences in seeding efficiencies. ThT-escaping fibrils might limit the detection of αSyn seeding activity[114]. Therefore, the seeding activity of PD and MSA should be further characterised using different amyloid fluorophores such as SYBR-green or luminescent conjugated oligothiophenes (LCOs)[111,114].

Furthermore, MSA showed longer T_{50} and lower V_{MAX}, which distinguished from

PD, as shown in published findings[146]. Interestingly, among the brain-derived fibrils, PD and MSA brain-derived αSyn fibrils showed similar αSyn seeding activity. Unlike CSF, the fibrillar fraction consists of concentrated αSyn conformers, and the microenvironment of the two biosamples is substantially different, which might affect the assay performance. A future investigation of combined biosample analysis with αSyn SAA might provide useful insights into how the assay performs differently with various biosamples and what could be the 'ideal' diagnostic biomarker.

The MSA αSyn SAA parameters also correlated with the clinical progression of MSA (UMSARS change). This novel finding requires further validation with larger cohorts. However, it is encouraging that a significant correlation was found in all parameters in 24 MSA patients. More severe clinical symptoms and rapid disease progression of MSA might explain why such a strong correlation is found in MSA but not PD.

6.3.1 Experimental limitations

Small cohort size is an important limiting factor in this chapter. The differences in kinetics parameters (T_{50} and V_{MAX}) between PD and MSA must be examined and confirmed in larger cohorts. Also, these parameters alone cannot yet stratify PD and MSA. In order to employ SAA as a diagnostic tool, a more disease-specific parameter or a variable should be further investigated from larger and well-characterised longitudinal cohorts.

Although SAA parameters significantly differed among PD clinical clusters, the low sample size limits the significance of the correlations. Power calculation equation 6.1[210] can be used to estimate the sample size required for this correlative study to have statistical significance.

$$N = \frac{Z^2_{\frac{\alpha}{2}} \times s(1-s)}{d^2 \times P} \tag{6.1}$$

The power calculation can be performed with 5 % significance level (α), 93.6 % SAA sensitivity for PD from a published literature[111] (s) and 10 % marginal error rate

(d). The expected prevalence of each clinical cluster (P) is 32.5 % (1), 17.7 % (2), 23.6 % (3) and 26.6 % (4) according to the previous cluster characterisation performed with the Discovery cohort[11].

As a result, a total of 68 (1), 127 (2), 94 (3) and 83 (4) cases are required for each cluster to have statistical power. Having a much smaller cohort than the estimated likely accounted for the unexpected observation of high SAA response (92.9 %) in the slow motor progression cluster (4) and lower SAA response (80 %) in the severe motor disease cluster (3). Therefore, to obtain statistical power on the correlation of SAA parameters between PD clinical clusters, a larger sample size is needed.

6.3.2 Summary

This chapter has shown the high sensitivity and specificity of CSF αSyn SAA for PD. The quantitative parameters lacked correlation with PD clinical progression but demonstrated association with four PD clinical clusters. Also, MSA and PD showed distinctive SAA kinetics, and quantitative kinetics correlated with disease progression of MSA. This finding might highlight the limitation of αSyn SAA as a PD progression marker but its value as a stratifying diagnostic marker that guides making a more robust diagnosis.

Chapter 7

Salivary biomarker for PD

7.1 Introduction

Saliva is an attractive biofluid for diagnostic purposes due to its non-invasive and cost-effective collection methods. Also, the salivary gland is anatomically connected to the central nervous system, and Lewy pathology has been observed in the submandibular glands of PD patients[211]. Therefore, saliva may be a useful diagnostic biomarker reflecting the clinical and pathological state of PD. Indeed, recent studies have already started investigating salivary biomarkers for PD using salivary genomic, transcriptomic, proteomic and metabolomic approaches[212].

According to previously published studies on PD saliva, αSyn is the most studied protein. Collective studies utilised ELISA assays and detected significantly lower total-αSyn levels in PD saliva than the healthy individuals[133,156,158–160]. However, one study found that salivary αSyn remains unchanged in PD[166]. Interestingly, an increased level of oligomeric αSyn in saliva was a consistent finding in PD compared to healthy individuals[156,159,160,166]. In addition, DJ-1 is another protein involved in PD pathology, and its significant increase in PD saliva has been reported[157,213]. Other molecular changes include increased acetylcholinesterase activity and higher concentration of heme oxygenase-1 protein in PD saliva compared to healthy individuals[214].

To date, most salivary biomarker studies employed antibody-based detection methods to observe proteins associated with PD pathology. Only recently, studies began to optimise the αSyn seed amplification assay (SAA) to detect pathological αSyn in PD saliva. Luan and colleagues detected αSyn seeding activity in 75 PD patients with 76.0 % sensitivity and 94.4 % specificity[172]. A study by Vivacqua and colleagues tested 37 PD salivary samples and detected PD with 86 % sensitivity and 78 % specificity[133]. The authors also combined the UPDRS and the Non-Motor Symptoms Scale (NMSS) scores, which positively correlated with a few SAA kinetic parameters, including the area under the curve (AUC). Such findings highlight the potential of salivary αSyn SAA as a diagnostic and progression biomarker for PD. Nevertheless, the robustness of the assay must be investigated, assessing the reproducibility in larger longitudinal cohorts.

Apart from proteins involved in PD pathology, more global proteomic changes have been investigated in PD saliva samples. Figura and colleagues analysed saliva samples from 24 PD patients and 14 healthy controls using liquid chromatography-tandem mass spectrometry (LC-MS/MS). They identified lower concentrations of three proteins (S100-A16, ARPC2A and VPS4B) in PD saliva compared to healthy controls[171]. The ability to detect changes in the salivary proteomic composition demonstrates the useful application of mass spectrometry (MS) in biomarker study.

This study combines multiple biochemical characterisation methods to overview signature protein changes in PD saliva comprehensively. As outlined above, previous studies applied a single approach to characterise human saliva. However, due to the heterogeneous nature of human saliva's molecular composition, a single methodological approach has limitations in identifying disease-related changes. Also, the reproducibility of published results is crucial when investigating a biosample with a highly variable composition. Therefore, the hypothesis was that the neuropathological changes in PD are reflected in the saliva, which can be measured by employing multiple biochemical characterisation methods. The aims of this chapter are the following:

1. Examine the levels of different αSyn conformers in PD and healthy saliva using Western blot and ELISA.

2. Examine salivary proteomic profiles using intact mass spectrometry and LC-MS/MS.

3. Assess αSyn seeding activity of PD and healthy saliva using SAA.

7.2 Results

7.2.1 Immunoblot analysis of salivary αSyn

First, immunoblot was used to examine αSyn in PD and HC saliva. Three antibodies were tested: Syn1 (total αSyn, mouse), SynO4 (oligomeric αSyn, mouse), and pS129 (S129 phosphorylated αSyn, rabbit). Eight PD and 8 HC saliva samples were chosen for a preliminary test. Also, in parallel, the immunoblots were incubated with anti-mouse (anti-Ms) and anti-rabbit (anti-Rb) antibodies only to test for non-specific binding of the secondary antibodies. Both anti-Ms and anti-Rb showed non-specific immunoreactivity in all the saliva samples (Figs. 7.1a&b). Anti-Ms showed non-specific immunoreactivity to a 25 kDa protein, which is present in the immunoblots of Syn1 (Fig. 7.1a). Furthermore, anti-Rb showed non-specific immunoreactivity to a 45 kDa protein, which is also present in the immunoblot of pS129 as shown in Fig. 7.1b.

Subsequently, among αSyn-specific antibodies, SynO4 was selected to examine salivary αSyn, as it showed specific immunoreactivity that did not overlap with the 25 kDa non-specific immunoreactivity of the anti-Ms secondary antibody. The 49 kDa protein bands detected by SynO4 in PD and HC saliva were quantified and plotted in Figs. 7.2a&b. The full immunoblot for 33 PD and 41 HC salivary samples are shown in Fig. A.6. The density of the 49 kDa band was significantly higher in PD saliva than in HC.

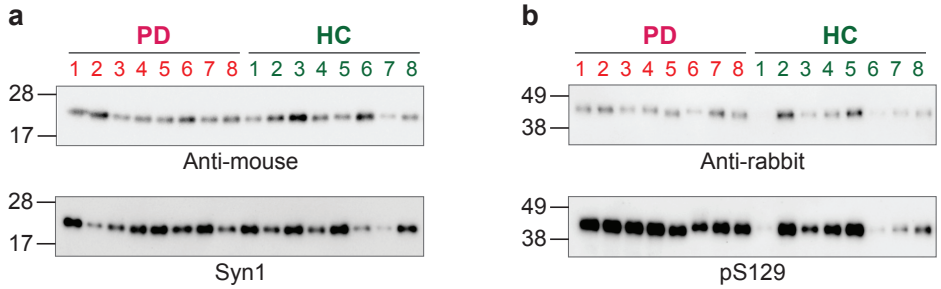

Figure 7.1 **Non-specific immunoreactivity of secondary antibodies towards salivary proteins. a&b**, Non-specific immunoreactivity of anti-mouse (Ms) (**a**) and anti-rabbit (Rb) (**b**) secondary antibodies towards salivary proteins from PD (n = 8) and HC (n = 8). (**a**) The top membrane was incubated with anti-Ms alone and the bottom membrane with Syn1 antibody. The 25 kDa band arises from the non-specific immunoreactivity of anti-Ms. (**b**) The top membrane was incubated with anti-Rb alone and the bottom membrane with pS129 antibody. The 45 kDa band comes from the non-specific immunoreactivity of anti-Rb. Molecular weights (kDa) are indicated on the left of each immunoblot.

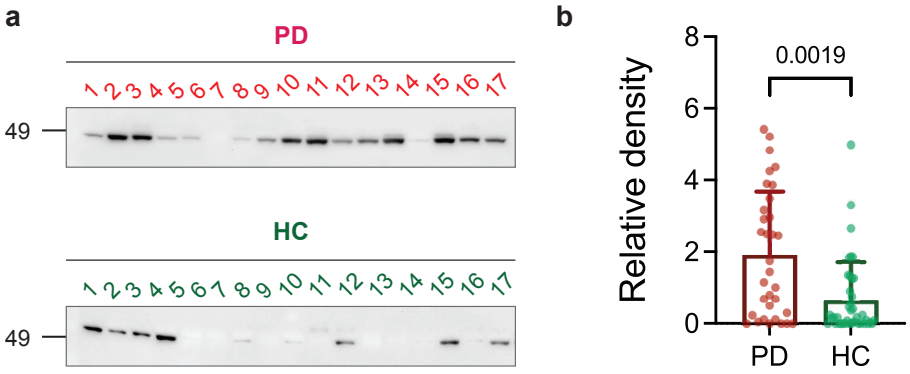

Figure 7.2 **SynO4 detection of salivary αSyn. a&b**, Immunoreactivity of SynO4 towards PD (n = 17) and HC (n = 17) saliva (**a**) and semi-quantitative analysis of the immunoreactivity (**b**). SynO4 showed specific immunoreactivity to a 49 kDa protein in PD and HC saliva. Mann-Whitney U test was used, and P-value is indicated above the plot. Molecular weights (kDa) are indicated on the left of each immunoblot.

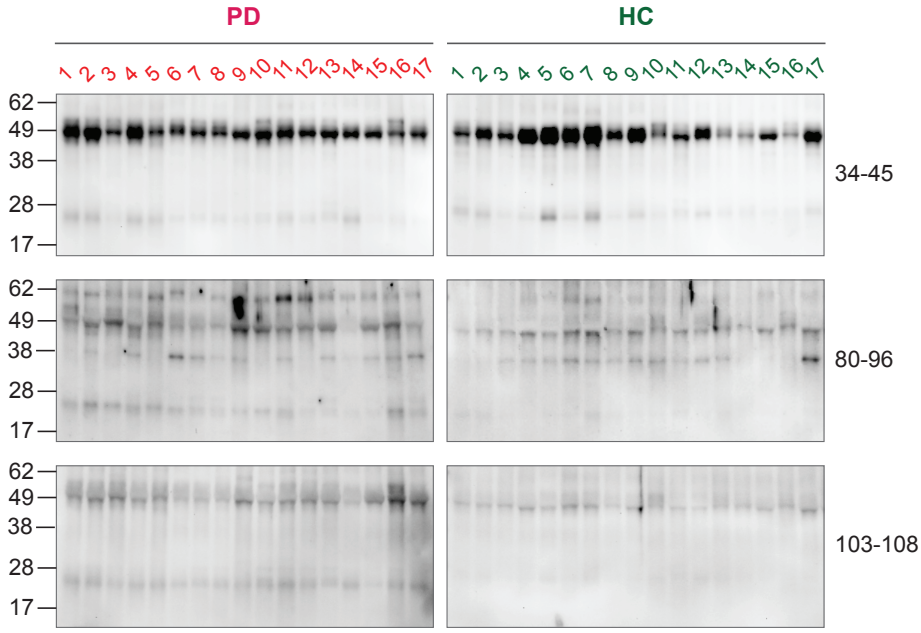

Figure 7.3 HRP-conjugated αSyn antibodies detect salivary αSyn. HRP-conjugated antibodies 34-45, 80-96, and 103-108 tested with PD (n = 17) and HC (n = 17) saliva. 34-45 and 103-108 antibodies detected 25 and 49 kDa αSyn. 80-96 antibody detected 25, 38, 49, and 62 kDa αSyn. Molecular weights (kDa) are indicated on the left of each immunoblot.

HRP-conjugated αSyn-specific antibodies were used to remove non-specificity arising from secondary antibodies. Three HRP-conjugated antibodies were selected, which target different regions of αSyn: 34-45, 80-96 and 103-108. Brain homogenates (BH) were included as a positive control. The full immunoblots are provided in Figs. A.7a-c. First, 34-45 showed immunoreactivity to 25 and 49 kDa proteins (Fig. 7.3) and when the band intensities were compared between PD and HC saliva, there were no significant differences (Fig. 7.4a). 80-96 showed immunoreactivity to four major proteins with a molecular weight of 25, 38, 49 and 62 kDa (Fig. 7.3). When these band intensities were quantified, their intensities were significantly higher in PD than in HC saliva (Fig. 7.4b). 103-08 showed immunoreactivity to 25 and 49 kDa proteins, similar to 34-45 (Fig. 7.3), and the intensities of these bands were significantly higher in PD than in HC saliva (Fig. 7.4c).

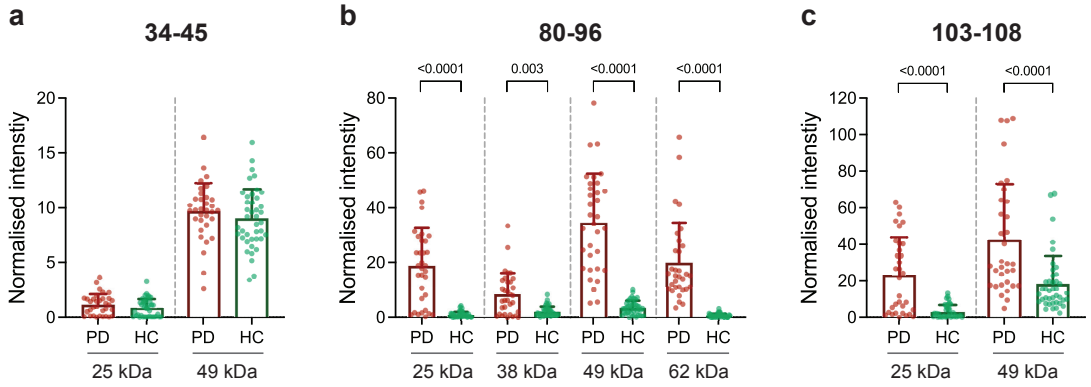

Figure 7.4 **Quantification of immunoreactivity from HRP-conjugated αSyn antibodies. a-c**, Intensity of distinct immunoblot bands detected with (**a**) 34-45, (**b**) 80-96, and (**c**) 103-108 HRP-conjugated antibodies towards PD and HC saliva. (**a**) The intensity of 25 and 49 kDa bands detected by 34-45 were not significantly different between PD and HC saliva. (**b**) The intensity of the 25, 38, 49, and 62 kDa bands detected by 80-96 were significantly higher in PD saliva than in HC. (**c**) The 25 and 49 kDa bands detected by 103-108 were significantly higher in PD saliva than in HC. Mann-Whitney *U* test was used for statistical analysis, and the *P*-values are indicated on each plot.

7.2.2 Measurement of salivary total and aggregated αSyn levels with ELISA

A more sensitive ELISA assay was employed to measure salivary αSyn levels. Using BCA, the concentration of total salivary protein was measured from PD and HC subjects. Salivary protein concentration was significantly higher in PD saliva than in HC (Fig. 7.5a). The mean $\pm$ SD of salivary protein concentration was 2.5 $\pm$ 1.5 and 1.4 $\pm$ 0.6 mg/mL for PD and HC, respectively.

Two different ELISA kits were used that detect total αSyn and aggregated αSyn. First, the total αSyn ELISA had a detection range from 10.2 to 325 pg/mL (Fig. 7.5b). A total of 25/33 PD and 24/41 HC samples showed αSyn levels within the assay sensitivity range and thus only considered for further analysis. As a result, the level of total αSyn in saliva was significantly, but weakly, higher in PD than in HC (Fig. 7.5c). The mean $\pm$ SD of total αSyn levels in saliva was 38.1 $\pm$ 37.8 and 27.6 $\pm$ 37.5 pg/mL for PD and HC,

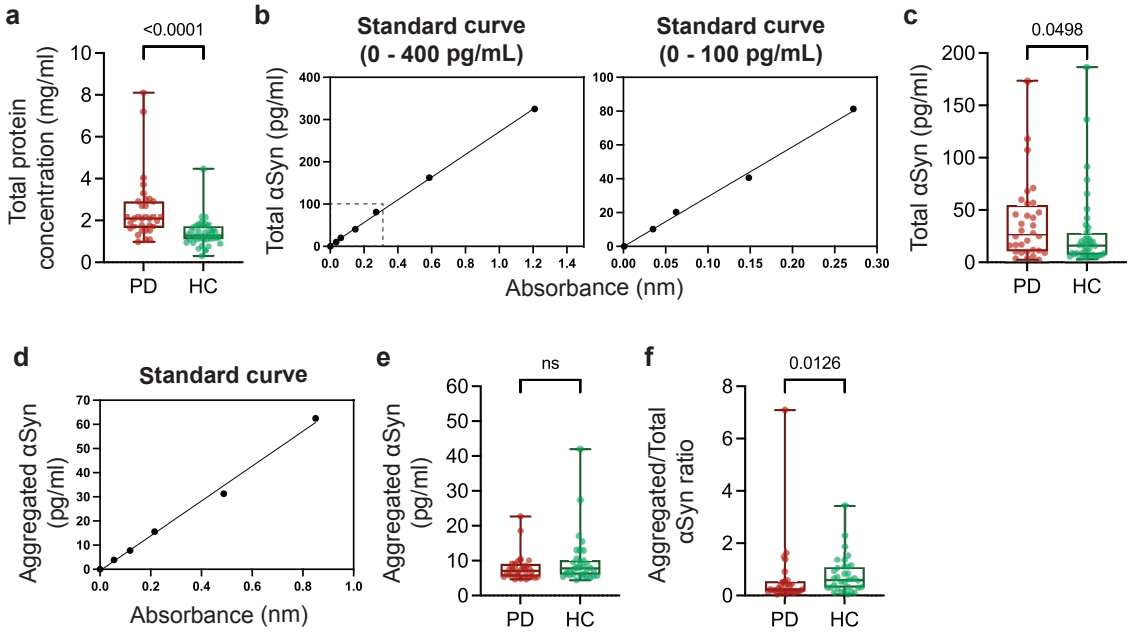

Figure 7.5 **Concentrations of total protein and αSyn in PD and healthy saliva.** **a**, Concentration of salivary total protein. **b**, Total αSyn ELISA standard curves displayed for range 0 - 400 pg/mL (left) and 0 - 100 pg/mL (right). **c**, Total αSyn levels in PD and HC saliva. **d**, Aggregated αSyn ELISA standard curve. **e**, Aggregated αSyn levels in PD and HC saliva. **f**, The ratio of aggregated and total αSyn in PD and HC saliva. Mann-Whitney *U* test was used and *P*-value is indicated above each plot. ns: not significant.

respectively.

Next, the detection range of the aggregated αSyn ELISA was 3.9 to 62.5 pg/mL (Fig. 7.5d). The levels of aggregated αSyn in all PD and HC samples were within the assay sensitivity range. The level of aggregated αSyn in saliva was not statistically different between PD and HC (Fig. 7.5e). The mean $\pm$ SD of aggregated αSyn levels in saliva was 8.0 $\pm$ 3.8 and 9.8 $\pm$ 7.1 pg/mL for PD and HC, respectively. In addition, the ratio of aggregated versus total αSyn level was significantly higher in HC than in PD (Fig. 7.5f). The mean $\pm$ SD of aggregated to total αSyn ratio in saliva was 0.6 $\pm$ 1.3 and 0.8 $\pm$ 0.7 for PD and HC, respectively.

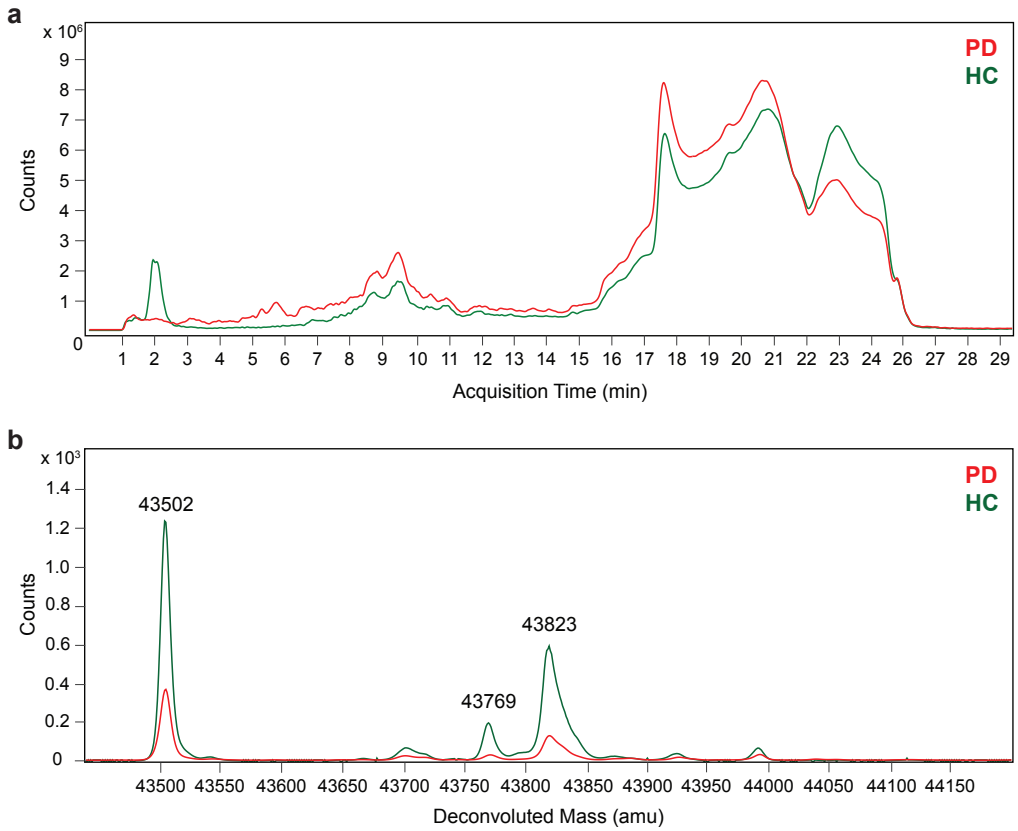

Figure 7.6 **Intact mass analysis of pooled saliva from PD and HC. a&b**, Size-exclusion chromatograms of pooled PD and HC saliva eluted through an HPLC column (**a**) and deconvoluted mass peaks for retention time between 22 and 25 mins (**b**). The mass peak at 43502 Da matched chitinase-3-like protein-2 (CH3L2), and a smaller mass peak 43823 Da represents a Gal-Glu glycosylation. PD and HC saliva are presented in red and green curves, respectively.

7.2.3 LC-MS intact mass analysis of PD saliva

Due to the highly heterogeneous nature of salivary protein composition, 33 PD and 41 HC saliva samples were pooled to examine an average proteomic profile of PD and HC saliva using LC-MS mass-spectrometry. A total of 5 µl of pooled saliva was loaded onto HPLC connected in line with MS. Protein elution was observed at retention times between 15.5 and 25.5 min (Fig. 7.6a). Between retention times of 22 and 25 min, a protein with a mass of 43504 Da was observed, which matched to chitinase-3-like protein-2 (CH3L2) (Fig. 7.6b). In HC saliva, a glycosylated form of this protein was present (43828 Da)

but absent in PD saliva. Also, the height of the mass peak of CH3L2 was approximately higher in HC by 3-fold than in PD, indicating a reduced abundance of this protein in PD saliva than in HC. In order to confirm whether the protein with mass 43828 Da is CH3L2, pooled saliva samples were tested with LC-MS/MS and identified the presence of Ch3L2 in PD and HC saliva with identical experimental mass.

7.2.4 Proteomic profiling of PD saliva

Using a single pooled sample limited statistical analysis between PD and HC samples. To perform LC-MS/MS label-free quantification and statistical analysis, each PD and HC (6 sub-pools in total) were divided into three sub-pools. A total of 386 proteins were identified among the 6 sub-pools, and 152 common proteins were identified. Among 152 proteins, only 5 showed significant fold change between PD and HC saliva, as presented in the volcano plot in Fig. 7.7. The abundance of uridylate-specific endoribonuclease (ENDOU, P21128) was 2.4-fold lower in PD than in HC saliva. The abundance of alpha-1-antitrypsin (A1AT, P01009) was 2.1-fold higher in PD than in HC saliva, and its fold change had the highest statistical significance. Three proteins – protein LEG1 homolog (LEG1H, Q6P5S2), immunoglobulin heavy constant gamma 2 (IGHG2, P01859), and immunoglobulin heavy constant gamma 2 (IGHG3, P01860) – also showed significant fold-change but the changes were less than 2-fold. CH3L2 identified from intact-mass LC-MS analysis was only detected from 2 PD and 2 HC sub-pools. Therefore, the fold-change calculation was not possible.

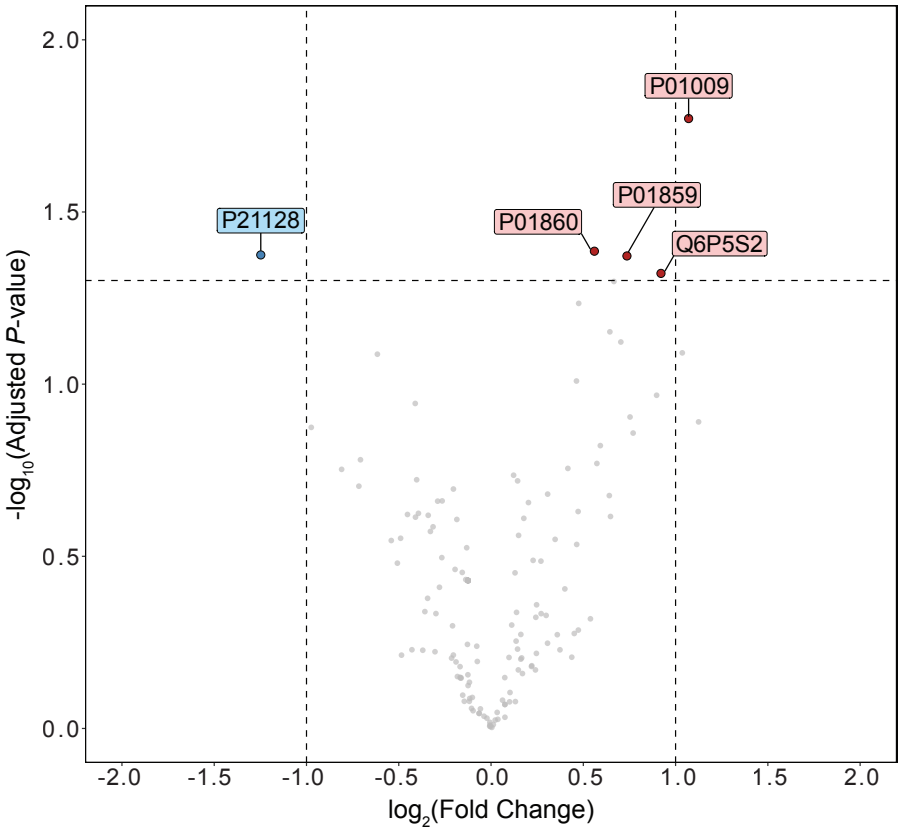

Figure 7.7 Salivary protein differences between PD and HC. The results from LC-MSMS data are presented according to the fold change (log_2(Fold change)) and its statistical significance ($-log_{10}$(Adjusted *P*-value)). A total of 5 proteins showed significant fold differences between PD and HC saliva. P01009 – Alpha-1-antitrypsin (A1AT), Q6P5S2 – Protein LEG1 homolog (LEG1H), P01859 – Immunoglobulin heavy constant gamma 2 (IGHG2), P01860 - Immunoglobulin heavy constant gamma 2 (IGHG3), and P21128 - Uridylate-specific endoribonuclease (ENDOU). Higher and lower protein expression in PD saliva relative to HC is indicated in red and blue, respectively. The two vertical dashed lines indicate where the fold change is 2 (log_2(Fold change) $\pm$ 1.0). The horizontal dashed line indicates the cut-off at $p = 0.05$ ($-log_{10}$(Adjusted *P*-value) = 1.3). *P*-values were adjusted for multiple comparisons using the Benjamini-Hochberg procedure.

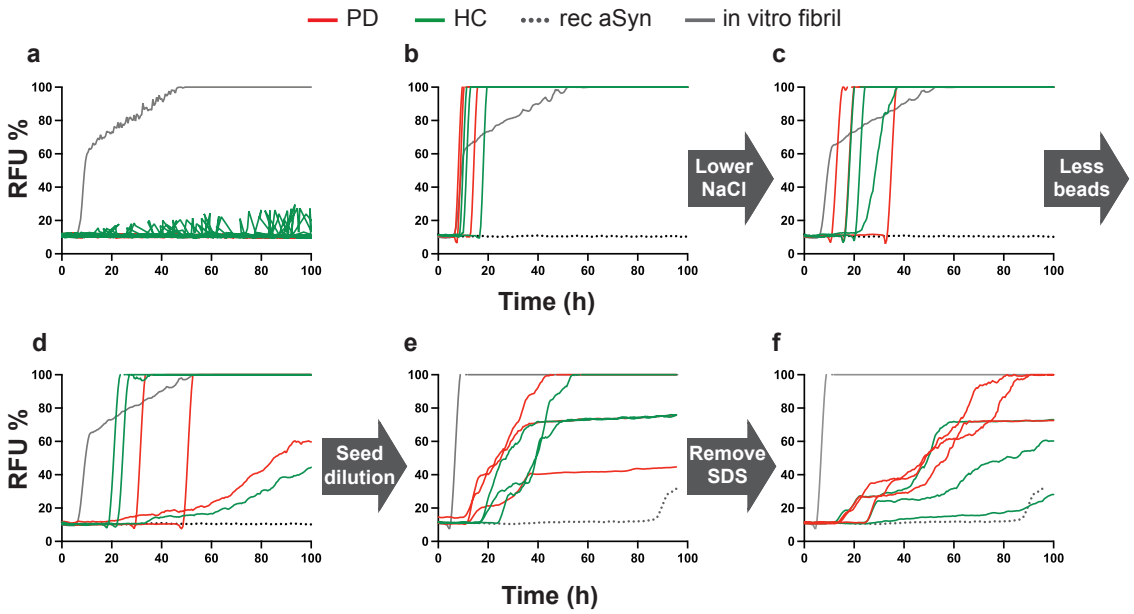

Figure 7.8 **Optimisation of salivary αSyn SAA. a&b**, Salivary SAA activities measured using protocols from Ref.[133] (**a**) and Ref.[172] (**b**). **c-f**, Optimisation of the protocol from Ref.[172] by removing NaCl (**c**), reducing the number of 1 mm silica beads (5 to 1) (**d**), increasing the dilution of seed (1:100 to 1:10,000) (**e**) and removing SDS (**f**). PD n = 3, HC n = 3. Each sample was run in triplicates and the fluorescence curves represent the average of the triplicates. The reactions with in vitro fibril seed and without seed (rec αSyn) are positive and negative controls, respectively.

7.2.5 Detection of αSyn seeding activity in PD saliva

αSyn SAA was employed to assess the presence of seeding-competent αSyn species in the saliva of PD patients. The assay conditions were optimised regarding published literature on salivary SAA[133,172]. Using the methods from Ref.[133] failed to detect any seeding activity in saliva samples (Fig. 7.8a). The assay conditions from Ref.[172] (10 mM PBS pH 7.4, 500 mM NaCl, 0.0015 % SDS, 10 µM ThT, three 1 mm beads) resulted in aggressive seeding from PD and HC saliva (Fig. 7.8b). Subsequently, this assay condition was further optimised by removing NaCl (Fig. 7.8c), using one 1 mm bead (Fig. 7.8d), increasing seed dilution to 10:10,000 (Fig. 7.8e), and removing SDS (Fig. 7.8f). As a result, the optimised condition induced slower seeding activity, improving separation between PD and HC, and dampening the seeding in HC saliva.

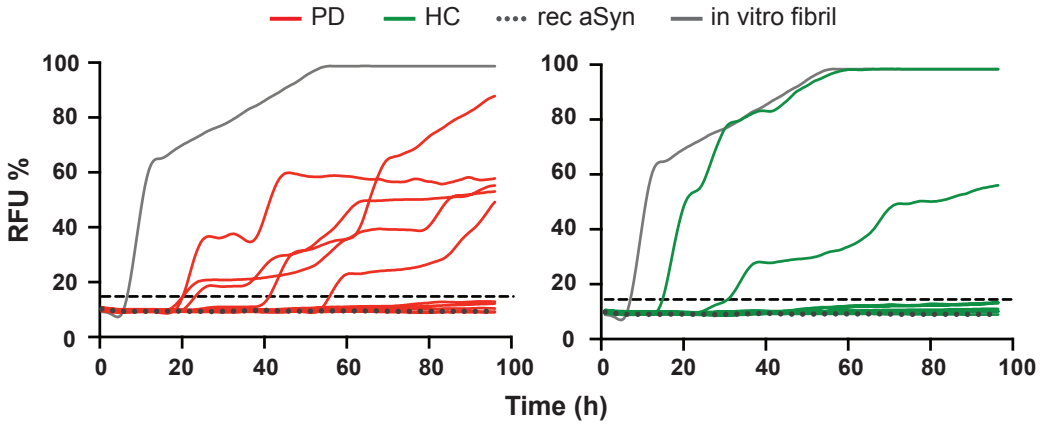

Figure 7.9 **SAA detection of αSyn seeding activity in PD saliva.** αSyn SAA analysis of αSyn seeding activity of 10 PD (red) and 10 HC (green) salivary samples. Each sample was run in triplicates and the fluorescence curves represent the average of the triplicates. The reactions with in vitro fibril seed and without seed (rec αSyn) are positive and negative controls, respectively. The threshold was set at 5 standard deviations from the averaged initial fluorescence.

Next, as a preliminary investigation, 10 samples from each PD and HC were examined using the optimised assay conditions. Saliva derived from PD patients showed greater seeding capacity compared to those from HC subjects. The averaged fluorescence readings of the replicates in Fig. 7.9 show that 5/10 PD samples and 2/10 HC samples crossed the threshold and showed positive seeding activity. As a result, the assay performed with 50 % sensitivity and 80 % specificity. Contrary to the stereotypical sigmoidal shape of SAA fluorescence curves, the results demonstrated a ladder-like curve. In addition, the fluorescence readings of each replicate highlight the variability of the seeding activity between replicates (Figs. A.8 & A.9). The curve shape and SAA kinetics varied significantly between the three replicates, especially for the PD salivary samples (Fig. A.8).

7.3 Discussion

7.3.1 Salivary αSyn

No significant differences were observed in the salivary levels of total and aggregated αSyn between PD and healthy subjects using ELISA, which aligns with previous findings[166]. However, most salivary αSyn ELISA studies reported lower salivary levels of total Syn and higher levels of aggregated αSyn in PD compared to healthy controls[133,156,158–160]. The differences could be caused by several factors. In this study, αSyn Legend MAX ELISA kit (BioLegend) was chosen due to its wider standard range and high sensitivity compared to the kits used in previous publications. The high sensitivity might have resulted in a more accurate measurement of salivary αSyn levels. Furthermore, the antibodies used in the commercial kits are unknown. It has been highlighted that αSyn antibodies are not specific for a particular 'species' of αSyn, and different antibodies show distinct immunoreactivity to αSyn monomers, oligomers, and fibrils[190]. Therefore, the αSyn 'species' detected by the ELISA kits and their representativeness of the salivary αSyn population is questionable.

7.3.2 Salivary proteomic profiling

This study reported a reduced salivary CH3L2 level in PD. To date, several chitinase-like proteins (CLPs) have been characterised in humans, including the chitinase-like protein-1 (CH3L1) and chitinase-like protein-2 (CH3L2). CLPs are involved in cartilage tissue differentiation and growth but also display cytokine-like properties[215]. They are secreted by immune cells and activated microglia, which might explain their elevated levels in diseases associated with infection and inflammation[216]. Interestingly, multiple findings demonstrated the association of CH3L2 level with the progression of several neurodegenerative diseases. For example, higher CSF levels of CH3L2 were associated with progressive multiple sclerosis (MS) and amyotrophic lateral sclerosis (ALS) patients[217,218].

Chitinases in PD have also been investigated, but current findings are limited to

CH3L1 and not CH3L2. The CSF levels of CH3L1 were negatively correlated to the Montreal cognitive assessment (MoCA) score in PD patients[219]. Nevertheless, the CSF levels of CH3L1 were not distinguishable between PD and healthy subjects[219,220]. CH3L1 was not detected in any of the saliva samples in this study.

Furthermore, the abundance of ENDOU and A1AT were more than 2-fold different in PD than in healthy saliva. According to published reports, ENDOU has not been investigated in neurodegenerative diseases, and the significance of finding this protein in PD saliva remains unclear. On the other hand, A1AT is a serine protease inhibitor known to attenuate microglial-mediated inflammation and retinal degeneration[221–223]. Interestingly, while reducing inflammatory effect, A1AT reduces β-amyloid phagocytosis by microglial cells in vitro[221]. Therefore, an increased level of A1AT in PD saliva might reflect an anti-inflammatory response, which simultaneously inhibits αSyn aggregate clearance mechanism.

7.3.3 αSyn seeding activity in PD saliva

The preliminary investigation demonstrates evidence of αSyn seeding activity in salivary samples from PD. The αSyn SAA resulted in 50% sensitivity and 80% specificity. The assay specificity is similar to previously published results, but the sensitivity is much lower[133,172]. It is critical to continue the investigation with all the samples and assess the reproducibility of the assay outcome to build rigour to the current finding.

The limited performance of the αSyn SAA with saliva might indicate the necessity for further optimisation. On the other hand, the possibility that the saliva matrix reduces the assay sensitivity cannot be excluded. Interestingly, αSyn SAA of nasal brushing samples from PD and iRBD patients also resulted in low assay sensitivity due to the nasal brushing matrix inhibiting αSyn aggregation during the SAA reaction[224]. Saliva is another complex matrix, which might also have an inhibitory effect on αSyn aggregation. Such possible effects should be assessed when further optimising salivary αSyn SAA.

7.3.4 Experimental limitations

Experimenting with different αSyn-specific antibodies and HRP-conjugated antibodies, multiple HMW bands were detected in PD and HC saliva using immunoblotting. However, 14 kDa monomeric αSyn bands were absent. Further analysis with more sensitive ELISA assays demonstrated that the salivary αSyn levels range between 10.3 - 186.6 pg/mL and aggregated αSyn ranged between 4.3 - 41.9 pg/mL. ELISA measurements indicate the presence of salivary αSyn in the scale of picograms, whilst the detection sensitivity of immunoblotting is restricted to the nanogram range[225]. Therefore, the low amount of αSyn present in saliva is non-detectable using immunoblot and the bands observed in this chapter are likely non-specific background signals resulting from the complex matrix of salivary composition.

The proteomic analysis was confronted with the inherent variability in the protein composition of saliva across individual subjects. As a result, the study employed a methodological approach that involved pooling saliva samples from groups of PD patients and healthy controls. This pooling strategy renders the representative 'average' salivary alterations in PD instead of individual-specific changes. Therefore, to validate the findings, it is crucial to examine individual saliva for reported molecular changes.

7.3.5 Summary

This chapter identified three main molecular changes in PD saliva: 1) no significant changes in the level of αSyn, 2) reduced CH3L2 and ENDOU and increased A1AT abundance and 3) αSyn seeding activity. The heterogeneous nature of the salivary complex was the major challenge in this study. Therefore, future investigation is needed in larger cohorts and instead of focusing on a single target, a combination of multiple measurements might facilitate biomarker research.

Chapter 8

General discussion

The overarching aims of this thesis were to investigate the brain-derived αSyn fibrils from different synucleinopathies and compare them to the counterpart SAA fibrils. Also, it aimed to investigate the diagnostic value of αSyn SAA for CSF from PD and MSA patients and salivary biomarkers for PD. This chapter recapitulates and summarises the key findings from each chapter. The significance and implications of the findings are discussed by contextualising the findings with existing literature. Also, the chapter examines the study's limitations and research directions, highlighting the opportunities for future work.

8.1 Key findings

Chapter 4 investigated the biochemical and biophysical properties of PD brain-derived αSyn fibrils. To achieve this, the sarkosyl-based extraction method was optimised to isolate the αSyn fibrils from the brain. Screening the fibrils with 12 αSyn antibodies showed that the C-terminal targeting antibodies were specific towards sarkosyl-insoluble αSyn from PD. Digesting the PD αSyn fibrils at low PK concentrations revealed the variable PK-resistant signatures between different PD cases, which might indicate the existence of multiple αSyn strains within PD. TEM images showed straight and twisted morphologies of the PD αSyn fibrils. Distinct immunogold-labelling patterns of different

antibodies demonstrated the structural heterogeneity of PD brain-derived αSyn fibrils.

Chapter 5 characterised the biochemical and biophysical properties of the brain-derived αSyn fibrils from PD, PDD, DLB and MSA and assessed whether these properties are replicated in the SAA fibrils. Distinct seeding kinetics, PK and GdnHCl resistance and morphology of the brain-derived fibrils provided evidence of αSyn strains in different synucleinopathies. However, the corresponding SAA fibrils demonstrated strikingly different profiles than the brain-derived fibrils. The uniform biochemical profiles of the SAA fibrils across the synucleinopathies suggest SAA might be 'printing' identical fibrils regardless of the seed. The SAA fibrils displayed a single dominant structure, either straight or twisted. Unexpectedly, the PDD/DLB SAA fibrils were weakly phosphorylated, while PD/MSA SAA fibrils were not. These observations demonstrate the limitation of the SAA αSyn fibrils in representing the biochemical and biophysical properties of the brain-derived αSyn fibrils.

Chapter 6 quantified αSyn seeding in CSF of PD and MSA patients to stratify PD versus MSA and assessed its association with disease progression. To achieve this, different kinetic parameters were extracted from the αSyn SAA reaction. Parameters T_{50} and V_{MAX} were distinguishable between PD and MSA, suggesting faster αSyn seeding activity in MSA. In PD patients, there were no clear correlations between the SAA parameters and clinical data. However, differences in the overall SAA reactivity and V_{MAX} across different PD clusters suggest evidence of distinct αSyn strains within a single disease entity. In MSA patients, all SAA parameters correlated with disease progression. Findings demonstrate the value of αSyn SAA as a diagnostic biomarker that could advance PD/MSA diagnosis and provide information about disease progression and phenotypes.

Chapter 7 explored signature molecular changes in PD salivary samples that could serve as a disease biomarker. ELISA revealed that the salivary levels of total and aggregated αSyn do not differ between PD and healthy subjects. Non-specific immunoreactivity of the secondary antibodies limited antibody-based characterisation of saliva using

immunoblot. To overcome this limitation, HRP-conjugated αSyn antibodies were used, which identified significantly higher levels of multimeric αSyn species in PD saliva than in healthy controls. The proteomic analysis found lower CH3L2 and ENDOU and a higher level of A1AT in PD saliva than in healthy controls. Preliminary αSyn SAA identified seeding activity in PD saliva, suggesting the presence of αSyn seeding competent and pathological αSyn species in PD saliva.

8.2 Implications of findings

This section will discuss the general implications of the main findings from each chapter and new hypotheses generated as a result. A more detailed speculation with the reflection of existing literature is elaborated in the discussion section of each chapter.

8.2.1 Characterisation of brain-derived αSyn fibrils

Characterising the brain-derived αSyn fibrils provides an investigative lens into the underlying molecular mechanisms of synucleinopathies. As analogised in the introduction, these fibrils resemble the 'broken parts' in a 'junkyard,' offering invaluable insights into the 'malfunctioning machinery' of neurodegenerative diseases. Chapter 4 examined the biochemical and biophysical heterogeneity of αSyn fibrils extracted from PD brains. This biochemical variability aligns with prior studies[109] and underscores the molecular diversity inherent in these fibrils. Importantly, this molecular heterogeneity may correlate with the clinical and phenotypic variability observed in PD patients[11], thereby offering a potential explanation for the diverse clinical manifestations of the disease.

While focusing on fibrils provides a targeted approach, it raises the question of potential bias. The sarkosyl-extraction method is designed to isolate fibrils, yet it may not preclude the presence of high molecular weight oligomers. It is crucial to recognise that fibrils, oligomers and monomers may coexist in a dynamic equilibrium within the neural environment. Consequently, the results obtained from immunoblotting and PK profiles may reflect a composite state of various αSyn conformers rather than exclusively fibrils.

This limitation, which is elaborated further in Section **??**, suggests that the biochemical findings from Chapter 4 could be more representative of the entire spectrum of αSyn conformers present in the diseased brain. Given that oligomers have been implicated as the primary toxic species in PD[84], future research should extend beyond fibrils to include other molecular states of αSyn. This broader approach will provide a more holistic view of the 'malfunctioning machinery'.

8.2.2 Strain-like properties of the brain-derived αSyn fibrils from different synucleinopathies

Do distinct synucleinopathies PD, PDD, DLB, and MSA each harbour a unique αSyn strain? Previous reports on the distinct structures, seeding kinetics, and pathological properties of brain-derived αSyn from synucleinopathies demonstrate evidence of αSyn strains[85,104,109,111]. Chapter 5 identified the distinct biochemical and biophysical properties of the αSyn fibrils from different synucleinopathies, adding further observations of αSyn strain-like properties.

Cryo-EM studies reported that brain-derived αSyn fibrils from LBDs share a common fibrillar architecture distinguishable from those of MSA[104]. Similarly, Chapter 5 showed that MSA brain-derived fibrils have distinct TEM morphologies compared to the LBDs. These observations might indicate the presence of distinct αSyn strains between LBDs and MSA and a common strain among the LBDs. PDD and DLB exhibited similar seeding kinetics, TEM morphologies and phosphorylation patterns. Perhaps a common fibril or strain exists in both PDD and DLB. In contrast, PD demonstrated weaker seeding capacity and conformational stability than PDD and DLB. It must be noted that the sarkosyl-insoluble fraction of PD brains contained fewer amounts of αSyn fibrils than PDD and DLB. Thus, such molecular differences observed in PD brain-derived fibrils might have been caused by limited amounts of fibrils. PDD and DLB might represent advanced stages of PD, characterised by the accumulation and higher amounts of identical fibrils or strains.

Furthermore, each synucleinopathy could be associated with a spectrum of αSyn strains. The cryo-EM study on the Lewy fold identified both twisted and straight fibrils but only characterised the twisted[104]. The uncharacterised, straight fibrils might possess a distinct architecture, potentially signifying a separate strain. Similarly, the finding of straight and twisted fibrils from PD, PDD and DLB brains might indicate the co-existence of multiple αSyn strains underlying the clinical and pathological heterogeneity of synucleinopathies.

8.2.3 Brain-derived versus SAA αSyn fibrils

Chapter 5 illustrated significant biochemical and biophysical differences between brain-derived and SAA αSyn fibrils. While SAA fibrils offer advantages such as higher fibril yield and purity, facilitating downstream fibril research, the pronounced differences underscore the importance of considering such limitations when applying SAA fibrils to studying αSyn strains.

Numerous factors might account for the differences. The SAA reaction is driven by templated aggregation, wherein the intrinsic properties of the seeds are replicated in the newly amplifying fibril. This appears to hold true for second-generation seeding by the SAA fibrils. However, primary seeding with brain-derived fibrils presents a conundrum. The limited purity of brain-derived fibrils may impede templated seeding. Moreover, the absence of PTMs on the SAA fibrils could play a role. Prior cryo-EM studies have revealed that bulky PTMs, such as ubiquitination at specific core residues, significantly alter the secondary structure of the fibrillar core[85].

The observed differences accentuate the necessity for more representative models for brain-derived αSyn fibrils. One potential avenue could involve using induced pluripotent stem cell (iPSC) - derived neurons to amplify fibrils. iPSC-derived neurons seeded with brain-derived αSyn fibrils could facilitate endogenous fibril amplification under more physiological conditions, allowing the incorporation of PTMs. Tanudjojo and colleagues have shown that SAA fibrils (amplified from PD and MSA brain homogenates)

induced distinct patterns of αSyn pathology and toxicity in iPSC-derived dopaminergic neurons[118]. Also, the PD and MSA-amplified fibrils from the cellular lysates showed different patterns of PK resistance. Findings indicate a successful amplification of distinct αSyn fibrils or strains. The same investigation can be done with brain-derived fibrils, which may result in the amplification of more biologically representative fibrils. However, this approach may entail a longer amplification period compared to SAA. Most importantly, the multi-dimensional differences, such as biological and pathological aspects, must be understood in brain-derived and SAA fibrils to better develop a representative model for brain-derived αSyn fibrils.

8.2.4 Quantification of αSyn seeding in CSF of PD and MSA patients

The results presented in chapter 6 emphasise the utility of αSyn SAA as a diagnostic instrument for PD and MSA. Notably, the assay's sensitivity was significantly lower for MSA than PD, indicating that a smaller proportion of MSA samples exhibited detectable αSyn seeding activity or that the amyloid dye ThT does not properly bind to the MSA fibrils. Intriguingly, several studies have even documented an absence of αSyn seeding activity in MSA CSF samples[113,209]. In contrast, research has shown that mice injected with MSA brain-derived αSyn aggregates exhibit accelerated disease propagation relative to LBD[92], suggesting fast αSyn seeding activity in MSA brains. Furthermore, data from Chapter 5 revealed similar seeding activities for brain-derived αSyn fibrils from both PD and MSA. This raises the possibility that in MSA, seeding-competent αSyn species present in the brain might be underrepresented in the CSF or that a distinct αSyn strain, which escapes ThT detection, might be prevalent.

Moreover, the SAA parameters did not correlate with PD clinical metrics, and only some unexpected correlations were found where lower seeding activity was associated with a more severe disease state. Further analyses would need to examine larger cohorts with longitudinal CSF samples representing a wider spectrum of PD disease severity. Nevertheless, identifying a correlation between SAA parameters and MSA disease pro-

gression implies its clinical use to predict and measure disease progression. However, this also needs to be repeated in a larger longitudinal cohort.

The identification of distinct PD clinical clusters, differentiated by a specific SAA parameter (specifically V_{MAX}), reinforces the hypothesis surrounding the existence of αSyn strains. Interestingly, clusters with more advanced disease manifestations exhibited elevated V_{MAX} values, indicative of faster seeding activities. However, this could potentially be attributed to higher accumulation of αSyn aggregates in the brain due to severe disease progression. To comprehensively characterise the αSyn strains associated with these PD clusters, biological and biochemical characterisation of these CSF samples, as presented in Chapter 4, would be important.

8.2.5 Salivary biomarkers and its limitations

Chapter 7 identified prospective salivary biomarker candidates for PD, a frontier that remains relatively unexplored, particularly in the context of salivary proteomics for PD. The findings from Chapter 7 and previous literature combined suggest an increase in the level of oligomeric αSyn in PD saliva. The precise explanation of how αSyn is found in saliva is unclear. However, it is hypothesised that αSyn is secreted from salivary glands. Also, findings from this chapter demonstrated αSyn seeding activity from PD saliva. These observations suggest that PD saliva contains seeding competent αSyn species.

Other than αSyn, general salivary molecular biomarker research has challenges. Salivary protein composition is influenced by circadian rhythm, diet, and oral health[226]. Additionally, the lack of standardised collection and processing methods for saliva samples has made it challenging to compare results across studies[227]. Despite these limitations, the non-invasive nature of saliva collection makes it an attractive biofluid for biomarker research in PD. Salivary biomarker research is in its early stages, and with improved standardised collection and processing protocols and large longitudinal studies, saliva has the potential as an attractive medium for biomarkers of PD and other synucleinopathies.

8.3 Future directions

To progress from the findings from this thesis, future research might aim to systematically compare various extraction methods for αSyn fibrils. This would involve both biochemical and structural characterisation to elucidate the nuances between different extraction techniques. The objective could be to identify optimal methods for isolating a larger or specific spectrum of αSyn conformers, reflecting the heterogeneous population of fibrils.

Another promising avenue for future research lies in exploring the relationship between molecular and clinical subtypes of PD. Specifically, studies could aim to correlate the biochemical properties of αSyn fibrils with the clinical manifestations of the disease. Achieving this would necessitate a longitudinal study design, incorporating a cohort with extensive clinical characterisation and post-mortem brain samples. While logistically challenging, such an approach is currently ongoing with the Oxford Discovery study[11] and is likely to yield invaluable insights into whether biochemical subtypes of αSyn fibrils correspond to distinct clinical subtypes of PD. This, in turn, could offer a molecular explanation for the heterogeneous phenotypes observed in PD patients.

Furthermore, αSyn fibril variability across different brain regions is worth investigating. The objective would be to conduct a comprehensive examination of the biochemical and biophysical properties of these fibrils in various brain regions. To date, a systematic assessment encompassing multiple brain regions is lacking in the literature. Moreover, existing studies frequently employ different brain regions for their analyses, complicating direct comparisons. Undertaking a region-specific profiling of αSyn fibrils could furnish a more holistic understanding of their variability.

Intriguingly, the twisted fibrils observed via TEM were largely undetected by αSyn-specific antibodies. Future research could benefit from cryo-EM to elucidate the precise nature of these twisted fibrils. Such an investigation would not only confirm their molecular identity but also reveal insight into their frequent occurrence in the brains of patients with PD, PDD and DLB.

This thesis focused on the biochemical and biophysical characterisation of αSyn fibrils. For future studies, the biological properties of the fibrils can be explored as strains are defined by the distinguishable disease phenotypes resulting from transmitting an identical host[96]. Cellular or mice models of synucleinopathy can be infected with brain-derived fibrils and examine seeding efficiency, disease incubation time and propagation of αSyn pathology throughout different brain regions[92, 109].

In order to further validate the value of αSyn SAA as a diagnostic and molecular marker, a large longitudinal study would be essential. For a given period of time, a routine CSF collection and αSyn SAA can be performed to build a timeline of disease progression and the corresponding quantitative SAA outcome. Such a study might produce an improved understanding of how the clinical trajectory is reflected by the SAA parameters and assessment of SAA as a prognostic biomarker.

Alternative to salivary protein biomarkers, metabolomics offers a promising direction for future research. The composition of salivary metabolites is intricately linked to the oral microbiome, an area that parallels the extensive research conducted on the gut microbiome in PD[228]. Given the emerging significance of microbiomes in PD pathophysiology, investigating the oral microbiome through salivary metabolomics could yield valuable insights. Previous studies have already undertaken metabolic profiling of saliva in PD patients, revealing elevated concentrations of specific metabolites such as taurine and gamma-aminobutyric acid (GABA)[229]. These findings suggest that metabolic dysregulation could serve as an additional hallmark of PD, thereby presenting a potential candidate for biomarker development.

8.4 Concluding remarks

The intricate heterogeneity of synucleinopathies raises perplexing questions: What role does αSyn play, and how can it be better diagnosed? This thesis addresses the complex landscape of αSyn fibrils, suggesting that the relationship between specific synu-

cleinopathies and αSyn strains may not be as straightforward as one disease-one strain. Distinct αSyn strains or a mixture of strains might represent different clinical subtypes of one disease. Developing representative αSyn fibril models could facilitate investigating the intricate relationship. Subsequently, understanding the molecular basis of distinct synucleinopathies could promote the innovation of disease-stratifying and more quantitative and non-invasive biomarkers.

Appendix A

Appendices

A.1 Chapter 4

A.1.1 Immunogold-TEM analysis of αSyn fibrils from PD brains

αSyn fibrils extracted from PD brains were screened for immunolabelling on TEM using 12 different αSyn specific antibodies. The NAC-region targeting antibodies (80-96, Syn1), three C-terminal antibodies (110-115, LB509, Syn211), and an oligomeric αSyn-specific antibody (5G4) did not label any fibrils on TEM as shown on Fig. A.1. This observation suggests that these regions might be embedded in the core.

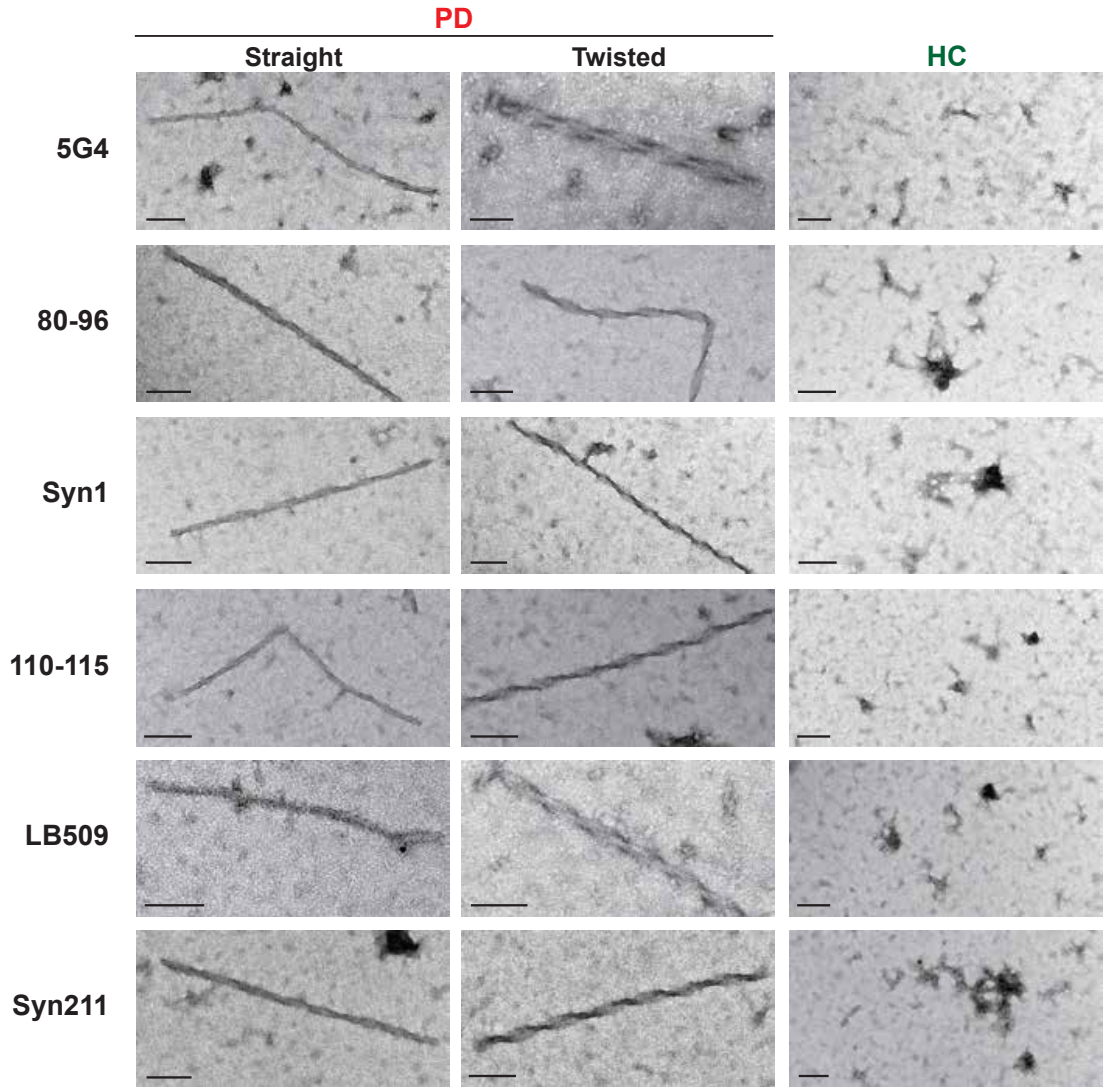

Figure A.1 **Immunogold-TEM images of unlabelled αSyn fibrils.** TEM images of αSyn fibrils from PD brains that were not labelled using 5G4, 80-96, Syn1, 110-115, LB509 and Syn211 antibodies. These 6 antibodies did not label both the straight and twisted fibrils. Sarkosyl-insoluble fraction from HC brain was used as a negative control. Scale bar = 100 nm.

A.2 Chapter 5

A.2.1 Conformational stability of brain-derived and SAA αSyn fibrils

The conformational stability of the brain-derived and SAA αSyn fibrils were assessed using GdnHCl denaturation combined with PK digestion (Fig. A.2a-d). The PD and MSA brain-derived fibrils showed rapid denaturation, whereas those of PDD and DLB were more resistant. The adjacent comparison of the brain-derived and SAA fibrils demonstrates the clear contrast in conformational stability between the two fibrils. All SAA fibrils were more conformationally stable compared to the brain-derived fibrils and revealed an identical resistance profile.

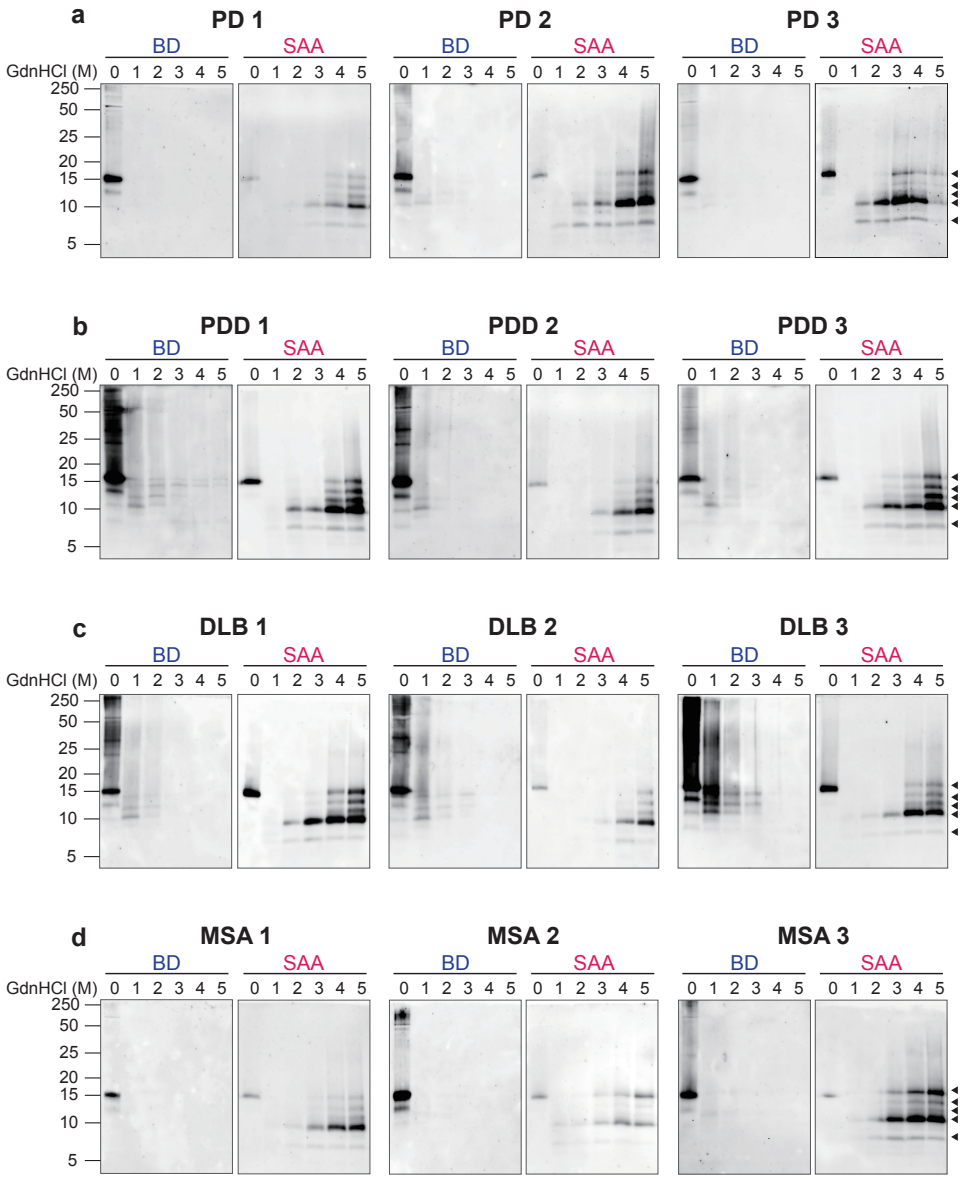

Figure A.2 **Conformational stability of brain-derived and SAA αSyn fibrils. a-d**, Brain-derived and SAA αSyn fibrils from PD (**a**), PDD (**b**), DLB (**c**), and MSA (**d**) were digested with increasing concentrations of GdnHCl (1-5 M) and 1 µg/ml of PK. The 0 M GdnHCl represents a non-treated sarkosyl-insoluble fraction (no PK digestion). The digested products were resolved with Western blot using Syn1 antibody. Results for all 3 cases are shown. Molecular weights (kDa) are indicated on the left of the immunoblots. Five black triangles on the right mark the uniform pattern of peptides revealed across all SAA fibrils.

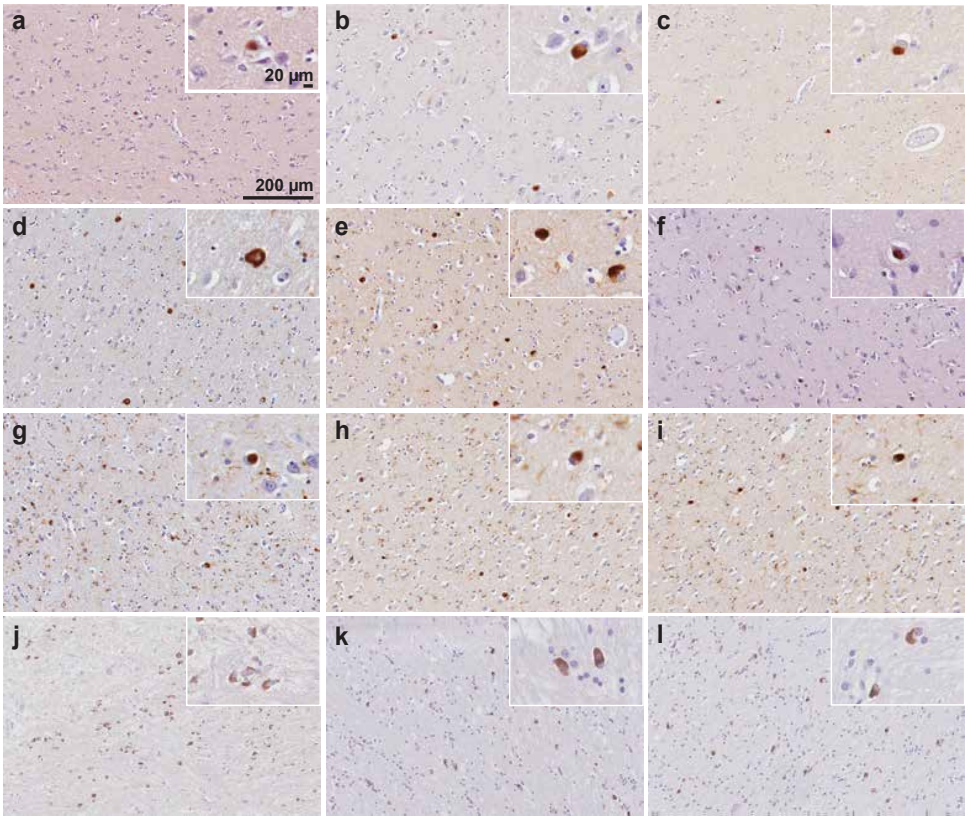

Figure A.3 **αSyn pathology in PD, PDD, DLB and MSA brains. a-l**, αSyn pathology in PD 1-3 (**a-c**), PDD 1-3 (**d-f**), DLB 1-3 (**g-i**), and MSA 1-3 (**j-l**) brains. The entorhinal cortex was selected for PD, PDD and DLB. Striatum was selected for MSA. Syn1 (BD Biosciences) was used to reveal the pathology. Scale bars, 200 µm and 20 µm (applies to all images).

A.2.2 Immunohistochemistry analysis of αSyn pathology in PD, PDD, DLB and MSA brains

Immunohistochemistry was performed to examine the αSyn pathology in the brains used in Chapter 5. Lewy bodies were present in the entorhinal cortex of PD, PDD and DLB (Fig. A.3a-i). Lewy neurites were also observed in PDD and DLB brains, revealing more severe pathology than PD. GCIs were observed in the striatum of MSA brains (Fig. A.3j-l).

A.2.3 Phosphorylated αSyn fibrils in PD, PDD, DLB and MSA brains

Sarkosyl-insoluble fractions of PD, PDD, DLB and MSA brains contained varying amounts of phosphorylated αSyn. Immunogold-TEM using pS129 antibody revealed that the fractions from PD and MSA contained a lower number of phosphorylated αSyn fibrils compared to those of PDD and DLB (Fig. A.4). This finding was further confirmed by immunoblot analysis.

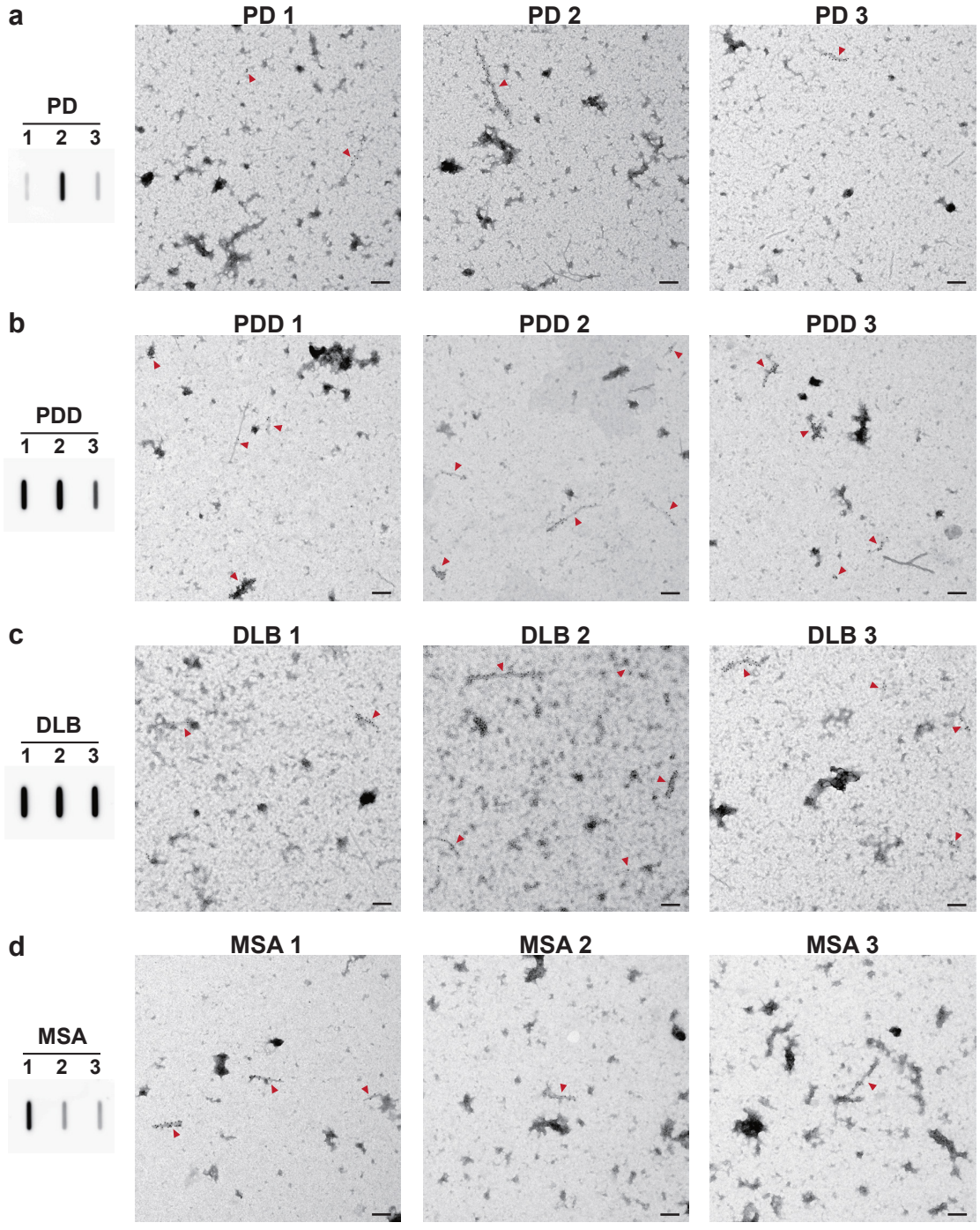

Figure A.4 **Immunogold-TEM images of phosphorylated αSyn from PD, PDD, DLB, and MSA brains.** **a-d**, Phosphorylated αSyn fibrils on TEM and immunoblot from the sarkosyl-insoluble fractions of PD (**a**), PDD (**b**), DLB (**c**) and MSA (**d**) brains. Phosphorylated αSyn fibrils are marked in red arrows on the TEM images. Scale bar = 100 nm (applies to all images).

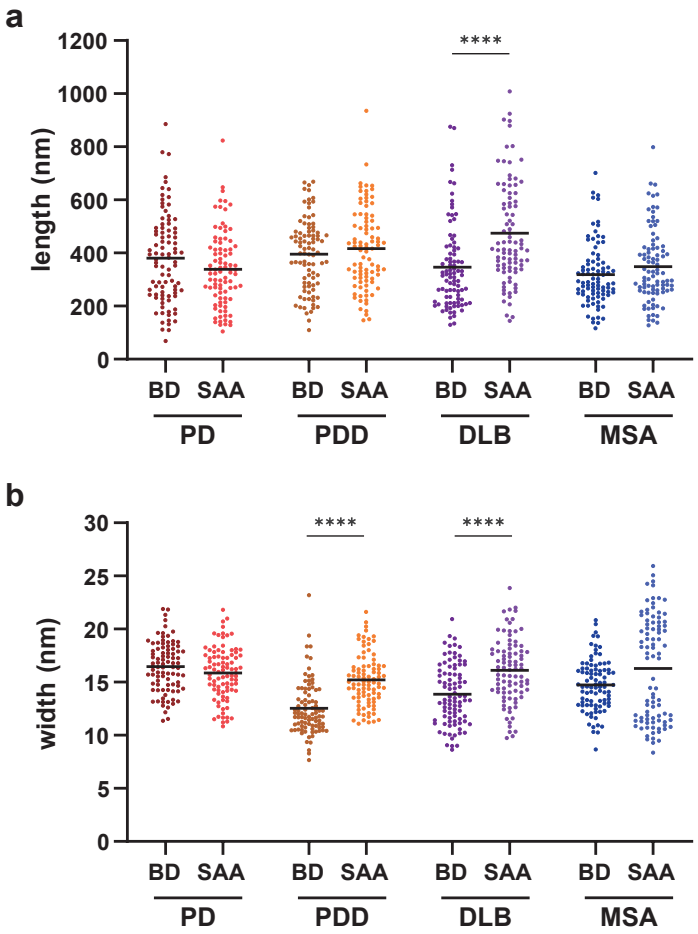

Figure A.5 **Length and width measurements of the brain-derived and SAA fibrils. a,b**, Comparison of the lengths (**a**) and widths (**b**) of the brain-derived (BD) and SAA fibrils. Thirty fibrils were measured for each disease case ($n = 3$). Thus, a total of 90 data points were plotted. The bold black line indicates an average. Mann-Whitney U test was used. ****$P \leq 0.001$.

A.2.4 Measurement of fibrils from TEM images

The lengths and widths of the fibrils were measured from the TEM images of brain-derived and SAA fibrils (Fig. A.5). Due to mixed straight and twisted morphologies of the fibrils, only straight fibrils were considered when measuring the lengths and the widths for direct comparison. However, MSA-SAA fibrils were twisted only, resulting in two different clusters of widths due to altering widths of the twists (Fig. A.5b).

A.3 Chapter 6

A.3.1 Association between SAA parameters and clinical symptoms of PD patients

Correlative analysis between SAA parameters and PD clinical symptoms is summarised in Table A.1. Highlighted in red, MDS-UPDRS I, MMSE and MoCA showed significant association with T_{50}. These correlations are visualised in Fig. 6.2.

Table A.1 Correlation analysis between SAA parameters and clinical data of PD patients. All data is estimate (95 % confidence interval); *P*-value. *P*-values < 0.05 are highlighted in red. Spearman rank correlation was used. UPDRS, Unified Parkinson's Disease Rating Scale; MDS-UPDRS, Movement Disorder Society Unified Parkinson's Disease Rating Scale; MoCA, Montreal Cognitive Assessment; MMSE, Mini-Mental state examination; LP, lumbar puncture.

Clinical data	SAA (+)	Lag phase	F_{MAX}	T_{50}	V_{MAX}	AUC
MDS-UPDRS I	0.69 (0.35, 1.36); $p = 0.28$	-0.20 (-0.44, 0.05); $p = 0.11$	-0.03 (-0.27, 0.21); $p = 0.82$	-0.33 (-0.56, -0.10); $p = 0.006$	-0.17 (-0.41, 0.07); $p = 0.16$	-0.15 (-0.40, 0.10); $p = 0.23$
MDS-UPDRS II	0.80 (0.39, 1.66); $p = 0.55$	-0.11 (-0.37, 0.14); $p = 0.38$	-0.04 (-0.29, 0.22); $p = 0.78$	-0.20 (-0.45, 0.06); $p = 0.13$	-0.12 (-0.37, 0.13); $p = 0.34$	-0.04 (-0.30, 0.22); $p = 0.76$
MDS-UPDRS III	0.92 (0.41, 2.05); $p = 0.84$	-0.13 (-0.38, 0.11); $p = 0.29$	-0.21 (-0.44, 0.03); $p = 0.090$	-0.15 (-0.40, 0.09); $p = 0.22$	-0.19 (-0.43, 0.05); $p = 0.12$	-0.19 (-0.43, 0.06); $p = 0.13$
MDS-UPDRS IV	0.92 (0.39, 2.17); $p = 0.85$	-0.03 (-0.27, 0.20); $p = 0.78$	0.09 (-0.14, 0.33); $p = 0.43$	-0.10 (-0.34, 0.13); $p = 0.38$	0.14 (-0.10, 0.38); $p = 0.24$	0.01 (-0.23, 0.25); $p = 0.91$
MMSE	1.88 (0.92, 3.84); $p = 0.084$	0.20 (-0.04, 0.45); $p = 0.11$	0.21 (-0.04, 0.45); $p = 0.094$	0.26 (0.02, 0.51); $p = 0.037$	0.24 (-0.00, 0.49); $p = 0.052$	0.12 (-0.13, 0.38); $p = 0.34$
MoCA	1.71 (0.76, 3.85); $p = 0.19$	0.25 (-0.00, 0.50); $p = 0.053$	0.07 (-0.18, 0.33); $p = 0.58$	0.33 (0.08, 0.58); $p = 0.010$	0.15 (-0.10, 0.41); $p = 0.24$	0.11 (-0.15, 0.37); $p = 0.39$
Disease duration	1.27 (0.60, 2.68); $p = 0.53$	-0.01 (-0.25, 0.23); $p = 0.95$	0.09 (-0.14, 0.33); $p = 0.42$	0.07 (-0.17, 0.30); $p = 0.59$	0.16 (-0.07, 0.40); $p = 0.17$	0.08 (-0.16, 0.32); $p = 0.53$
Age at LP	0.78 (0.39, 1.57); $p = 0.49$	0.04 (-0.21, 0.28); $p = 0.77$	-0.09 (-0.32, 0.15); $p = 0.47$	0.02 (-0.22, 0.27); $p = 0.84$	-0.01 (-0.25, 0.23); $p = 0.93$	-0.09 (-0.33, 0.16); $p = 0.48$
Gender	0.25 (0.03, 2.27); $p = 0.22$	-0.32 (-0.82, 0.18); $p = 0.21$	-0.41 (-0.90, 0.08); $p = 0.10$	-0.32 (-0.82, 0.18); $p = 0.21$	-0.29 (-0.79, 0.20); $p = 0.24$	-0.03 (-0.53, 0.48); $p = 0.92$

A.3.2 SAA parameter is associated with PD clinical clusters

The SAA parameters were compared across the four different PD clinical clusters, which is summarised in Table A.2. The proportion of SAA-positive samples was significantly different between clusters 1 and 2. Also, V_{MAX} significantly differed across the four clusters. The parametric values of each cluster are plotted in Fig. 6.3.

Table A.2 SAA parameters and PD clinical clusters. Data is presented as mean ± SD. Kruskal-Wallis test was used for statistical analysis. *P*-values < 0.05 are highlighted in red.

SAA parameter	Cluster 1 (n = 27)	Cluster 2 (n = 13)	Cluster 3 (n = 15)	Cluster 4 (n = 14)	*P*-value
SAA (+)	27 (100 %)	9 (69.2 %)	12 (80 %)	13 (92.9 %)	0.008
Lag phase	61.2 ± 21.8	73.5 ± 36.1	76.8 ± 28.0	62.6 ± 27.1	0.35
F_{MAX} (x 10^5)	2.07 ± 0.71	1.62 ± 1.10	1.67 ± 0.99	1.81 ± 0.94	0.35
T_{50}	72.6 ± 23.1	81.8 ± 31.2	90.9 ± 24.7	75.6 ± 26.8	0.17
V_{MAX} (x 10^4)	5.41 ± 3.74	3.00 ± 3.53	2.91 ± 2.33	6.87 ± 7.18	0.018
AUC (x 10^6)	8.90 ± 4.99	9.74 ± 8.59	5.95 ± 3.42	8.00 ± 5.24	0.41

A.3.3 SAA parameters correlate with MSA disease progression

Correlative analysis between SAA parameters and clinical symptoms of MSA patients is summarised in Table A.3. Highlighted in red, all five parameters showed a significant correlation with the change in UMSARS. These correlations are visualised in Fig. 6.4.

Table A.3 Correlation analysis between SAA parameters and clinical data of MSA patients. All data is estimate (95 % confidence interval); *P*-value. *P*-values < 0.05 are highlighted in red. Spearman rank correlation was used. NA indicates that the model could not be formulated due to perfect prediction. Only 20 patients had UMSARS follow-up data. MSA-C, Multiple System Atrophy-cerebellar type; MSA-P, Multiple System Atrophy-parkinsonian type; UMSARS, Unified Multiple System Atrophy Rating Scale; LP, lumbar puncture.

Clinical data	SAA (+)	Lag phase	F_{MAX}	T_{50}	V_{MAX}	AUC
MSA-C vs MSA-P	NA	0.59 (–0.42, 1.60); $p = 0.23$	0.74 (–0.24, 1.72); $p = 0.13$	0.19 (–0.86, 1.24); $p = 0.70$	0.54 (–0.46, 1.54); $p = 0.27$	0.85 (–0.10, 1.80); $p = 0.077$
UMSARS baseline	0.70 (0.18, 2.74); $p = 0.61$	–0.54 (–1.11, 0.03); $p = 0.063$	–0.15 (–0.77, 0.46); $p = 0.61$	–0.60 (–1.19, –0.02); $p = 0.045$	–0.38 (–0.98, 0.22); $p = 0.20$	–0.41 (–0.97, 0.16); $p = 0.14$
UMSARS follow-up	1.62 (0.32, 8.13); $p = 0.56$	–0.37 (–1.18, 0.45); $p = 0.35$	0.03 (–0.76, 0.82); $p = 0.93$	–0.49 (–1.31, 0.34); $p = 0.23$	–0.21 (–1.04, 0.62); $p = 0.60$	–0.19 (–0.96, 0.57); $p = 0.60$
UMSARS change	NA	0.69 (0.12, 1.25); $p = 0.021$	0.67 (0.15, 1.19); $p = 0.015$	0.56 (–0.08, 1.20); $p = 0.083$	0.70 (0.15, 1.26); $p = 0.016$	0.68 (0.18, 1.18); $p = 0.011$
Age at LP	0.96 (0.37, 2.47); $p = 0.93$	–0.18 (–0.65, 0.30); $p = 0.45$	–0.18 (–0.64, 0.28); $p = 0.42$	0.12 (–0.38, 0.61); $p = 0.63$	–0.19 (–0.66, 0.28); $p = 0.41$	0.03 (–0.42, 0.48); $p = 0.89$
Disease duration	1.77 (0.54, 5.80); $p = 0.34$	0.09 (–0.38, 0.57); $p = 0.69$	0.11 (–0.35, 0.57); $p = 0.62$	0.01 (–0.48, 0.51); $p = 0.96$	0.13 (–0.34, 0.60); $p = 0.57$	0.05 (–0.40, 0.50); $p = 0.81$
Gender	1.40 (0.21, 9.49); $p = 0.73$	–0.21 (–1.20, 0.79); $p = 0.67$	–0.28 (–1.25, 0.68); $p = 0.55$	–0.15 (–1.18, 0.89); $p = 0.77$	0.03 (–0.96, 1.01); $p = 0.96$	–0.67 (–1.60, 0.27); $p = 0.15$

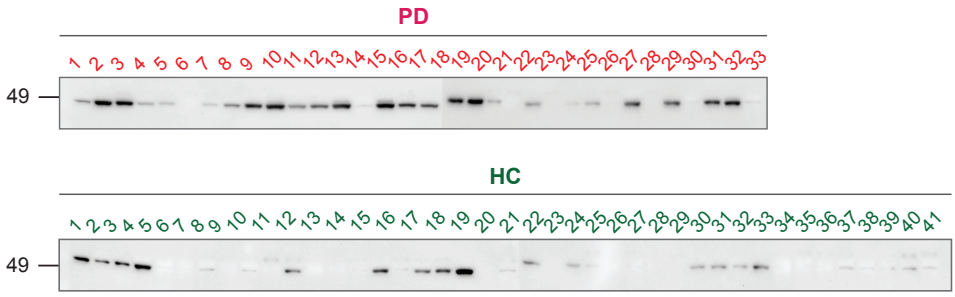

Figure A.6 Complete immunoblots of SynO4. Immunoreacitivity of SynO4 towards PD (n = 33) and HC (n = 41) saliva. SynO4 showed specific immunoreactivity to a 49 kDa protein in PD and HC saliva.

A.4 Chapter 7

A.4.1 SynO4 detects salivary αSyn

The immunoreactivity of SynO4 antibody was examined towards salivary samples from 33 PD and 41 HC subjects. The SynO4 antibody detected a 49 kDa αSyn in 25/33 PD and 15/41 HC salivary samples. The complete immunoblot of all the samples is presented in Fig. A.6.

A.4.2 HRP-conjugated αSyn antibodies detect salivary αSyn

The immunoreactivity of HRP-conjugated antibodies (34-45, 80-96, 103-108) was examined towards salivary samples from 33 PD and 41 HC subjects. The complete immunoblots of 33 PD and 41 HC salivary samples are presented in Fig. A.7a-c. All three antibodies detected a common 25 and 49 kDa αSyn species. The 80-96 antibody detected additional 38 and 62 kDa αSyn species (Fig. A.7b).

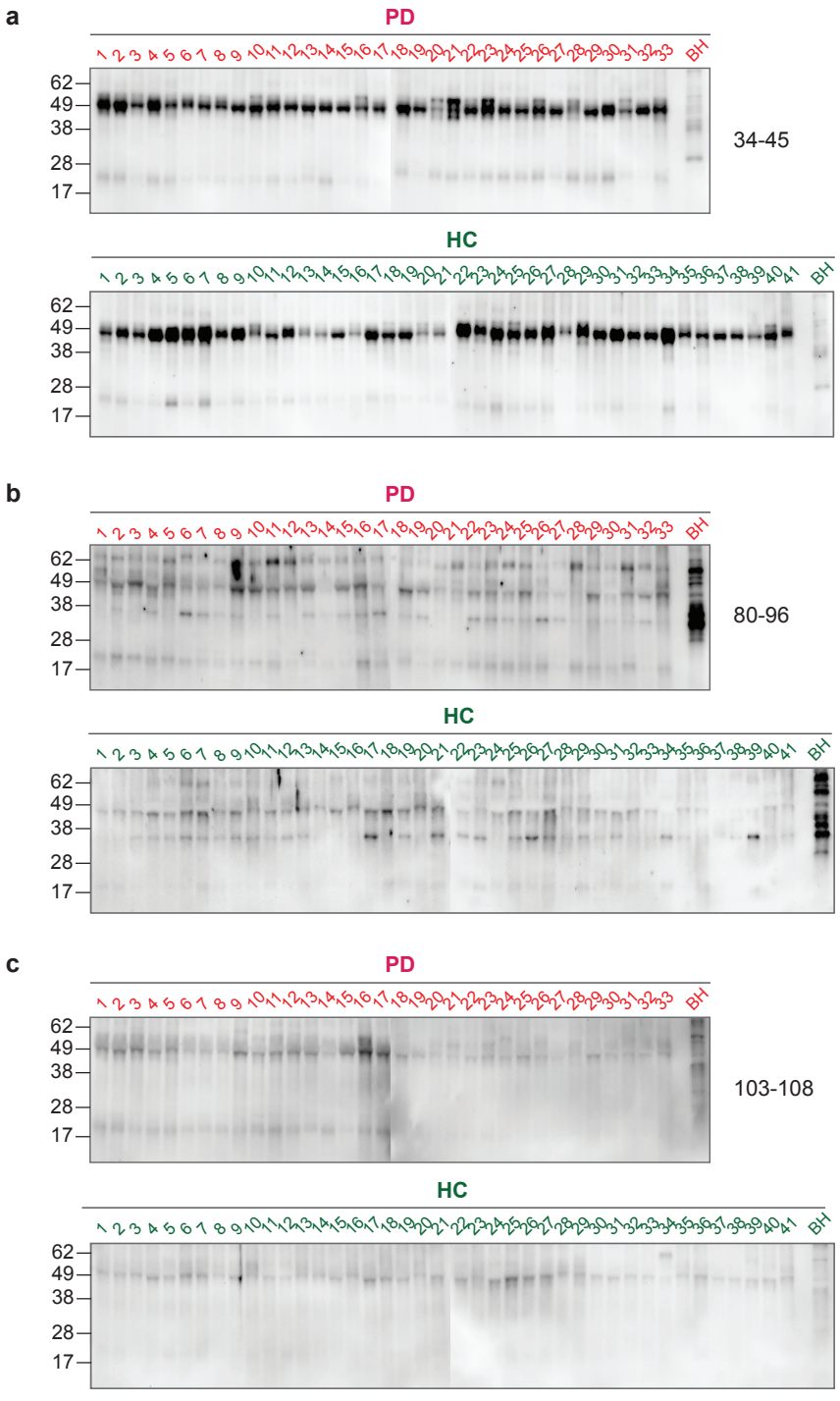

Figure A.7 **Complete immunoblots of HRP-conjugated antibodies. a-c**, Immunoreacitivity of HRP-conjugated antibodies 34-45 (**a**), 80-96 (**b**), and 103-108 (**c**) towards PD (n = 33) and HC (n = 41) saliva. BH (brain homogenate) was included as a positive control.

A.4.3 Detection of αSyn seeding activity in PD saliva

αSyn seeding activity was measured in the saliva samples from PD and HC subjects using SAA. Ten PD and 10 HC salivary samples were tested in triplicates. The averaged measurements are presented in Fig. 7.9. Here, the raw measurements of all the replicates are presented in Figs. A.8 & A.9.

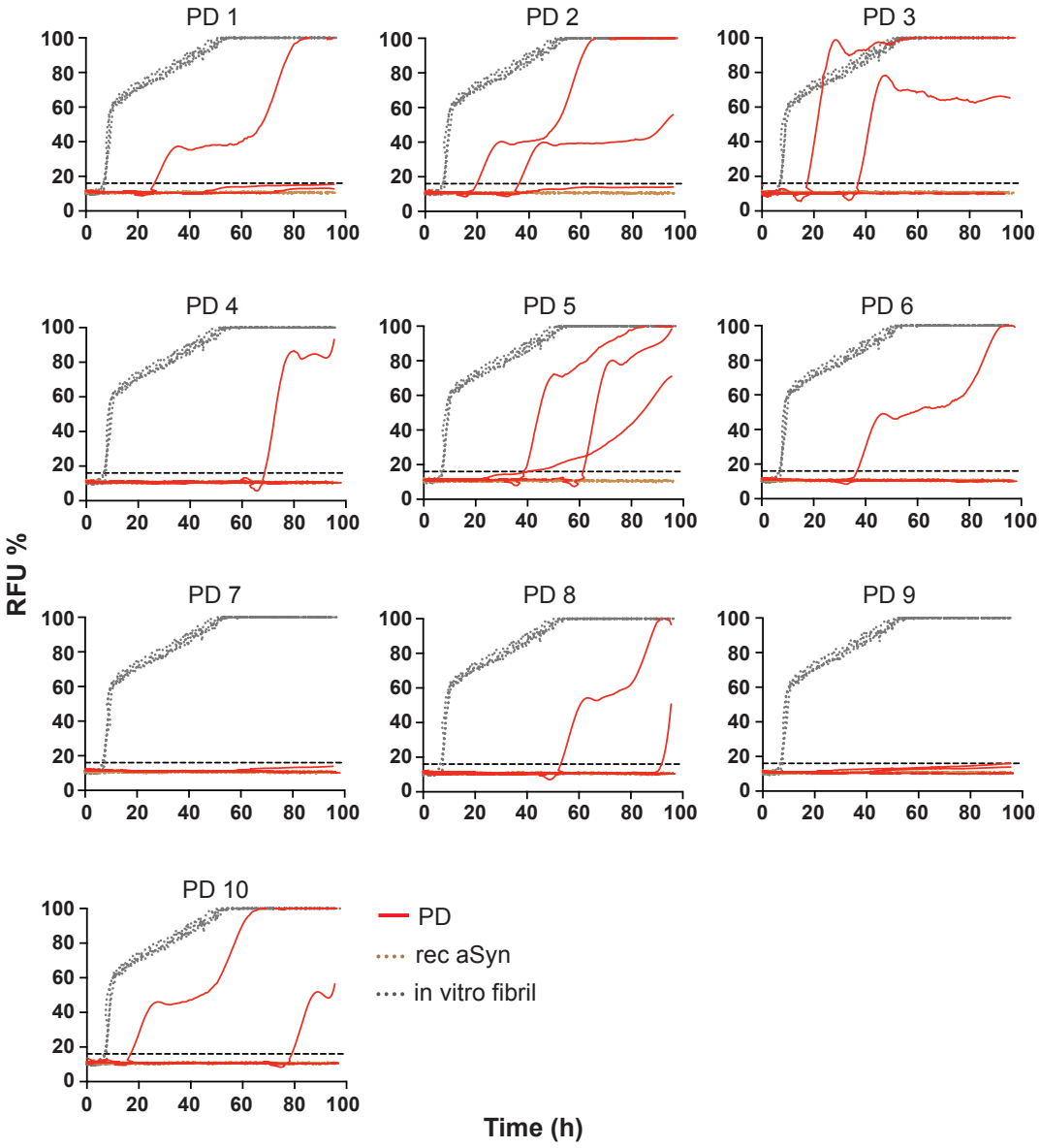

Figure A.8 **Raw SAA measures of αSyn seeding activity in PD saliva.** SAA analysis of αSyn seeding activity of 10 PD (red) salivary samples. Each sample (PD 1 - 10) was run in triplicates. The reactions with in vitro fibril seed and without seed (rec αSyn) are positive and negative controls, respectively.

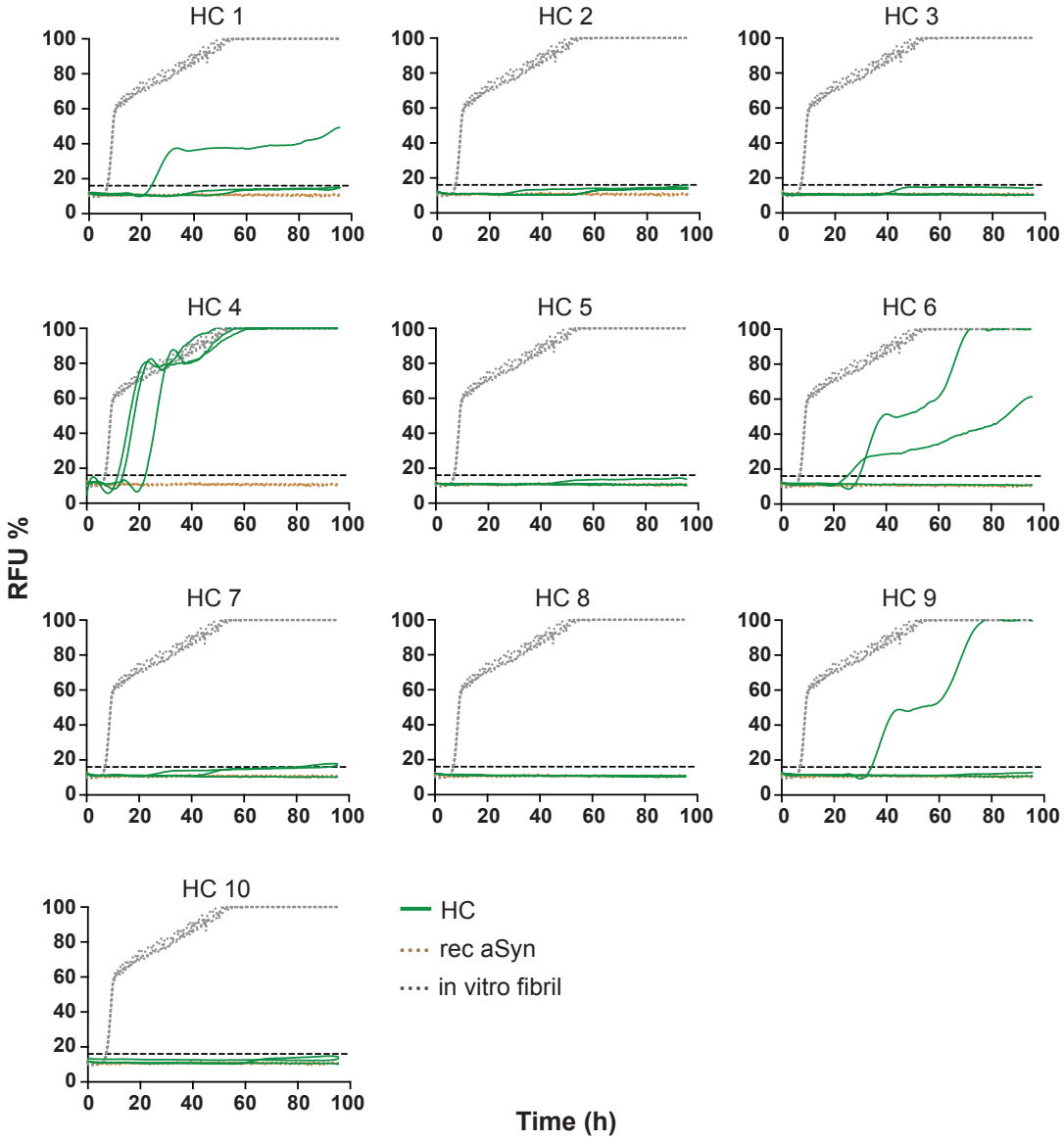

Figure A.9 **Raw SAA measures of αSyn seeding activity in HC saliva.** SAA analysis of αSyn seeding activity of 10 HC (green) salivary samples. Each sample (HC 1 - 10) was run in triplicates. The reactions with in vitro fibril seed and without seed (rec αSyn) are positive and negative controls, respectively.

References

1. Lewy, F. & Lewandowsky, M. Handbuch der neurologie. *Berlin: Julius Springer* (1912).

2. Altay, M. F., Liu, A. K. L., Holton, J. L., Parkkinen, L. & Lashuel, H. A. Prominent astrocytic alpha-synuclein pathology with unique post-translational modification signatures unveiled across lewy body disorders. *Acta Neuropathol. Commun.* **10**, 163 (2022).

3. Tysnes, O.-B. & Storstein, A. Epidemiology of parkinson's disease. *J. neural transmission* **124**, 901–905 (2017).

4. Hoehn, M. M., Yahr, M. D. *et al.* Parkinsonism: onset, progression, and mortality. *Neurology* **50**, 318–318 (1998).

5. Tolosa, E., Garrido, A., Scholz, S. W. & Poewe, W. Challenges in the diagnosis of parkinson's disease. *The Lancet Neurol.* **20**, 385–397 (2021).

6. Schenck, C. H., Boeve, B. F. & Mahowald, M. W. Delayed emergence of a parkinsonian disorder or dementia in 81% of older men initially diagnosed with idiopathic rapid eye movement sleep behavior disorder: a 16-year update on a previously reported series. *Sleep medicine* **14**, 744–748 (2013).

7. Emre, M. *et al.* Clinical diagnostic criteria for dementia associated with parkinson's disease. *Mov. disorders: official journal Mov. Disord. Soc.* **22**, 1689–1707 (2007).

8. Aarsland, D., Andersen, K., Larsen, J. P. & Lolk, A. Prevalence and characteristics of dementia in parkinson disease: an 8-year prospective study. *Arch. neurology* **60**, 387–392 (2003).

9. Goetz, C. G. *et al.* Movement disorder society-sponsored revision of the unified parkinson's disease rating scale (mds-updrs): scale presentation and clinimetric testing results. *Mov. disorders: official journal Mov. Disord. Soc.* **23**, 2129–2170 (2008).

10. Hoops, S. *et al.* Validity of the moca and mmse in the detection of mci and dementia in parkinson disease. *Neurology* **73**, 1738–1745 (2009).

11. Lawton, M. *et al.* Developing and validating parkinson's disease subtypes and their motor and cognitive progression. *J. Neurol. Neurosurg. & Psychiatry* **89**, 1279–1287 (2018).

12. Dijkstra, A. A. *et al.* Stage-dependent nigral neuronal loss in incidental lewy body and parkinson's disease. *Mov. disorders* **29**, 1244–1251 (2014).

13. Spillantini, M. G. *et al.* Filamentous alpha-synuclein inclusions link multiple system atrophy with parkinson's disease and dementia with lewy bodies. *Neurosci Lett* **251**, 205–8, DOI: 10.1016/s0304-3940(98)00504-7 (1998).

14. Braak, H. *et al.* Staging of brain pathology related to sporadic parkinson's disease. *Neurobiol Aging* **24**, 197–211, DOI: 10.1016/s0197-4580(02)00065-9 (2003).

15. Giguère, N., Burke Nanni, S. & Trudeau, L.-E. On cell loss and selective vulnerability of neuronal populations in parkinson's disease. *Front. neurology* 455 (2018).

16. Surmeier, D. J., Obeso, J. A. & Halliday, G. M. Selective neuronal vulnerability in parkinson disease. *Nat. Rev. Neurosci.* **18**, 101–113 (2017).

17. Parkkinen, L. *et al.* Disentangling the relationship between lewy bodies and nigral neuronal loss in parkinson's disease. *J. Park. disease* **1**, 277–286 (2011).

18. Parkkinen, L., Pirttilä, T. & Alafuzoff, I. Applicability of current staging/categorization of α-synuclein pathology and their clinical relevance. *Acta neuropathologica* **115**, 399–407 (2008).

19. Kalaitzakis, M. E., Graeber, M. B., Gentleman, S. M. & Pearce, R. K. Controversies over the staging of α-synuclein pathology in parkinson's disease. *Acta neuropathologica* **116**, 125–128 (2008).

20. McKeith, I. *et al.* Dementia with lewy bodies. *The Lancet Neurol.* **3**, 19–28 (2004).

21. Luis, C. A. *et al.* Sensitivity and specificity of three clinical criteria for dementia with lewy bodies in an autopsy-verified sample. *Int. journal geriatric psychiatry* **14**, 526–533 (1999).

22. McKeith, I. G. *et al.* Diagnosis and management of dementia with lewy bodies: Fourth consensus report of the dlb consortium. *Neurology* **89**, 88–100 (2017).

23. Walker, L., Stefanis, L. & Attems, J. Clinical and neuropathological differences between parkinson's disease, parkinson's disease dementia and dementia with lewy bodies–current issues and future directions. *J. neurochemistry* **150**, 467–474 (2019).

24. Nelson, P. T. *et al.* Low sensitivity in clinical diagnoses of dementia with lewy bodies. *J. neurology* **257**, 359–366 (2010).

25. Ballard, C., Kahn, Z. & Corbett, A. Treatment of dementia with lewy bodies and parkinson's disease dementia. *Drugs & aging* **28**, 769–777 (2011).

26. Kosaka, K. Lewy bodies in cerebral cortex. report of three cases. *Acta neuropathologica* **42**, 127–134 (1978).

27. Outeiro, T. F. *et al.* Dementia with lewy bodies: an update and outlook. *Mol. neurodegeneration* **14**, 1–18 (2019).

28. Poewe, W. *et al.* Multiple system atrophy. *Nat. Rev. Dis. Primers* **8**, 56 (2022).

29. Low, P. *et al.* Natural history study of msa in north america: A prospective cohort study. *Auton. Neurosci. Basic Clin.* **192**, 126–127 (2015).

30. Kim, H.-J., Jeon, B. S., Lee, J.-Y. & Yun, J. Y. Survival of korean patients with multiple system atrophy. *Mov. disorders* **26**, 909–912 (2011).

31. Wenning, G. K. *et al.* The natural history of multiple system atrophy: a prospective european cohort study. *The lancet neurology* **12**, 264–274 (2013).

32. Wenning, G. K. *et al.* Development and validation of the unified multiple system atrophy rating scale (umsars). *Mov. Disord.* **19**, 1391–1402 (2004).

33. Trojanowski, J., Revesz, T. & on MSA, N. W. G. Proposed neuropathological criteria for the post mortem diagnosis of multiple system atrophy. *Neuropathol. applied neurobiology* **33**, 615–620 (2007).

34. Papp, M. I., Kahn, J. E. & Lantos, P. L. Glial cytoplasmic inclusions in the cns of patients with multiple system atrophy (striatonigral degeneration, olivopontocerebellar atrophy and shy-drager syndrome). *J Neurol Sci* **94**, 79–100, DOI: 10.1016/0022-510x(89)90219-0 (1989).

35. Shibasaki, Y., Baillie, D., St. Clair, D. & Brookes, A. High-resolution mapping of snca encoding α-synuclein, the non-aβ component of alzheimer's disease amyloid precursor, to human chromosome 4q21. 3$\rightarrow$ q22 by fluorescence in situ hybridization. *Cytogenet. Genome Res.* **71**, 54–55 (1995).

36. Maroteaux, L., Campanelli, J. T. & Scheller, R. H. Synuclein: a neuron-specific protein localized to the nucleus and presynaptic nerve terminal. *J. Neurosci.* **8**, 2804–2815 (1988).

37. Kahle, P. J. *et al.* Subcellular localization of wild-type and parkinson's disease-associated mutant α-synuclein in human and transgenic mouse brain. *J. Neurosci.* **20**, 6365–6373 (2000).

38. Davidson, W. S., Jonas, A., Clayton, D. F. & George, J. M. Stabilization of α-synuclein secondary structure upon binding to synthetic membranes. *J. Biol. Chem.* **273**, 9443–9449 (1998).

39. Iwai, A., Yoshimoto, M., Masliah, E. & Saitoh, T. Non-a. beta. component of alzheimer's disease amyloid (nac) is amyloidogenic. *Biochemistry* **34**, 10139–10145 (1995).

40. Qin, Z., Hu, D., Han, S., Hong, D.-P. & Fink, A. L. Role of different regions of α-synuclein in the assembly of fibrils. *Biochemistry* **46**, 13322–13330 (2007).

41. Schrödinger, L. & DeLano, W. Pymol.

42. Ulmer, T. S., Bax, A., Cole, N. B. & Nussbaum, R. L. Structure and dynamics of micelle-bound human α-synuclein. *J. Biol. Chem.* **280**, 9595–9603 (2005).

43. Ulmer, T., Bax, A., Cole, N. & Nussbaum, R. Human micelle-bound alpha-synuclein, DOI: 10.2210/pdb1xq8/pdb (2005).

44. Lautenschläger, J. *et al.* C-terminal calcium binding of α-synuclein modulates synaptic vesicle interaction. *Nat. communications* **9**, 712 (2018).

45. Sorrentino, Z. A. & Giasson, B. I. The emerging role of α-synuclein truncation in aggregation and disease. *J. Biol. Chem.* **295**, 10224–10244 (2020).

46. Krüger, R. *et al.* Alasopro mutation in the gene encoding α-synuclein in parkinson's disease. *Nat. genetics* **18**, 106–108 (1998).

47. Zarranz, J. J. *et al.* The new mutation, e46k, of α-synuclein causes parkinson and lewy body dementia. *Annals Neurol. Off. J. Am. Neurol. Assoc. Child Neurol. Soc.* **55**, 164–173 (2004).

48. Proukakis, C. *et al.* A novel α-synuclein missense mutation in parkinson disease. *Neurology* **80**, 1062–1064 (2013).

49. Lesage, S. *et al.* G51d α-synuclein mutation causes a novel parkinsonian–pyramidal syndrome. *Annals neurology* **73**, 459–471 (2013).

50. Pasanen, P. *et al.* A novel α-synuclein mutation a53e associated with atypical multiple system atrophy and parkinson's disease-type pathology. *Neurobiol. aging* **35**, 2180–e1 (2014).

51. Polymeropoulos, M. H. *et al.* Mutation in the α-synuclein gene identified in families with parkinson's disease. *science* **276**, 2045–2047 (1997).

52. Yoshino, H. *et al.* Homozygous alpha-synuclein p. a53v in familial parkinson's disease. *Neurobiol. aging* **57**, 248–e7 (2017).

53. Bussell, R. & Eliezer, D. Residual structure and dynamics in parkinson's disease-associated mutants of α-synuclein. *J. Biol. Chem.* **276**, 45996–46003 (2001).

54. Perrin, R. J., Woods, W. S., Clayton, D. F. & George, J. M. Interaction of human α-synuclein and parkinson's disease variants with phospholipids: structural analysis using site-directed mutagenesis. *J. Biol. Chem.* **275**, 34393–34398 (2000).

55. Jakes, R., Spillantini, M. G. & Goedert, M. Identification of two distinct synucleins from human brain. *FEBS letters* **345**, 27–32 (1994).

56. Lavedan, C. *et al.* Identification, localization and characterization of the human γ-synuclein gene. *Hum. genetics* **103**, 106–112 (1998).

57. Chandra, S. *et al.* Double-knockout mice for α-and β-synucleins: effect on synaptic functions. *Proc. Natl. Acad. Sci.* **101**, 14966–14971 (2004).

58. Robertson, D. C. *et al.* Developmental loss and resistance to mptp toxicity of dopaminergic neurones in substantia nigra pars compacta of γ-synuclein, α-synuclein and double α/γ-synuclein null mutant mice. *J. neurochemistry* **89**, 1126–1136 (2004).

59. Frey, B. *et al.* Monitoring alpha-synuclein oligomerization and aggregation using bimolecular fluorescence complementation assays: What you see is not always what you get. *J. neurochemistry* **157**, 872–888 (2021).

60. Spillantini, M. G. *et al.* Alpha-synuclein in lewy bodies. *Nature* **388**, 839–40, DOI: 10.1038/42166 (1997).

61. Lavedan, C. *et al.* Absence of mutation in the β-and γ-synuclein genes in familial autosomal dominant parkinson's disease. *DNA research* **5**, 401–402 (1998).

62. Ohtake, H. *et al.* β-synuclein gene alterations in dementia with lewy bodies. *Neurology* **63**, 805–811 (2004).

63. Uversky, V. N., Li, J. & Fink, A. L. Metal-triggered structural transformations, aggregation, and fibrillation of human α-synuclein: a possible molecular link between parkinson's disease and heavy metal exposure. *J. Biol. Chem.* **276**, 44284–44296 (2001).

64. Hashimoto, M., Rockenstein, E., Mante, M., Mallory, M. & Masliah, E. β-synuclein inhibits α-synuclein aggregation: a possible role as an anti-parkinsonian factor. *Neuron* **32**, 213–223 (2001).

65. Greten-Harrison, B. *et al.* $\alpha\beta\gamma$-synuclein triple knockout mice reveal age-dependent neuronal dysfunction. *Proc. Natl. Acad. Sci.* **107**, 19573–19578 (2010).

66. Iwai, A. *et al.* The precursor protein of non-aβ component of alzheimer's disease amyloid is a presynaptic protein of the central nervous system. *Neuron* **14**, 467–475 (1995).

67. Abeliovich, A. *et al.* Mice lacking α-synuclein display functional deficits in the nigrostriatal dopamine system. *Neuron* **25**, 239–252 (2000).

68. Cabin, D. E. *et al.* Synaptic vesicle depletion correlates with attenuated synaptic responses to prolonged repetitive stimulation in mice lacking α-synuclein. *J. Neurosci.* **22**, 8797–8807 (2002).

69. Lee, S.-J., Jeon, H. & Kandror, K. V. Alpha-synuclein is localized in a subpopulation of rat brain synaptic vesicles. *Acta Neurobiol Exp (Wars)* **68**, 509–515 (2008).

70. Burré, J. *et al.* α-synuclein promotes snare-complex assembly in vivo and in vitro. *Science* **329**, 1663–1667 (2010).

71. Yavich, L., Tanila, H., Vepsäläinen, S. & Jäkälä, P. Role of α-synuclein in presynaptic dopamine recruitment. *J. Neurosci.* **24**, 11165–11170 (2004).

72. Nemani, V. M. *et al.* Increased expression of α-synuclein reduces neurotransmitter release by inhibiting synaptic vesicle reclustering after endocytosis. *Neuron* **65**, 66–79 (2010).

73. Kragh, C. L., Ubhi, K., Wyss-Corey, T. & Masliah, E. Autophagy in dementias. *Brain pathology* **22**, 99–109 (2012).

74. Chartier-Harlin, M.-C. *et al.* α-synuclein locus duplication as a cause of familial parkinson's disease. *The Lancet* **364**, 1167–1169 (2004).

75. Seidel, K. *et al.* First appraisal of brain pathology owing to a30p mutant alpha-synuclein. *Annals neurology* **67**, 684–689 (2010).

76. Lashuel, H. A., Overk, C. R., Oueslati, A. & Masliah, E. The many faces of α-synuclein: from structure and toxicity to therapeutic target. *Nat. Rev. Neurosci.* **14**, 38–48 (2013).

77. Cuervo, A. M., Stefanis, L., Fredenburg, R., Lansbury, P. T. & Sulzer, D. Impaired degradation of mutant α-synuclein by chaperone-mediated autophagy. *Science* **305**, 1292–1295 (2004).

78. Crews, L. *et al.* Selective molecular alterations in the autophagy pathway in patients with lewy body disease and in models of α-synucleinopathy. *PloS one* **5**, e9313 (2010).

79. Tayebi, N. *et al.* Gaucher disease and parkinsonism: a phenotypic and genotypic characterization. *Mol. genetics metabolism* **73**, 313–321 (2001).

80. Uversky, V. N. Neuropathology, biochemistry, and biophysics of α-synuclein aggregation. *J. neurochemistry* **103**, 17–37 (2007).

81. Chen, S. W. *et al.* Structural characterization of toxic oligomers that are kinetically trapped during α-synuclein fibril formation. *Proc. Natl. Acad. Sci.* **112**, E1994–E2003 (2015).

82. Cremades, N. *et al.* Direct observation of the interconversion of normal and toxic forms of α-synuclein. *Cell* **149**, 1048–1059 (2012).

83. Danzer, K. M. *et al.* Different species of α-synuclein oligomers induce calcium influx and seeding. *J. Neurosci.* **27**, 9220–9232 (2007).

84. Winner, B. *et al.* In vivo demonstration that α-synuclein oligomers are toxic. *Proc. Natl. Acad. Sci.* **108**, 4194–4199 (2011).

85. Schweighauser, M. *et al.* Structures of α-synuclein filaments from multiple system atrophy. *Nature* **585**, 464–469 (2020).

86. Schweighauser, M. *et al.* Multiple system atrophy type i alpha-synuclein filament, DOI: 10.2210/pdb6xyo/pdb (2020).

87. Conway, K. A., Harper, J. D. & Lansbury, P. T. Accelerated in vitro fibril formation by a mutant α-synuclein linked to early-onset parkinson disease. *Nat. medicine* **4**, 1318–1320 (1998).

88. Wood, S. J. *et al.* α-synuclein fibrillogenesis is nucleation-dependent: Implications for the pathogenesis of parkinson's disease. *J. Biol. Chem.* **274**, 19509–19512 (1999).

89. Desplats, P. *et al.* Inclusion formation and neuronal cell death through neuron-to-neuron transmission of α-synuclein. *Proc. Natl. Acad. Sci.* **106**, 13010–13015 (2009).

90. Hansen, C. *et al.* α-synuclein propagates from mouse brain to grafted dopaminergic neurons and seeds aggregation in cultured human cells. *The J. clinical investigation* **121**, 715–725 (2011).

91. Luk, K. C. *et al.* Pathological α-synuclein transmission initiates parkinson-like neurodegeneration in nontransgenic mice. *Science* **338**, 949–953 (2012).

92. Lau, A. *et al.* alpha-synuclein strains target distinct brain regions and cell types. *Nat Neurosci* **23**, 21–31, DOI: 10.1038/s41593-019-0541-x (2020).

93. Luk, K. C. *et al.* Intracerebral inoculation of pathological α-synuclein initiates a rapidly progressive neurodegenerative α-synucleinopathy in mice. *J. Exp. Medicine* **209**, 975–986 (2012).

94. Li, J.-Y. *et al.* Lewy bodies in grafted neurons in subjects with parkinson's disease suggest host-to-graft disease propagation. *Nat. medicine* **14**, 501–503 (2008).

95. Kordower, J. H., Chu, Y., Hauser, R. A., Freeman, T. B. & Olanow, C. W. Lewy body–like pathology in long-term embryonic nigral transplants in parkinson's disease. *Nat. medicine* **14**, 504–506 (2008).

96. Aguzzi, A., Heikenwalder, M. & Polymenidou, M. Insights into prion strains and neurotoxicity. *Nat. reviews Mol. cell biology* **8**, 552–561 (2007).

97. Bousset, L. *et al.* Structural and functional characterization of two alpha-synuclein strains. *Nat Commun* **4**, 2575, DOI: 10.1038/ncomms3575 (2013).

98. Fusco, G. *et al.* Structural basis of membrane disruption and cellular toxicity by α-synuclein oligomers. *Science* **358**, 1440–1443 (2017).

99. Shrivastava, A. N. *et al.* Differential membrane binding and seeding of distinct α-synuclein fibrillar polymorphs. *Biophys. journal* **118**, 1301–1320 (2020).

100. Guerrero-Ferreira, R. *et al.* Two new polymorphic structures of human full-length alpha-synuclein fibrils solved by cryo-electron microscopy. *Elife* **8**, DOI: 10.7554/eLife.48907 (2019).

101. Peelaerts, W. *et al.* alpha-synuclein strains cause distinct synucleinopathies after local and systemic administration. *Nature* **522**, 340–4, DOI: 10.1038/nature14547 (2015).

102. Gribaudo, S. *et al.* Propagation of α-synuclein strains within human reconstructed neuronal network. *Stem Cell Reports* **12**, 230–244 (2019).

103. Makky, A., Bousset, L., Polesel-Maris, J. & Melki, R. Nanomechanical properties of distinct fibrillar polymorphs of the protein α-synuclein. *Sci. Reports* **6**, 37970 (2016).

104. Yang, Y. *et al.* Structures of α-synuclein filaments from human brains with lewy pathology. *Nature* **610**, 791–795 (2022).

105. Yang, Y. *et al.* Cryo-EM structure of alpha-synuclein filaments from parkinson's disease and dementia with lewy bodies, DOI: 10.2210/pdb8a9l/pdb (2022).

106. Malfertheiner, K., Stefanova, N. & Heras-Garvin, A. The concept of α-synuclein strains and how different conformations may explain distinct neurodegenerative disorders. *Front. Neurol.* **12**, 737195 (2021).

107. Spillantini, M. G., Crowther, R. A., Jakes, R., Hasegawa, M. & Goedert, M. alpha-synuclein in filamentous inclusions of lewy bodies from parkinson's disease and dementia with lewy bodies. *Proc Natl Acad Sci U S A* **95**, 6469–73, DOI: 10.1073/pnas.95.11.6469 (1998).

108. Crowther, R. A., Daniel, S. E. & Goedert, M. Characterisation of isolated alpha-synuclein filaments from substantia nigra of parkinson's disease brain. *Neurosci Lett* **292**, 128–30, DOI: 10.1016/s0304-3940(00)01440-3 (2000).

109. Guo, J. L. *et al.* Distinct α-synuclein strains differentially promote tau inclusions in neurons. *Cell* **154**, 103–117 (2013).

110. Peng, C. *et al.* Cellular milieu imparts distinct pathological alpha-synuclein strains in alpha-synucleinopathies. *Nature* **557**, 558–563, DOI: 10.1038/s41586-018-0104-4 (2018).

111. Shahnawaz, M. *et al.* Discriminating alpha-synuclein strains in parkinson's disease and multiple system atrophy. *Nature* **578**, 273–277, DOI: 10.1038/s41586-020-1984-7 (2020).

112. Poggiolini, I. *et al.* Diagnostic value of cerebrospinal fluid alpha-synuclein seed quantification in synucleinopathies. *Brain* **145**, 584–595 (2022).

113. Rossi, M. *et al.* Ultrasensitive rt-quic assay with high sensitivity and specificity for lewy body-associated synucleinopathies. *Acta neuropathologica* **140**, 49–62 (2020).

114. De Giorgi, F. *et al.* Novel self-replicating α-synuclein polymorphs that escape tht monitoring can spontaneously emerge and acutely spread in neurons. *Sci. Adv.* **6**, eabc4364 (2020).

115. Lövestam, S. *et al.* Seeded assembly in vitro does not replicate the structures of αSyn-synuclein filaments from multiple system atrophy. *FEBS open bio* **11**, 999–1013 (2021).

116. Strohaker, T. *et al.* Structural heterogeneity of alpha-synuclein fibrils amplified from patient brain extracts. *Nat Commun* **10**, 5535, DOI: 10.1038/s41467-019-13564-w (2019).

117. Van der Perren, A. *et al.* The structural differences between patient-derived α-synuclein strains dictate characteristics of parkinson's disease, multiple system atrophy and dementia with lewy bodies. *Acta neuropathologica* **139**, 977–1000 (2020).

118. Tanudjojo, B. *et al.* Phenotypic manifestation of α-synuclein strains derived from parkinson's disease and multiple system atrophy in human dopaminergic neurons. *Nat. communications* **12**, 3817 (2021).

119. De Luca, C. M. G. *et al.* The alpha-synuclein rt-quic products generated by the olfactory mucosa of patients with parkinson's disease and multiple system atrophy induce inflammatory responses in sh-sy5y cells. *Cells* **11**, 87 (2022).

120. Watts, J. C. *et al.* Transmission of multiple system atrophy prions to transgenic mice. *Proc Natl Acad Sci U S A* **110**, 19555–60, DOI: 10.1073/pnas.1318268110 (2013).

121. Prusiner, S. B. *et al.* Evidence for α-synuclein prions causing multiple system atrophy in humans with parkinsonism. *Proc. Natl. Acad. Sci.* **112**, E5308–E5317 (2015).

122. Lovestam, S., Schweighauser, M. & Scheres, S. Type 3 alpha-synuclein filament seeded in vitro by filaments purified from multiple systems atrophy case 5, DOI: 10.2210/pdb7nck/pdb (2021).

123. Fan, Y. *et al.* Conformational change of α-synuclein fibrils in cerebrospinal fluid from different clinical phases of parkinson's disease. *Structure* **31**, 78–87 (2023).

124. Fan, Y., Sun, Y., Wang, J. & Liu, C. Major polymorph in alpha-synuclein fibril seeded by cerebrospinal fluid from a mid-to-late stage (mid-PD-1) parkinson's disease patient, DOI: 10.2210/pdb7xo1/pdb (2022).

125. Fairfoul, G. *et al.* Alpha-synuclein rt-quic in the csf of patients with alpha-synucleinopathies. *Ann Clin Transl Neurol* **3**, 812–818, DOI: 10.1002/acn3.338 (2016).

126. Strimbu, K. & Tavel, J. A. What are biomarkers? *Curr. Opin. HIV AIDS* **5**, 463 (2010).

127. Blennow, K., Hampel, H., Weiner, M. & Zetterberg, H. Cerebrospinal fluid and plasma biomarkers in alzheimer disease. *Nat. Rev. Neurol.* **6**, 131–144 (2010).

128. Prusiner, S. B. Prions. *Proc. Natl. Acad. Sci.* **95**, 13363–13383 (1998).

129. Sano, K. *et al.* Prion-like seeding of misfolded α-synuclein in the brains of dementia with lewy body patients in rt-quic. *Mol. neurobiology* **55**, 3916–3930 (2018).

130. De Luca, C. M. G. *et al.* Efficient rt-quic seeding activity for α-synuclein in olfactory mucosa samples of patients with parkinson's disease and multiple system atrophy. *Transl. neurodegeneration* **8**, 1–14 (2019).

131. Kuzkina, A. *et al.* Dermal real-time quaking-induced conversion is a sensitive marker to confirm isolated rapid eye movement sleep behavior disorder as an early α-synucleinopathy. *Mov. Disord.* (2023).

132. Okuzumi, A. *et al.* Propagative α-synuclein seeds as serum biomarkers for synucleinopathies. *Nat. Medicine* 1–8 (2023).

133. Vivacqua, G. *et al.* Salivary α-synuclein rt-quic correlates with disease severity in de novo parkinson's disease. *Mov. Disord.* **38**, 153 (2023).

134. Candelise, N. *et al.* Effect of the micro-environment on α-synuclein conversion and implication in seeded conversion assays. *Transl. neurodegeneration* **9**, 1–16 (2020).

135. Schmitz, M. *et al.* The real-time quaking-induced conversion assay for detection of human prion disease and study of other protein misfolding diseases. *Nat. protocols* **11**, 2233–2242 (2016).

136. Groveman, B. R. *et al.* Rapid and ultra-sensitive quantitation of disease-associated alpha-synuclein seeds in brain and cerebrospinal fluid by alphasyn rt-quic. *Acta Neuropathol Commun* **6**, 7, DOI: 10.1186/s40478-018-0508-2 (2018).

137. Bargar, C. *et al.* Discrimination of msa-p and msa-c by rt-quic analysis of olfactory mucosa: the first assessment of assay reproducibility between two specialized laboratories. *Mol. neurodegeneration* **16**, 1–19 (2021).

138. Poggiolini, I. *et al.* Rt-quic using c-terminally truncated α-synuclein forms detects differences in seeding propensity of different brain regions from synucleinopathies. *Biomolecules* **11**, 820 (2021).

139. Iranzo, A. *et al.* Misfolded α-synuclein assessment in the skin and csf by rt-quic in isolated rem sleep behavior disorder. *Neurology* **100**, e1944–e1954 (2023).

140. Iranzo, A. *et al.* Detection of α-synuclein in csf by rt-quic in patients with isolated rapid-eye-movement sleep behaviour disorder: a longitudinal observational study. *The Lancet Neurol.* **20**, 203–212 (2021).

141. Concha-Marambio, L. *et al.* Accurate detection of α-synuclein seeds in cerebrospinal fluid from isolated rapid eye movement sleep behavior disorder and patients with parkinson's disease in the denovo parkinson (denopa) cohort. *Mov. Disord.* **38**, 567–578 (2023).

142. Liguori, R. *et al.* A comparative blind study between skin biopsy and seed amplification assay to disclose pathological α-synuclein in rbd. *npj Park. Dis.* **9**, 34 (2023).

143. Stefani, A. *et al.* Alpha-synuclein seeds in olfactory mucosa of patients with isolated rem sleep behaviour disorder. *Brain* **144**, 1118–1126 (2021).

144. Kang, U. J. *et al.* Comparative study of cerebrospinal fluid α-synuclein seeding aggregation assays for diagnosis of parkinson's disease. *Mov. Disord.* **34**, 536–544 (2019).

145. Orrù, C. D. *et al.* A rapid α-synuclein seed assay of parkinson's disease csf panel shows high diagnostic accuracy. *Annals Clin. Transl. Neurol.* **8**, 374–384 (2021).

146. Shahnawaz, M. *et al.* Development of a biochemical diagnosis of parkinson disease by detection of alpha-synuclein misfolded aggregates in cerebrospinal fluid. *JAMA Neurol* **74**, 163–172, DOI: 10.1001/jamaneurol.2016.4547 (2017).

147. Siderowf, A. *et al.* Assessment of heterogeneity among participants in the parkinson's progression markers initiative cohort using α-synuclein seed amplification: a cross-sectional study. *The Lancet Neurol.* **22**, 407–417 (2023).

148. Russo, M. J. *et al.* High diagnostic performance of independent alpha-synuclein seed amplification assays for detection of early parkinson's disease. *Acta neuropathologica communications* **9**, 1–13 (2021).

149. Mitchell, T. *et al.* Emerging neuroimaging biomarkers across disease stage in parkinson disease: a review. *JAMA neurology* **78**, 1262–1272 (2021).

150. Bongianni, M. *et al.* Olfactory swab sampling optimization for α-synuclein aggregate detection in patients with parkinson's disease. *Transl. neurodegeneration* **11**, 1–11 (2022).

151. Kuzkina, A. *et al.* Diagnostic value of skin rt-quic in parkinson's disease: a two-laboratory study. *npj Park. Dis.* **7**, 99, DOI: 10.1038/s41531-021-00242-2 (2021).

152. Schenkels, L. C., Veerman, E. C. & Nieuw Amerongen, A. V. Biochemical composition of human saliva in relation to other mucosal fluids. *Critical reviews oral biology & medicine* **6**, 161–175 (1995).

153. Ferreira, J. N. & Hoffman, M. P. Interactions between developing nerves and salivary glands. *Organogenesis* **9**, 199–205 (2013).

154. Proctor, G. & Shaalan, A. Disease-induced changes in salivary gland function and the composition of saliva. *J. dental research* **100**, 1201–1209 (2021).

155. Cersosimo, M. G. *et al.* Dry mouth: an overlooked autonomic symptom of parkinson's disease. *J. Park. Dis.* **1**, 169–173 (2011).

156. Vivacqua, G. *et al.* Abnormal salivary total and oligomeric alpha-synuclein in parkinson's disease. *PloS one* **11**, e0151156 (2016).

157. Devic, I. *et al.* Salivary α-synuclein and dj-1: potential biomarkers for parkinson's disease. *Brain* **134**, e178–e178 (2011).

158. Al-Nimer, M. S., Mshatat, S. F. & Abdulla, H. I. Saliva α-synuclein and a high extinction coefficient protein: a novel approach in assessment biomarkers of parkinson's disease. *North Am. journal medical sciences* **6**, 633 (2014).

159. Shaheen, H., Sobhy, S., El Mously, S., Abuomira, M. & Mansour, M. Salivary alpha-synuclein (total and oligomeric form): potential biomarkers in parkinson's disease. *The Egypt. J. Neurol. Psychiatry Neurosurg.* **56**, 1–6 (2020).

160. Vivacqua, G. *et al.* Salivary alpha-synuclein in the diagnosis of parkinson's disease and progressive supranuclear palsy. *Park. & related disorders* **63**, 143–148 (2019).

161. Sabaei, M. *et al.* Salivary levels of disease-related biomarkers in the early stages of parkinson's and alzheimer's disease: A cross-sectional study. *IBRO Neurosci. Reports* **14**, 285–292 (2023).

162. Kang, W. *et al.* Salivary total α-synuclein, oligomeric α-synuclein and snca variants in parkinson's disease patients. *Sci. reports* **6**, 28143 (2016).

163. Cao, Z. *et al.* α-synuclein in salivary extracellular vesicles as a potential biomarker of parkinson's disease. *Neurosci. letters* **696**, 114–120 (2019).

164. Goldman, J. G. *et al.* Cerebrospinal fluid, plasma, and saliva in the biofind study: relationships among biomarkers and parkinson's disease features. *Mov. Disord.* **33**, 282–288 (2018).

165. Fernández-Espejo, E. *et al.* Native α-synuclein, 3-nitrotyrosine proteins, and patterns of nitro-α-synuclein-immunoreactive inclusions in saliva and submandibulary gland in parkinson's disease. *Antioxidants* **10**, 715 (2021).

166. De Bartolo, M. I. *et al.* A combined panel of salivary biomarkers in de novo parkinson's disease. *Annals Neurol.* **93**, 446–459 (2023).

167. Angius, F. *et al.* Combined measure of salivary alpha-synuclein species as diagnostic biomarker for parkinson's disease. *J. Neurol.* 1–9 (2023).

168. Compta, Y. *et al.* Cerebrospinal tau, phospho-tau, and beta-amyloid and neuropsychological functions in parkinson's disease. *Mov. disorders: official journal Mov. Disord. Soc.* **24**, 2203–2210 (2009).

169. Pan, L. *et al.* Tau accelerates α-synuclein aggregation and spreading in parkinson's disease. *Brain* **145**, 3454–3471 (2022).

170. Youn, J. *et al.* Cerebrospinal fluid levels of autophagy-related proteins represent potentially novel biomarkers of early-stage parkinson's disease. *Sci. Reports* **8**, 16866 (2018).

171. Figura, M. *et al.* Proteomic profile of saliva in parkinson's disease patients: A proof of concept study. *Brain Sci.* **11**, 661 (2021).

172. Luan, M. *et al.* Diagnostic value of salivary real-time quaking-induced conversion in parkinson's disease and multiple system atrophy. *Mov. Disord.* **37**, 1059–1063 (2022).

173. Clarke, C. *et al.* Uk parkinson's disease society brain bank diagnostic criteria. *NIHR Journals Libr.* (2016).

174. Gilman, S. *et al.* Second consensus statement on the diagnosis of multiple system atrophy. *Neurology* **71**, 670–676 (2008).

175. Foubert-Samier, A. *et al.* Disease progression and prognostic factors in multiple system atrophy: a prospective cohort study. *Neurobiol. Dis.* **139**, 104813 (2020).

176. Fedorova, T. *et al.* Salivary acetylcholinesterase activity is increased in parkinson's disease: a potential marker of parasympathetic dysfunction. *Park. Dis.* **2015** (2015).

177. Navazesh, M. & Christensen, C. A comparison of whole mouth resting and stimulated salivary measurement procedures. *J. dental research* **61**, 1158–1162 (1982).

178. Sayer, R., Law, E., Connelly, P. J. & Breen, K. C. Association of a salivary acetylcholinesterase with alzheimer's disease and response to cholinesterase inhibitors. *Clin. biochemistry* **37**, 98–104 (2004).

179. Sanderson, J. B. *et al.* Analysis of α-synuclein species enriched from cerebral cortex of humans with sporadic dementia with lewy bodies. *Brain communications* **2**, fcaa010 (2020).

180. Tofaris, G. K., Razzaq, A., Ghetti, B., Lilley, K. S. & Spillantini, M. G. Ubiquitination of α-synuclein in lewy bodies is a pathological event not associated with impairment of proteasome function. *J. Biol. Chem.* **278**, 44405–44411 (2003).

181. Holec, S. A. & Woerman, A. L. Evidence of distinct α-synuclein strains underlying disease heterogeneity. *Acta Neuropathol.* **142**, 73–86 (2021).

182. Shi, Y. *et al.* Structure-based classification of tauopathies. *Nature* **598**, 359–363 (2021).

183. Woerman, A. L. *et al.* Propagation of prions causing synucleinopathies in cultured cells. *Proc Natl Acad Sci U S A* **112**, E4949–58, DOI: 10.1073/pnas.1513426112 (2015).

184. Woerman, A. L. *et al.* Msa prions exhibit remarkable stability and resistance to inactivation. *Acta Neuropathol.* **135**, 49–63, DOI: 10.1007/s00401-017-1762-2 (2018).

185. Bernis, M. E. *et al.* Prion-like propagation of human brain-derived alpha-synuclein in transgenic mice expressing human wild-type alpha-synuclein. *Acta Neuropathol Commun* **3**, 75, DOI: 10.1186/s40478-015-0254-7 (2015).

186. Woerman, A. L. *et al.* Familial parkinson's point mutation abolishes multiple system atrophy prion replication. *Proc. Natl. Acad. Sci.* **115**, 409–414, DOI: 10.1073/pnas.1719369115 (2018).

187. Woerman, A. L. *et al.* Multiple system atrophy prions retain strain specificity after serial propagation in two different tg(snca*a53t) mouse lines. *Acta Neuropathol.* **137**, 437–454, DOI: 10.1007/s00401-019-01959-4 (2019).

188. Woerman, A. L. *et al.* Kinetics of α-synuclein prions preceding neuropathological inclusions in multiple system atrophy. *PLoS pathogens* **16**, e1008222 (2020).

189. Bartz, J. C. Prion strain diversity. *Cold Spring Harb. perspectives medicine* **6** (2016).

190. Kumar, S. T. *et al.* How specific are the conformation-specific α-synuclein antibodies? characterization and validation of 16 α-synuclein conformation-specific antibodies using well-characterized preparations of α-synuclein monomers, fibrils and oligomers with distinct structures and morphology. *Neurobiol. disease* **146**, 105086 (2020).

191. Mahul-Mellier, A.-L. *et al.* The process of lewy body formation, rather than simply α-synuclein fibrillization, is one of the major drivers of neurodegeneration. *Proc. Natl. Acad. Sci.* **117**, 4971–4982 (2020).

192. Gram, H., Theologidis, V., Boesen, T. & Jensen, P. H. Sarkosyl differentially solubilizes patient-derived alpha-synuclein fibril strains. *Front. Mol. Biosci.* **10** (2023).

193. Li, B. *et al.* Cryo-em of full-length α-synuclein reveals fibril polymorphs with a common structural kernel. *Nat. communications* **9**, 3609 (2018).

194. Ayers, J. I. *et al.* Different αSyn synuclein prion strains cause dementia with lewy bodies and multiple system atrophy. *Proc. Natl. Acad. Sci.* **119**, e2113489119 (2022).

195. Holec, S. A. *et al.* Multiple system atrophy prions transmit neurological disease to mice expressing wild-type human α-synuclein. *Acta Neuropathol.* **144**, 677–690 (2022).

196. Frieg, B. *et al.* Quaternary structure of patient-homogenate amplified α-synuclein fibrils modulates seeding of endogenous α-synuclein. *Commun. biology* **5**, 1040 (2022).

197. Sano, K. *et al.* Conformational properties of prion strains can be transmitted to recombinant prion protein fibrils in real-time quaking-induced conversion. *J Virol* **88**, 11791–801, DOI: 10.1128/jvi.00585-14 (2014).

198. Chahine, L. M. *et al.* In vivo distribution of α-synuclein in multiple tissues and biofluids in parkinson disease. *Neurology* **95**, e1267–e1284 (2020).

199. Smith, W. W. *et al.* α-synuclein phosphorylation enhances eosinophilic cytoplasmic inclusion formation in sh-sy5y cells. *J. Neurosci.* **25**, 5544–5552 (2005).

200. Karampetsou, M. *et al.* Phosphorylated exogenous alpha-synuclein fibrils exacerbate pathology and induce neuronal dysfunction in mice. *Sci. Reports* **7**, 16533, DOI: 10.1038/s41598-017-15813-8 (2017).

201. Ma, M.-R., Hu, Z.-W., Zhao, Y.-F., Chen, Y.-X. & Li, Y.-M. Phosphorylation induces distinct alpha-synuclein strain formation. *Sci. Reports* **6**, 37130, DOI: 10.1038/srep37130 (2016).

202. Ghanem, S. S. *et al.* α-synuclein phosphorylation at serine 129 occurs after initial protein deposition and inhibits seeded fibril formation and toxicity. *Proc. Natl. Acad. Sci.* **119**, e2109617119 (2022).

203. Swirski, M. *et al.* Evaluating the relationship between amyloid-β and α-synuclein phosphorylated at ser129 in dementia with lewy bodies and parkinson's disease. *Alzheimer's research & therapy* **6**, 1–17 (2014).

204. Legname, G. *et al.* Continuum of prion protein structures enciphers a multitude of prion isolate-specified phenotypes. *Proc. Natl. Acad. Sci.* **103**, 19105–19110 (2006).

205. Gustavsson, N., Savchenko, E., Klementieva, O. & Roybon, L. The intracellular milieu of Parkinson's disease patient brain cells modulates alpha-synuclein protein aggregation. *Acta Neuropathol. Commun.* **9**, 1–6, DOI: 10.1186/s40478-021-01256-w (2021).

206. Balana, A. T. *et al.* O-glcnac modification forces the formation of an α-synuclein amyloid-strain with notably diminished seeding activity and pathology. *bioRxiv* 2023–03 (2023).

207. Hughes, A. J., Daniel, S. E., Kilford, L. & Lees, A. J. Accuracy of clinical diagnosis of idiopathic parkinson's disease: a clinico-pathological study of 100 cases. *J. neurology, neurosurgery & psychiatry* **55**, 181–184 (1992).

208. Orrú, C. D. *et al.* Factors that improve rt-quic detection of prion seeding activity. *Viruses* **8**, 140 (2016).

209. Van Rumund, A. *et al.* α-synuclein real-time quaking-induced conversion in the cerebrospinal fluid of uncertain cases of parkinsonism. *Annals neurology* **85**, 777–781 (2019).

210. Thanapornsangsuth, P., Chongsuksantikul, A., Saraya, A. W., Hiransuthikul, A. & Hemachudha, T. Real-time quaking-induced conversion assay using a small-scale substrate production workflow for the diagnosis of creutzfeldt-jakob disease. *J. Neurochem.* **166**, 403–413 (2023).

211. Del Tredici, K., Hawkes, C. H., Ghebremedhin, E. & Braak, H. Lewy pathology in the submandibular gland of individuals with incidental lewy body disease and sporadic parkinson's disease. *Acta neuropathologica* **119**, 703–713 (2010).

212. Bonne, N. J. & Wong, D. T. Salivary biomarker development using genomic, proteomic and metabolomic approaches. *Genome medicine* **4**, 1–12 (2012).

213. Kang, W.-Y. *et al.* Salivary dj-1 could be an indicator of parkinson's disease progression. *Front. aging neuroscience* **6**, 102 (2014).

214. Song, W. *et al.* Evaluation of salivary heme oxygenase-1 as a potential biomarker of early parkinson's disease. *Mov. Disord.* **33**, 583–591 (2018).

215. Pinteac, R., Montalban, X. & Comabella, M. Chitinases and chitinase-like proteins as biomarkers in neurologic disorders. *Neurol. Neuroinflammation* **8** (2021).

216. Russo, C., Valle, M. S., Casabona, A. & Malaguarnera, L. Chitinase signature in the plasticity of neurodegenerative diseases. *Int. J. Mol. Sci.* **24**, 6301 (2023).

217. Comabella, M. *et al.* Csf chitinase 3–like 2 is associated with long-term disability progression in patients with progressive multiple sclerosis. *Neurol. Neuroinflammation* **8** (2021).

218. Thompson, A. G. *et al.* Csf chitinase proteins in amyotrophic lateral sclerosis. *J. Neurol. Neurosurg. & Psychiatry* **90**, 1215–1220 (2019).

219. Bartl, M. *et al.* Biomarkers of neurodegeneration and glial activation validated in alzheimer's disease assessed in longitudinal cerebrospinal fluid samples of parkinson's disease. *PLoS One* **16**, e0257372 (2021).

220. Wennström, M. *et al.* The inflammatory marker ykl-40 is elevated in cerebrospinal fluid from patients with alzheimer's but not parkinson's disease or dementia with lewy bodies. *PloS one* **10**, e0135458 (2015).

221. Gold, M. *et al.* α 1-antitrypsin modulates microglial-mediated neuroinflammation and protects microglial cells from amyloid-β-induced toxicity. *J. neuroinflammation* **11**, 1–11 (2014).

222. Ortiz, G. *et al.* Alpha-1-antitrypsin ameliorates inflammation and neurodegeneration in the diabetic mouse retina. *Exp. Eye Res.* **174**, 29–39 (2018).

223. Zhou, T. *et al.* Alpha-1 antitrypsin attenuates m1 microglia-mediated neuroinflammation in retinal degeneration. *Front. Immunol.* **9**, 1202 (2018).

224. Kuzkina, A. *et al.* Combining skin and olfactory α-synuclein seed amplification assays (saa)—towards biomarker-driven phenotyping in synucleinopathies. *npj Park. Dis.* **9**, 79 (2023).

225. Xiang, Y. *et al.* Comparison of the sensitivity of western blotting between pvdf and nc membranes. *Sci. Reports* **11**, 12022 (2021).

226. Esser, D. *et al.* Sample stability and protein composition of saliva: implications for its use as a diagnostic fluid. *Biomark. insights* **3**, BMI–S607 (2008).

227. Schepici, G., Silvestro, S., Trubiani, O., Bramanti, P. & Mazzon, E. Salivary biomarkers: Future approaches for early diagnosis of neurodegenerative diseases. *Brain Sci.* **10**, 245 (2020).

228. Gardner, A., Carpenter, G. & So, P.-W. Salivary metabolomics: From diagnostic biomarker discovery to investigating biological function. *Metabolites* **10**, 47 (2020).

229. Kumari, S. *et al.* Quantitative metabolomics of saliva using proton nmr spectroscopy in patients with parkinson's disease and healthy controls. *Neurol. Sci.* **41**, 1201–1210 (2020).